



This is to certify that the  
dissertation entitled

STUDIES OF TWO IRON-CONTAINING ENZYMES FROM  
ESCHERICHIA COLI: PYRUVATE FORMATE-LYASE  
ACTIVATING ENZYME AND ALKB

presented by

TIMOTHY FLEMING HENSHAW

has been accepted towards fulfillment  
of the requirements for the

Doctoral degree in Chemistry



Major Professor's Signature

5/25/04

Date

**LIBRARY**  
**Michigan State**  
**University**

**PLACE IN RETURN BOX to remove this checkout from your record.**  
**TO AVOID FINES return on or before date due.**  
**MAY BE RECALLED with earlier due date if requested.**

| DATE DUE | DATE DUE | DATE DUE |
|----------|----------|----------|
|          |          |          |
|          |          |          |
|          |          |          |
|          |          |          |
|          |          |          |
|          |          |          |
|          |          |          |
|          |          |          |
|          |          |          |
|          |          |          |
|          |          |          |

**STUDIES OF TWO IRON-CONTAINING ENZYMES FROM ESCHERICHIA COLI:  
PYRUVATE FORMATE-LYASE ACTIVATING ENZYME AND ALKB**

**By**

**Timothy Fleming Henshaw**

**A DISSERTATION**

**Submitted to  
Michigan State University  
in partial fulfillment of the requirements  
for the degree of**

**DOCTOR OF PHILOSOPHY**

**Department of Chemistry**

**2004**

## ABSTRACT

### STUDIES OF TWO IRON-CONTAINING ENZYMES FROM ESCHERICHIA COLI: PFL-AE and ALKB

By

Timothy Fleming Henshaw

Pyruvate formate-lyase activating enzyme (PFL-AE) is an iron-sulfur protein that catalyzes the generation of an essential radical at glycine-734 of pyruvate formate-lyase (PFL). This radical-generating reaction is dependent on S-adenosylmethionine (AdoMet) and is thought to involve a 5'-deoxyadenosyl radical that is generated by the reductive cleavage of AdoMet. PFL-AE was purified under anaerobic conditions and the iron-sulfur cluster was characterized by a combination of EPR, Mössbauer, and UV-visible spectroscopies. As isolated, PFL-AE was found to contain a variety of iron-sulfur clusters, including  $[4\text{Fe-4S}]^{2+}$ ,  $[2\text{Fe-2S}]^{2+}$ , and linear and cuboidal  $[3\text{Fe-4S}]^+$  clusters, with the cuboidal  $[3\text{Fe-4S}]^+$  being the dominant form of the cluster. These preparations were found to exhibit high specific activity in the absence of added iron. Under reducing conditions, these cluster types were converted to a mixture of  $[4\text{Fe-4S}]^{2+}$  and  $[4\text{Fe-4S}]^{1+}$  clusters.

In order to investigate the possibility of a unique iron site in the cluster of PFL-AE, a dual-isotope approach ( $^{56}\text{Fe}/^{57}\text{Fe}$ ) was used to selectively label the  $[4\text{Fe-4S}]^{2+}$  cluster. Mössbauer spectroscopy of these samples demonstrated that the  $^{57}\text{Fe}$  was incorporated into the unique site. In the presence of AdoMet, a large increase in the isomer shift was observed (0.43 mm/s to 0.73 mm/s) indicating that AdoMet binds

directly to this site in the cluster. In addition, detailed characterization of a single turnover of PFL-AE shows that the  $[4\text{Fe-4S}]^{1+}$  cluster provided the electron that is required for the reductive cleavage of AdoMet.

AlkB from *Escherichia coli* is a component of the “Ada response,” which is a coordinated defense against the toxic and mutagenic effects of environmental and endogenous alkylating agents. Despite its identification in 1983, the function of AlkB had not been determined. Theoretical fold prediction had suggested that AlkB might be a member of the iron and  $\alpha$ -ketoglutarate dependent dioxygenase superfamily. This possibility was tested, and the results in this dissertation show that AlkB functions by coupling the oxidative decarboxylation of  $\alpha$ -ketoglutarate to the oxidation of the aberrant methyl group, resulting in release of formaldehyde and restoration of the original base. In addition, in the absence of primary substrate, AlkB was found to catalyze the oxidation of a tryptophan residue located close to the metal center.

Dedicated to the memory of  
Judith Fleming Henshaw  
April 17, 1945 – June 30, 2003

## Table of Contents

|   |     |
|---|-----|
| List of Figures .....   | vii |
| List of Schemes .....   | ix  |
| List of Tables .....  | x   |
| List of Abbreviations .....   | xi  |
| INTRODUCTION .....  | 1   |
| The Fe/S AdoMet enzymes.....  | 2   |
| Pyruvate formate-lyase .....  | 2   |
| Pyruvate formate-lyase activating enzyme .....  | 3   |
| Ribonucleotide reductase activating enzyme.....   | 7   |
| Lysine aminomutase .....  | 8   |
| Sulfur insertion: BioB and LipA.....  | 10  |
| Spore photoproduct lyase.....   | 11  |
| DNA repair and Fe(II)/ $\alpha$ -ketoglutarate dioxygenases .....                               | 12  |
| The Adaptive response to alkylating agents .....  | 13  |
| Fe(II)/ $\alpha$ -ketoglutarate Dioxygenases.....   | 16  |
| Amino Acid Hydroxylases.....  | 17  |
| Fe(II)/ $\alpha$ -KG Dioxygenase Mechanism .....  | 18  |
| Non-heme Models.....  | 20  |
| Identification of an Fe(IV)=O Intermediate.....   | 20  |
| AlkB as an Fe(II)/ $\alpha$ -ketoglutarate Dioxygenase .....                                    | 22  |
| References.....   | 23  |
| CHARACTERIZATION OF THE IRON-SULFUR CENTER OF PYRUVATE<br>FORMATE-LYASE ACTIVATING ENZYME ..... | 29  |
| II.1 Introduction .....   | 30  |
| II.2 Experimental Methods .....   | 32  |
| Growth and expression of PFL .....  | 32  |
| Subcloning, growth, and expression of PFL-AE .....  | 32  |
| Purification of pyruvate formate-lyase-activating enzyme (PFL-AE).....                          | 33  |
| Activity, protein and iron assays.....  | 34  |
| EPR and Mössbauer Spectroscopy .....  | 35  |
| II.3 Results .....  | 36  |
| Enzyme Activity .....   | 36  |
| Characterization of purified PFL-AE.....  | 36  |
| Characterization of the dithionite-reduced enzyme .....   | 45  |
| II.4 Discussion .....   | 51  |
| References.....   | 53  |
| IDENTIFICATION OF A UNIQUE IRON SITE .....  | 55  |
| III.1 Introduction.....   | 56  |
| III.2 Experimental Methods .....  | 57  |

|  |            |
|--|------------|
| Preparation of Specifically Labeled Samples .....                  | 58         |
| III.3 Results and Discussion .....                                 | 58         |
| References .....   | 63         |
| <b>THE ACTIVE FORM OF THE CLUSTER: SINGLE TURNOVER EXPERIMENTS</b> | <b>64</b>  |
| IV.1 Introduction.....   | 65         |
| IV.2 Methods .....   | 67         |
| Preparation of single turnover samples.....                        | 67         |
| EPR Spectroscopy.....  | 68         |
| IV.2 Results and Discussion .....                                  | 68         |
| <b>OXIDATIVE DNA REPAIR.....</b>                                   | <b>74</b>  |
| V.1 Introduction.....  | 75         |
| V.2 Experimental Methods.....                                      | 76         |
| Expression and purification of AlkB .....                          | 76         |
| Radioactive substrates and assays.....                             | 76         |
| HPLC assays .....  | 77         |
| High-level methylation of an oligonucleotide .....                 | 77         |
| UV-visible spectroscopy .....                                      | 78         |
| Gas chromatography/mass spectrometry .....                         | 78         |
| Oxygen consumption .....   | 78         |
| V.3 Results and Discussion.....                                    | 79         |
| Release of ethanol-soluble radioactivity .....                     | 79         |
| UV-visible spectroscopy .....                                      | 79         |
| Identification of 1-meA and 3-meC as AlkB substrates .....         | 83         |
| Formaldehyde release and oxygen consumption .....                  | 84         |
| References.....  | 88         |
| <b>ABBERANT ACTIVITY OF THE DNA REPAIR ENZYME ALKB.....</b>        | <b>90</b>  |
| VI.1 Introduction.....   | 91         |
| VI.2 Experimental.....   | 92         |
| Sample Preparation .....   | 92         |
| UV-visible (UV-vis) spectroscopy .....                             | 92         |
| Mass Spectrometry (MS) .....                                       | 93         |
| Structural Modeling .....  | 94         |
| VI.3 Results and Discussion .....                                  | 95         |
| Chromophore Formation.....   | 95         |
| Mass spectrometric analysis .....                                  | 96         |
| Protein Modeling .....   | 99         |
| Conclusions.....   | 101        |
| References.....  | 103        |
| <b>CONCLUSIONS AND FUTURE DIRECTIONS.....</b>                      | <b>105</b> |
| References.....  | 110        |

## List of Figures

|  |    |
|--|----|
| Figure II.1 UV–visible absorption spectrum of pyruvate formate-lyase activating enzyme as isolated.....  | 37 |
| Figure II.2 X-band EPR spectra of pyruvate formate-lyase-activating enzyme as a function of temperature.....   | 38 |
| Figure II.3 Mössbauer spectra of anaerobically purified native PFL-AE.....   | 40 |
| Figure II.4 Mössbauer spectrum of dithionite-reduced native PFL-AE recorded at 4.2 K in a magnetic field of 0.05 T applied parallel to the $\gamma$ -beam..... | 46 |
| Figure II.5 Mössbauer spectra of dithionite-reduced PFL-AE .....   | 47 |
| Figure II.6 EPR spectrum of dithionite-reduced PFL-AE showing a weak signal originating from the $[4\text{Fe-4S}]^+$ cluster.....                              | 48 |
| Figure III.1 Mossbauer spectra of $^{56}\text{Fe}$ PFL-AE reconstituted with $^{57}\text{Fe}$ and DTT in the absence (A) and presence (B) of AdoMet.....       | 59 |
| Figure IV.1 X-band EPR spectra of photoreduced PFL-AE before and after addition of PFL.....  | 69 |
| Figure IV.2 Spin quantitation of the EPR spectra shown in Figure IV.1A ( $[4\text{Fe-4S}]^{1+}$ ) and 1B (gly•) as a function of illumination time. ....       | 70 |
| Figure V.1 Release of ethanol-soluble material from methylated poly(dA) by AlkB in the presence of Fe(II) and $\alpha$ -ketoglutarate. ....                    | 80 |
| Figure V.2 Repair of 1-methyladenine (1-meA) and 3-methylcytosine (3-meC) by AlkB. ....  | 81 |

|   |     |
|---|-----|
| Figure V.3 Production of formaldehyde and consumption of O <sub>2</sub> by AlkB.....                | 85  |
| Figure VI.1 UV-visible spectroscopic analysis of the reaction of αKG-Fe(II)AlkB with<br>oxygen..... | 97  |
| Figure VI.2 LC/MS/MS identification of hydroxy-Trp 178 in AlkB. ....                                | 98  |
| Figure VI.3 Structure of AlkB determined by protein modeling.....                                   | 100 |

## List of Schemes

|   |    |
|---|----|
| Scheme I.1 Reaction catalyzed by PFL-AE and ARR-AE .....  | 3  |
| Scheme I.2 Activation of PFL.....   | 4  |
| Scheme I.3 Formation of an adenosyl adduct.....   | 4  |
| Scheme I.4 Structural comparison of AdoCbl and AdoMet.....  | 5  |
| Scheme I.5 Reaction catalyzed by lysine aminomutase .....   | 9  |
| Scheme I.6 Reaction catalyzed by BioB.....  | 11 |
| Scheme I.7 Proposed mechanism of spore photoproduct repair by SPL.....                              | 12 |
| Scheme I.8 Sites of Methylation in DNA .....  | 13 |
| Scheme I.9 1-methyladenosine and 3-methylcytosine.....  | 16 |
| Scheme I.10 Other Fe(II)/ $\alpha$ -KG catalyzed reactions .....                                    | 18 |
| Scheme I.11 Fe(II)/ $\alpha$ -KG Dioxygenase Mechanism .....  | 20 |
| Scheme I.12 Proposed Fe(II)/ $\alpha$ -KG dependent AlkB mechanism: “oxidative DNA repair”<br>..... | 22 |
| Scheme IV.1 Proposed redox role for the iron-sulfur cluster of PFL-AE .....                         | 66 |
| Scheme IV.2 Proposed Mechanism of PFL-AE .....  | 73 |
| Scheme V.1 Oxidative DNA repair mechanism catalyzed by AlkB .....                                   | 87 |

## List of Tables

|  |    |
|--|----|
| Temperature-Dependent Mössbauer Parameters of the Fe-S Clusters in Native PFL-AE . |    |
| .....  | 43 |

## List of Abbreviations

|              |  |
|--------------|--|
| $\alpha$ -KG | $\alpha$ -ketoglutarate                                  |
| BioB         | biotin synthase  |
| 1-meA        | 1-methyladenine  |
| 3-meC        | 3-methylcytosine   |
| 5'-dAdo      | 5'-deoxyadenosine  |
| AdoCbl       | adenosylcobalamin  |
| AdoMet       | S-adenosylmethionine                                     |
| CAS          | clavamate synthase                                       |
| CoA          | coenzyme-A   |
| DAOCS        | deacetoxycephalosporin C synthase                        |
| DMS          | dimethylsulfate  |
| DTT          | dithiothreitol   |
| EDTA         | ethylenediaminetetraacetic acid                          |
| ENDOR        | electron-nuclear double resonance                        |
| EPR          | electron paramagnetic resonance                          |
| FeS          | iron-sulfur cluster                                      |
| GC/MS        | gas chromatography/mass spectrometry                     |
| IPTG         | isopropyl- $\beta$ -D-thiogalactopyranoside              |
| LAM          | lysine aminomutase                                       |
| LB           | Luria Bertini media                                      |
| LMCT         | ligand to metal charge transfer transition               |
| MLCT         | metal to ligand charge transfer transition               |
| MMS          | methyl methanesulphonate                                 |
| MNNG         | N-methyl-N-nitro-N-nitroguanidine                        |
| NMNU         | N-methyl-N-nitrosourea                                   |
| PFL          | pyruvate formate-lyase                                   |
| PFL-AE       | pyruvate formate-lyase activating enzyme                 |
| PFPH         | pentafluorophenylhydrazine                               |
| RNR          | ribonucleotide reductase                                 |
| SDS-PAGE     | sodium dodecylsulfate polyacrylamine gel electrophoresis |
| TauD         | taurine/ $\alpha$ KG dioxygenase                         |
| TfdA         | 2,4-dichlorophenoxyacetic acid/ $\alpha$ KG dioxygenase  |
| Tris         | tris(hydroxymethyl)aminomethane                          |
| UV-vis       | ultraviolet-visible                                      |

# **CHAPTER I**

## **INTRODUCTION**

Many crucial biological processes require steps that involve single electron chemistry. This dissertation investigates two enzymes from *Escherichia coli* that catalyze reactions utilizing single electron chemistry. The first, pyruvate formate-lyase activating enzyme (PFL-AE, encoded by *pflA*) catalyzes the reductive cleavage of S-adenosylmethionine (AdoMet) to generate a carbon radical intermediate. The second, the gene product of *alkB*, is an iron and  $\alpha$ -ketoglutarate dependent dioxygenase that initiates the repair of alkylated DNA by a hydrogen atom abstraction step.

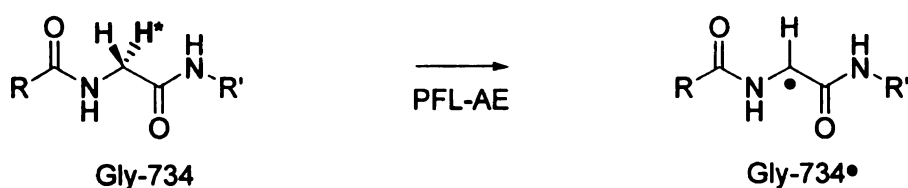
### **The Fe/S AdoMet enzymes**

The classical role of AdoMet in biological systems is that of a methylating agent, for example in the methylation of cytosine bases - a crucial mechanism of epigenetic regulation (1). In recent years, there has been an explosion of interest in AdoMet dependent enzymes that do not involve methylation (2). Rather, they utilize AdoMet and an iron-sulfur (FeS) cluster to generate substrate and enzyme-based radicals. The reactions accomplished by Fe-S/AdoMet enzymes include rearrangements, sulfur insertion, DNA repair, and glycy radical generation. I will describe the chemistry of several of these enzymes, focusing on exciting recent developments in the generation of 5'-deoxyadenosyl radicals and the fascinating ways in which they are employed.

#### *Pyruvate formate-lyase*

Pyruvate formate-lyase (PFL) catalyzes the first committed step in the anaerobic glucose catabolism by *Escherichia coli*; i.e. the reversible conversion of pyruvate and

coenzyme-A (CoA) to formate and acetyl-CoA . As isolated from aerobically growing cells, PFL is inactive and contains no metals or organic cofactors but the enzyme may be activated under strict anaerobic conditions. This activation is catalyzed by another enzyme, pyruvate formate-lyase activating enzyme, and involves the introduction of a glycy radical at Gly-734 (3-6)(Scheme 1). This radical is absolutely required for PFL activity and accounts for the extreme oxygen lability of the enzyme. Upon exposure to oxygen, the radical is irreversibly quenched and the peptide chain is cleaved at the radical site, leading to the formation of 3 kDa and 82 kDa protein fragments (4).

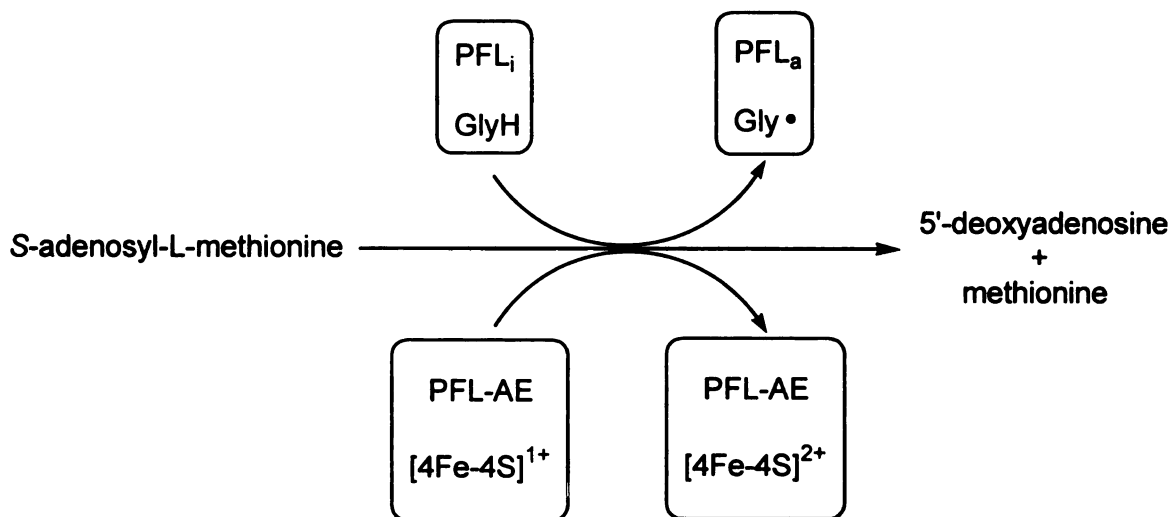


### **Scheme I.1 Reaction catalyzed by PFL-AE and ARR-AE**

The glycy radical does not directly participate in catalysis. Rather, the radical is transferred to one of two active site cysteine residue which attacks the carbonyl carbon of pyruvate, displacing formate and generating an acyl-enzyme intermediate.

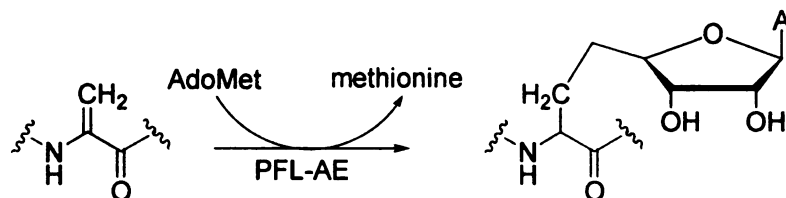
#### *Pyruvate formate-lyase activating enzyme*

The post-translational introduction of the glycy radical into PFL requires PFL-AE, AdoMet, and a source of electrons (Scheme I.2) (7). AdoMet is reductively cleaved to yield methionine and 5' deoxyadenosine (5'dAdo) (8).



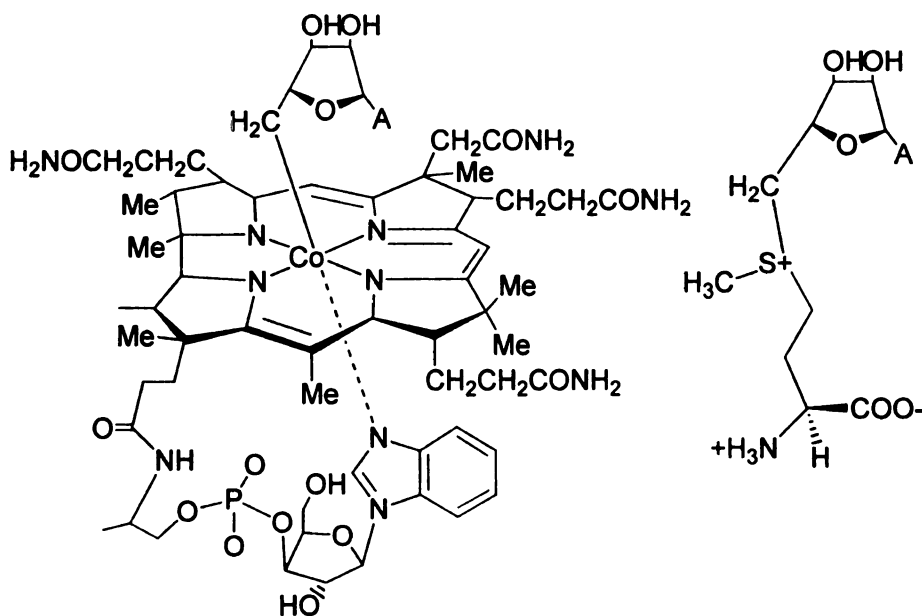
### Scheme I.2 Activation of PFL

In important early experiments, Knappe and coworkers labeled Gly-734 with deuterium and showed that the label was incorporated into 5'-deoxyadenosine, thus implicating a 5'-deoxyadenosyl radical as the hydrogen atom abstracting species (9). More recently, the same laboratory used a PFL peptide analog that contained dehydroalanine in place of Gly-734 as a substrate for PFL-AE (10). Using mass spectrometry, the authors characterized a 5'-deoxyadenosyl adduct of the peptide where the adenosyl moiety was linked to the  $\beta$ -carbon of the modified amino acid, thereby providing further evidence for the involvement of a 5'-deoxyadenosyl radical in the activation of PFL (10). (Scheme I.3)



### Scheme I.3 Formation of an adenosyl adduct

Deoxyadenosyl radicals had long been proposed as intermediates in adenosylcobalamin-dependent reactions, including rearrangements and nucleoside reduction. Enzymes generate 5'-deoxyadenosyl radicals from AdoCbl by destabilizing the weak carbon-cobalt bond and promoting its homolysis. AdoMet is a much simpler molecule with no metal cofactors (Scheme I.4) and it was unclear how a 5'-deoxyadenosyl radical might be generated, prompting Perry Frey to ask the question, "Is adenosylmethionine a poor man's adenosylcobalamin?" (11) A significant portion of this dissertation addresses that question. It is interesting to note that Professor Frey has changed his rhetoric regarding the radical generating role of AdoMet. Ten years after his previous query, he recently asked the question "S-adenosylmethionine: a wolf in sheep's clothing or a rich man's adenosylcobalamin" (2) as a reflection of the rapid pace of progress in this field.



**Scheme I.4 Structural comparison of AdoCbl and AdoMet**

Early evidence suggested that an organic cofactor (7) or mononuclear metal site (12) plays a role in PFL-AE catalyzed radical generation. The correct line of

investigation was found when an iron-sulfur cluster was identified in the enzyme (13). Broderick and coworkers used a combination of resonance Raman, ultraviolet-visible, and variable-temperature magnetic circular dichroism spectroscopies to identify a mixture of  $[4\text{Fe-4S}]^{2+}$  and  $[2\text{Fe-2S}]^{2+}$  clusters in the as-isolated enzyme. Reduction with dithionite yielded entirely cuboidal  $[4\text{Fe-4S}]$  clusters, with the more reduced and electron paramagnetic resonance active  $1+$  cluster oxidation state reached only in the presence of AdoMet (13).

Knappe and coworkers also identified an FeS cluster in PFL-AE that had been artificially reconstituted with iron and sulfide (14). They observed an axial EPR signal consistent with the presence of an  $[4\text{Fe-4S}]^{1+}$  cluster that underwent a shift to a rhombic signal upon AdoMet binding. Significantly, using site-directed mutagenesis, they identified three cysteine residues that were critical for cluster reconstitution and enzymatic activity.

The identification of an FeS cluster and the suggestion that AdoMet interacts with the cluster led to the proposal that the cluster could serve a redox role in the AE reaction (13). The cleavage of AdoMet to methionine and 5'-deoxyadenosine is a two-electron reduction. A hydrogen atom is abstracted from Gly-734, accounting for one electron. A reasonable proposal is that the cluster serves as the source of the additional electron, as shown in Scheme I.2. One aim of this dissertation is to test this mechanism and determine the active form of the cluster.

Another interesting question is the identity of the fourth ligand to the cluster. The C-X<sub>3</sub>-C-X<sub>2</sub>-C motif is conserved in all FeS/AdoMet enzymes (15). An interesting proposal is that AdoMet itself is the fourth ligand in the active form of the enzyme. The

observations that AdoMet seemed to alter the reduction potential or the anisotropy and the cluster electronic environment suggest an interaction between these species, but they do not necessarily indicate a direct interaction. A precise determination of the cluster/AdoMet interaction would greatly enhance our understanding of the mechanism of glycy radical generation.

### *Ribonucleotide reductase activating enzyme*

The reduction of ribonucleotides to deoxyribonucleotides is the rate-determining step in DNA synthesis (16). All three classes of ribonucleotide reductases utilize a radical mechanism in the reduction of the sugar, but vary in the mechanism by which the radical is generated. The class I enzymes use a diiron center and dioxygen as a radical generating mechanism. Class II enzymes use AdoCbl. Class III reductases function under anaerobic conditions and utilize AdoMet to generate a stable glycy radical in a manner directly analogous to the PFL system (Scheme I.1) (17-19). A small subunit, also termed the activating enzyme or  $\beta$  subunit, generates the radical that resides on Gly-681 of the larger or  $\alpha$  subunit. The glycy radical reacts with the active site cysteine that in turn abstracts a hydrogen atom from substrate to initiate reduction of the sugar at the 5'-carbon.

As in the case of the PFL system, AdoMet and a source of electrons is required to generate the glycy radical on the  $\alpha$  subunit (17). Like PFL-AE, the  $\beta$  subunit also contains a [4Fe-4S] cluster that can access both the 2+ and 1+ oxidation states (20, 21). Thus, it has been hypothesized that the [4Fe-4S]<sup>1+</sup> cluster provides the electron needed for the reductive cleavage of AdoMet, allowing subsequent activation of the

ribonucleotide reductase. Fontecave and coworkers correlated the production of methionine with the oxidation of the  $[4\text{Fe-4S}]^{1+}$  cluster and determined similar first order rate constants for both processes (22). They initially determined a stoichiometry of two methionines produced for each cluster oxidized, a ratio that is inconsistent with the reaction scheme. More recent work by the same lab has resolved the stoichiometry with regard to the activation, but they also observed reductive AdoMet cleavage catalyzed by the  $\beta$  subunit in the absence of the  $\alpha$  subunit (23). This side reaction produced two methionines for each cluster that was oxidized. An unprecedented mechanism was proposed that invokes a “hyper-reduced”  $[3\text{Fe-4S}]^{2-}$  cluster which could donate two electrons to reduce two equivalents of AdoMet, thus accounting for the observed methionine production. Experimental evidence to support this novel redox state has not been reported.

### *Lysine aminomutase*

Lysine 2,3-aminomutase (LAM) catalyzes the reversible conversion of L-lysine and L- $\beta$ -lysine, a reaction that is highly reminiscent of adenosylcobalamin dependent rearrangements (2)(Scheme I.5), but LAM activity is strictly dependent on AdoMet, not AdoCbl (24). When [*adenosyl-5'-<sup>3</sup>H]AdoMet is used, the radioactive label is incorporated into both L-lysine and L- $\beta$ -lysine (25). This result shows that AdoMet mediates hydrogen exchange in a manner directly analogous to the AdoCbl systems and strongly suggests that a 5'-deoxyadenosyl radical participates in this process.*



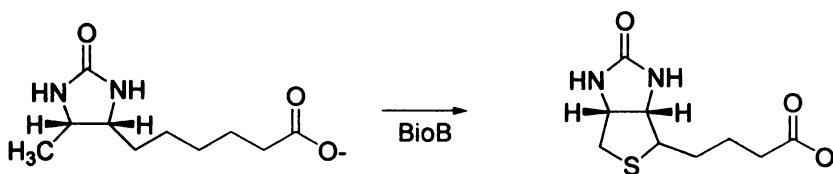
**Scheme I.5 Reaction catalyzed by lysine aminomutase**

Like other family members, LAM may accommodate a variety of cluster types. Of the various clusters and redox states that have been identified, Frey and coworkers have shown that the  $[4\text{Fe-4S}]^{1+}$  cluster participates in the catalytic cycle (26, 27). Recent creative work has provided the first direct spectroscopic evidence for a 5'-deoxyadenosyl radical in the AdoMet dependent systems. AnhydroAdoMet was used to stabilize and allow characterization of a 5'allylic radical in the LAM reaction (28, 29).

Recent work also has shed light on the interaction between AdoMet and the cluster in LAM (30). Frey and coworkers used selenoAdoMet (which contains selenium instead of sulfur) and were able to detect a Fe-Se interaction at 2.7 Å using X-ray absorption spectroscopy. This scattering was only observable in samples that contained the substrate analog *trans*-4,5-dehydrolysine, which traps the enzymatic reaction at an intermediate after cleavage of AdoMet. The new FT peak is then a reflection of methionine, a cleavage product of AdoMet, bound to the cluster (30). In addition to the information gained from X-ray spectroscopy, electron-nuclear double resonance (ENDOR) spectroscopy has been used to probe the interaction between AdoMet and the cluster (31). AdoMet was specifically labeled with <sup>17</sup>O at the carboxylate group and <sup>15</sup>N at the amino group. The results show that AdoMet chelates an iron of the cluster through the amino acid groups to form a five-membered ring. (Similar experiments have been done with the iron-sulfur cluster of PFL-AE and will be introduced in the final chapter (32, 33).)

*Sulfur insertion: BioB and LipA*

BioB catalyzes the insertion of a sulfur atom across two unactivated C-H bonds of dethiobiotin in the final biosynthetic step of biotin, an essential vitamin that is only produced by plants and certain microorganisms (for reviews see (2, 34)) (Scheme I.6). Like other family members, BioB is able to accommodate a wide variety of cluster types, however BioB binds two distinct clusters *simultaneously* (35). Jarrett and coworkers used specific  $^{57}\text{Fe}$  labeling and Mössbauer spectroscopy to identify two cluster types in BioB: a  $[\text{4Fe-4S}]^{2+}$  and a  $[\text{2Fe-2S}]^{2+}$  cluster (36). In addition, they were able to show that the  $[\text{2Fe-2S}]$  cluster was degraded during turnover while the  $[\text{4Fe-4S}]$  cluster remained intact (37). From these results they postulate that the  $[\text{2Fe-2S}]$  cluster serves as the sulfur source for the reaction, while the  $[\text{4Fe-4S}]$  cluster catalyzed the reductive cleavage of AdoMet to generate 5'-deoxyadenosyl radicals that activate the C-H bonds of dethiobiotin. The Fontecave group has detected a PLP-dependent cysteine desulfurase activity catalyzed by BioB and has shown that this activity is dependent on two (non-cluster ligand) cysteine residues (38). They postulate that the cysteine-derived sulfide forms a persulfide at the required cysteines and is then incorporated into dethiobiotin. It is possible that the results of both groups are correct and self-consistent. If the  $[\text{2Fe-2S}]$  cluster is degraded during turnover to provide the sulfur source, a regeneration mechanism (perhaps in the form of a cysteine desulfurase activity) would allow for multiple turnovers, a feat that has not yet been detected *in vitro*.



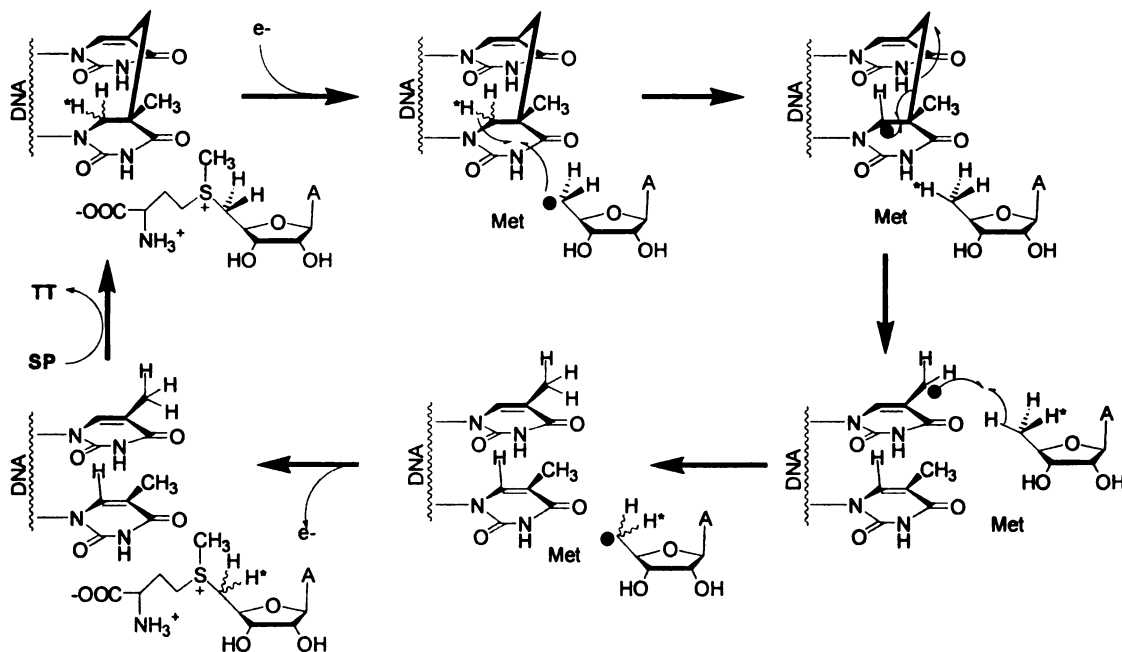
**Scheme I.6 Reaction catalyzed by BioB**

Recent exciting results include the determination of the crystal structures of BioB (39) and HemN (40), another FeS/AdoMet enzyme. These will be discussed in the context of the results presented in this dissertation in Chapters IV and VII.

#### *Spore photoproduct lyase*

In addition to the reactions already discussed, Fe/S/AdoMet enzymes also participate in DNA repair. Spores of *Bacillus subtilis* form specific thiamine dimers upon exposure to UV radiation, which are repaired by the spore photoproduct lyase (SPL) in a reaction that is dependent on AdoMet (41-43). (Scheme I.7). A [4Fe-4S] cluster has been identified in SPL and it has been reported that AdoMet undergoes reductive cleavage to methionine and 5'-deoxyadenosine (44). In contrast, later experiments have demonstrated that AdoMet functions as a cofactor rather than a cosubstrate in SPL (45). Cheek and Broderick generated photoproduct-containing DNA that was labeled with tritium at either the C-6 or methyl positions. When substrate was labeled at C-6, significant radioactivity was incorporated into AdoMet, but not when substrate was labeled at the methyl group (45). The results support the mechanism first suggested by Mehl and Begley (46) as shown in Scheme I.7. AdoMet is reduced by the Fe/S cluster to generate a 5'dAdo radical which abstracts a hydrogen atom from C-6 of the photoproduct

dimer. The substrate radical then undergoes  $\beta$ -scission and the abstracts a hydrogen atom from 5'dAdo to regenerate the 5'dAdo radical which recombined with methionine to regenerate AdoMet.



**Scheme I.7 Proposed mechanism of spore photoproduct repair by SPL**

Reflecting the diversity of chemistry that has already been demonstrated, Sophia *et al.* used PSI-BLAST and other bioinformatic tools to identify over 500 unique sequences that are thought to encode FeS/AdoMet enzymes (15). Some of the enzymes they identified had been characterized by biochemical methods, but most had not yet been identified as members of the FeS/AdoMet family.

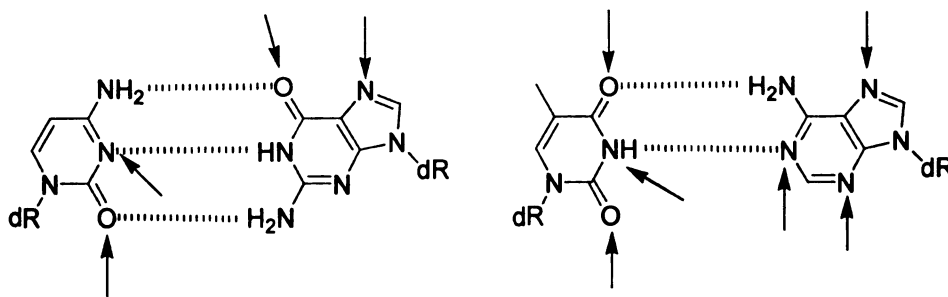
### DNA repair and Fe(II)/ $\alpha$ -ketoglutarate dioxygenases

DNA is constantly under attack. The molecule that carries our genetic information can be damaged or modified by oxidation, radiation, or toxins, as well as by

some endogenous biomolecules (47). To counter this constant threat to the security of the genetic information, elaborate and diverse mechanisms have evolved to reverse the DNA damage. Three general strategies for DNA repair are base excision, nucleotide excision, or direct repair. In base excision repair, the glycosidic bond is hydrolyzed by a glycosylase, removing the nucleoside base and resulting in an abasic site. Specialized endonucleases then must remove the remaining sugar phosphate and a DNA polymerase fills in the resulting gap. In nucleotide excision repair, a variable DNA segment that contains the lesion is removed and replaced.

#### *The Adaptive response to alkylating agents*

Alkylating agents are a broad class of toxins that have been shown to target DNA and other biomolecules. These methylating agents have been broadly separated into  $S_N1$  and the  $S_N2$  categories, based on the mechanism of nucleophilic substitution reaction they employ to alkylate the DNA base. As shown in Scheme I.8, a plethora of sites in the four bases are subject to damage from of methylating agents (48).



**Scheme I.8 Sites of Methylation in DNA**

*Escherichia coli* has developed an elegant response to the stress caused by exposure to alkylating agents that is described as both the “adaptive response to alkylating agents” and the “Ada response,” and includes four genes: *ada*, *alkB*, *alkA*, and *aidB*. The proteins encoded by these genes serve differing roles that all seem to protect the cell from acute exposure to alkylating agents.

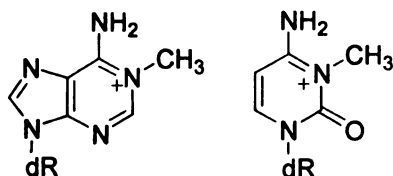
Ada is a fascinating trifunctional protein. It activates the transcription of the adaptive response and also repairs two types alkylated DNA lesions. The C-terminal domain is responsible for one type of DNA repair activity. Alkyl groups from the mutagenic lesions 6-methylguanine and 4-methylthymine are directly transferred to a specific nucleophilic cysteine residue (Cys-321) (49). After completing one DNA repair turnover the C-terminal domain is rendered inactive and *de novo* protein synthesis is required to provide additional resistance. The N-terminal domain of Ada similarly exhibits methyltransferase activity, but also serves as the transcriptional regulator of the adaptive response. A methyl group from the phosphotriester backbone is transferred to Cys-38, made possible by the coordination of a  $Zn^{2+}$  ion which enhances the nucleophilicity of the cysteine thiol (50, 51). Upon methylation of the N-terminal domain, the binding of Ada to the promoter regions of the *ada-alkB* operon and the *alkA* and *aidB* genes is enhanced, thus promoting expression of the adaptive response.

AlkA was quickly identified as a 3-methyladenosine glycosylase (52, 53). The function of AidB remains a mystery, but it may function by metabolizing  $S_N1$  alkylating agents, decomposing modified nucleotide precursors, or reversing damage to DNA . These hypotheses are currently being tested in our lab. It is interesting that in addition to these activities encoded to genes in the Ada response, *E. coli* has alkylation defense genes

that are constitutively expressed, suggesting that the cells are exposed to alkylating agents in both persistent and acute mechanisms. For example, *ogt* encodes a O<sup>6</sup>-methylguanine methyltransferase (54) and *tag* encodes a 3-methyladenosine glycosylase (55).

The protein encoded by *alkB* has been an enigma for two decades. In 1983 *alkB* mutants were isolated that were defective in their ability to reactivate methyl methanesulfonate-treated lambda phage (56). The gene was cloned (57) and the protein was purified without clarification of its role (58). AlkB was shown to protect cells from the toxic effects of the S<sub>N</sub>2 alkylating agents dimethylsulfate (DMS) and methyl iodide (MeI), but is less effective in protection against the S<sub>N</sub>1 reagents *N*-methyl-*N*-nitro-*N*-nitroguanidine (MNNG) and *N*-methyl-*N*-nitrosourea (NMNU). AlkB mutants are not defective in repairing 3-methyladenine, DNA strand breaks, abasic sites, and other lesions that may arise at abasic sites such as DNA–protein cross-links and DNA interstrand cross-links (59). Expression of the *E. coli* gene in human cells afforded similar resistance to alkylating agents, suggesting that AlkB functioned in the absence of other factors (60). A major piece of the AlkB puzzle was put in place when Sedgewick and coworkers found that *alkB* mutants were defective in reactivating single-stranded lambda phage that had been treated with S<sub>N</sub>2 alkylating agents (61). There was very little defect in the mutants' ability to reactivate double stranded phage that had been treated in the same manner, and the effect of S<sub>N</sub>2 methylating agents was much greater than that of S<sub>N</sub>1 agents. These results strongly suggest that AlkB repairs DNA lesions created in single stranded DNA. This may be because AlkB shows preference toward single-stranded substrate or it may repair lesions that are formed more readily in single- rather

than double-stranded DNA. Two prospective lesions that are formed primarily in single-stranded DNA were identified as potential substrates: 1-methyladenosine and 3-methylcytosine (Scheme I.9) (48, 61). The nitrogens that are methylated in these lesions are protected by Watson-Crick base pairing in double-stranded DNA.



**Scheme I.9 1-methyladenosine and 3-methylcytosine**

Recent *in silico* work also has contributed to our understanding of AlkB. Aravinid and Koonin used structural prediction tools to show that that AlkB likely adopts a fold that is characteristic of  $\alpha$ -ketoglutarate and iron dependent dioxygenases (62).

#### *Fe(II)/ $\alpha$ -ketoglutarate Dioxygenases*

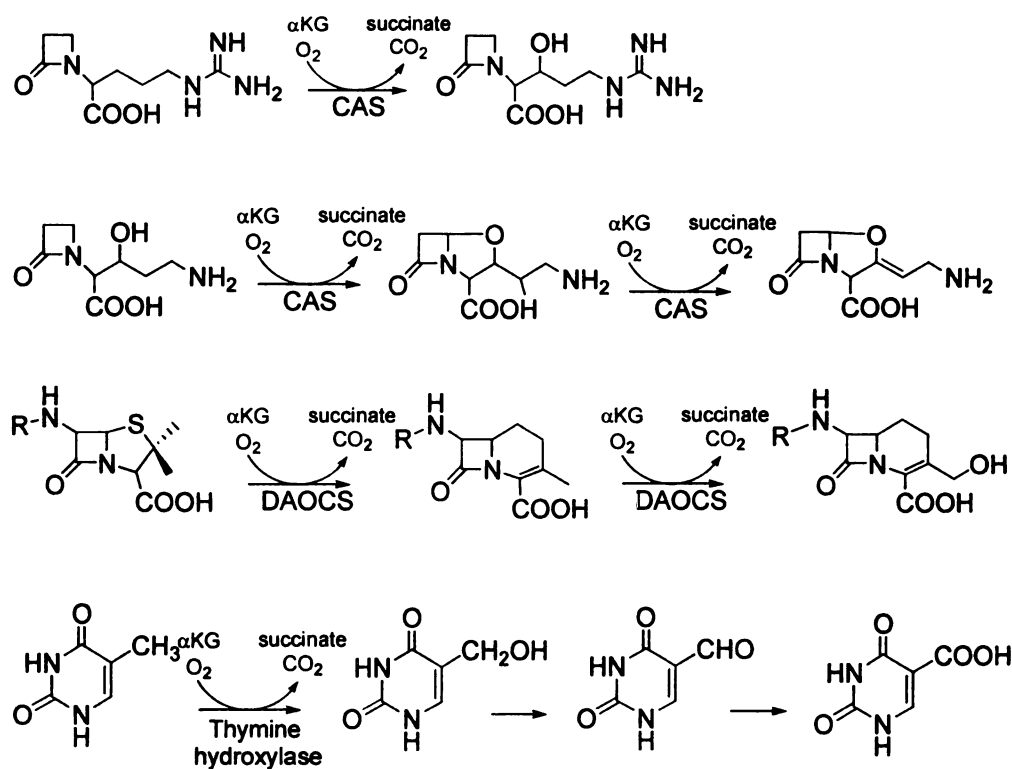
The enzymes that make up the iron and  $\alpha$ -ketoglutarate (Fe(II)/ $\alpha$ KG) dependent dioxygenase superfamily catalyze a wide variety of oxidations. Each enzyme couples the reduction of dioxygen to the oxidative decarboxylation of  $\alpha$ -ketoglutarate to generate high-valent iron-oxo intermediates that are responsible for the oxidation of the primary substrate. The following paragraphs briefly summarize the critical features of this enzyme family before returning to AlkB.

## *Amino Acid Hydroxylases*

Prolyl 4-hydroxylase, a representative Fe(II)/ $\alpha$ -KG dioxygenase, catalyzes the hydroxylation of proline within many structural and transcriptional proteins. In type I collagen, these hydroxylated proline residues stabilize the triple helical structure of the protein, accounting for its structural elasticity (63). Although studied for decades, interest in this sidechain hydroxylase has intensified with the discovery that the hypoxia response is regulated by an Fe(II)/ $\alpha$ -KG dioxygenase. The hypoxia inducible factor is a dimeric (HIF $\alpha$  and HIF $\beta$ ) transcription factor that is constitutively expressed and activates the transcription of a variety of genes (reviewed in (64)). Under normal oxygen conditions, Pro-564 of HIF $\alpha$  is hydroxylated by a prolyl 4-hydroxylase, targeting the transcription factor for ubiquitinylation and degradation, thus suppressing transcription (65-68). In an additional mechanism, hydroxylation of Asn 803 of HIF $\alpha$  prevents its interaction with p300, a coactivator that is required for HIF-dependent transcriptional activation. The enzyme responsible for this hydroxylation has been identified as an  $\alpha$ -KG dioxygenase (69). The medical significance in these systems is noteworthy, as hypoxia plays a significant role in a variety of disease processes, including tumor growth, diabetes, and other ischemic diseases (64).

Although the work presented in Chapters V and VI concerns an  $\alpha$ -KG dependent hydroxylase, other Fe(II)/ $\alpha$ -KG family members catalyze remarkably varied chemistry. For example, clavamate synthase (CAS) catalyzes three oxidative steps in the synthesis of clavulanic acid: a hydroxylation, an oxidative ring closure, and a desaturation, all of which consume O<sub>2</sub> and  $\alpha$ -KG (Scheme I.10) (70). Deacetoxycephalosporin C synthase (DAOCS) catalyzes both a ring expansion and a hydroxylation (Scheme I.10) (71-73).

Thymine hydroxylase catalyzes three successive oxidations of the methyl group of thymine, from the alcohol to the aldehyde to the acid (Scheme I.10) (74).



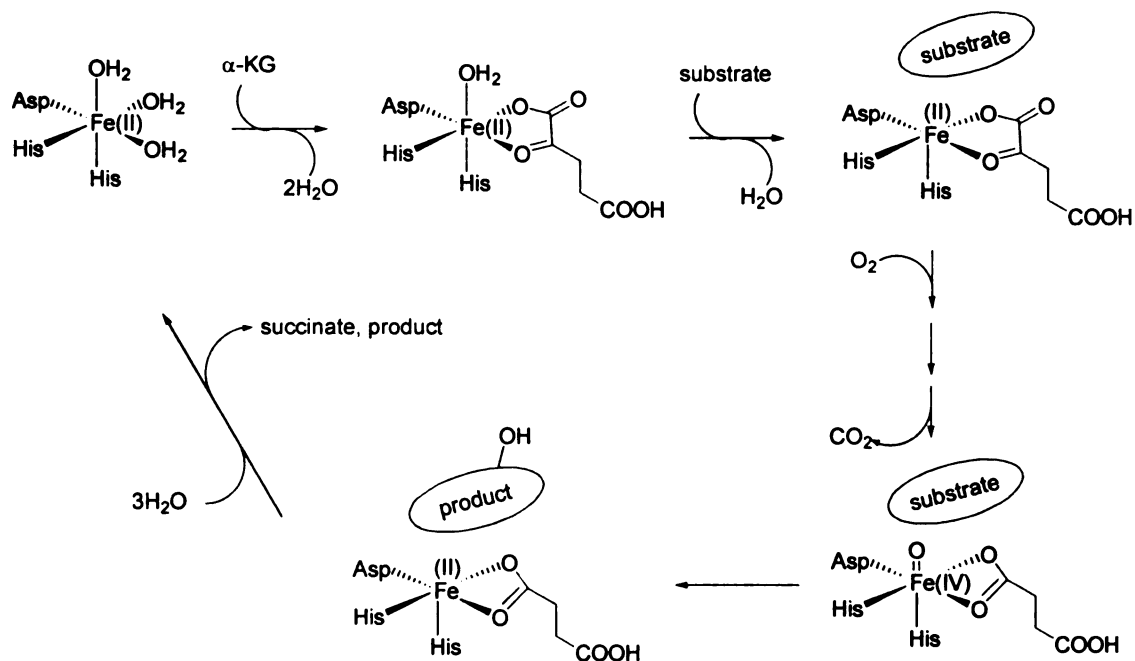
### Scheme I.10 Other Fe(II)/ $\alpha$ -KG catalyzed reactions

#### *Fe(II)/ $\alpha$ -KG Dioxygenase Mechanism*

An abundance of spectroscopic, structural and kinetic studies have dramatically improved our understanding of these enzymes in recent years (for reviews see (75, 76)) and have unveiled a number of reoccurring themes. From structural and spectroscopic studies, a clear picture of the first few steps of the catalytic cycle is clear (Scheme I.11). In the resting state of the enzyme, the Fe(II) is coordinated by two histidines and one acidic residue, and the remaining three sites in the distorted octahedral environment are

occupied by water.  $\alpha$ -Ketoglutarate chelates the iron through the C-1 carboxylate and C-2 ketone oxygens, displacing two waters, while the water in the sixth coordination site remains bound. The primary substrate binds to the enzyme, but not directly to the iron, causing a shift in the coordination environment as water disassociates, thus opening a coordination site for oxygen binding and activation. This communication via the protein matrix serves a critical regulatory role, since initiation of oxidative chemistry in the absence of primary substrate is destructive to the enzyme (77, 78) (Chapter VI).

Significant strides have been made towards understanding the later steps of the cycle, although some steps remain uncertain. Oxygen binds to the iron, most likely at the open coordination site, and may be reduced to either the superoxo or peroxy state. The oxygen then attacks the carbonyl carbon of  $\alpha$ -KG to yield an alkylperoxy intermediate which decomposes to release  $\text{CO}_2$  and generate an Fe(IV)-oxo intermediate. This high-valent iron species abstracts a hydrogen atom from the substrate, resulting in an Fe(III)-hydroxide and a substrate radical. Recombination of the substrate radical with the hydroxide restores the Fe(II) state of the enzyme and results in the hydroxylated substrate.



**Scheme I.11 Fe(II)/ $\alpha$ -KG Dioxygenase Mechanism**

### *Non-heme Models*

The inorganic community has provided model systems that mimic the coordination environment and reactivity of Fe(II)/ $\alpha$ -KG dioxygenases. Specifically, Que and coworkers have demonstrated ligand hydroxylation in an Fe(II)/ $\alpha$ -keto acid complex upon exposure to dioxygen, an activity that directly mimics the  $\alpha$ -KG hydroxylases (79). An exciting recent result is the crystallographic characterization of an Fe(IV)-oxo complex in a non-heme mononuclear environment (80). This proves that the long-postulated high valent intermediate is a viable possibility and provides an important spectroscopic point of reference for comparison to enzyme systems.

### *Identification of an Fe(IV)=O Intermediate*

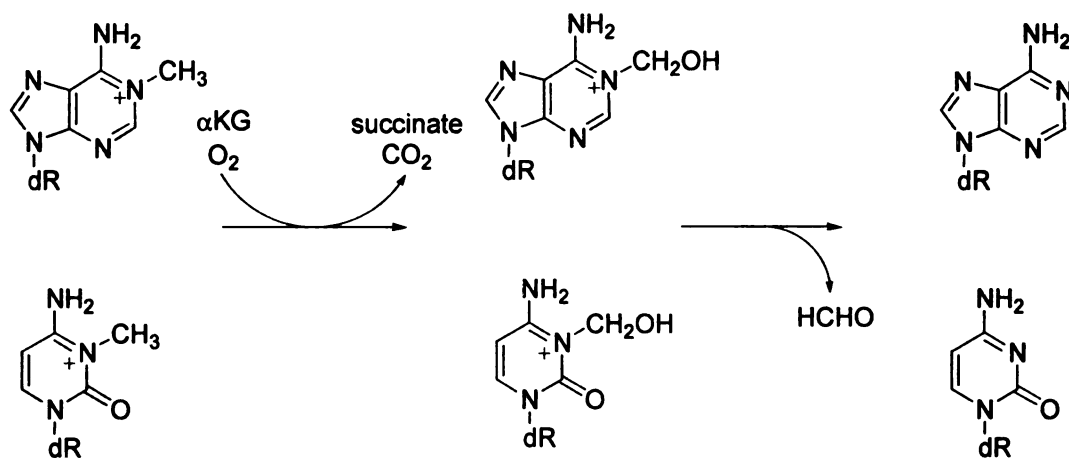
A likely Fe(IV) intermediate has also been identified in the cycle catalyzed by TauD. Bollinger, Krebs and coworkers used freeze-quench techniques to trap

intermediates and characterized them by Mössbauer and EPR spectroscopies (81). The Mössbauer parameters were consistent with a formal Fe(IV) oxidation state. The intermediate exhibited an integer spin state with  $S \geq 2$  and cryoreduction by gamma irradiation led to an EPR signal typical of a high-spin Fe(III)  $S = 5/2$  ground state. Taken together, these data provide strong evidence for the participation of an Fe(IV) intermediate. In an additional report, the same researchers determined that the rate of decay of this intermediate exhibits a 37-fold decrease when deuterated taurine is used (82). This substantial kinetic isotope effect indicates that the Fe(IV) intermediate is responsible for direct hydrogen atom abstraction from the primary substrate.

In a crucial extension of this work, our laboratory has used isotope difference time-resolved electronic absorption and resonance Raman (rR) spectroscopy to probe the nature of this intermediate (83). The experimental apparatus used a continuous flow technique that allows rR excitement at a selected delay time. When the chromophore associated with the Fe(IV) intermediate is excited, the dominant oxygen dependent mode is observed at  $821 \text{ cm}^{-1}$  and shifts to  $787 \text{ cm}^{-1}$  when  $^{18}\text{O}_2$  is used in place of  $^{16}\text{O}_2$ . The position and isotope shift of this mode compares favorably with the well characterized Fe(IV)-oxo intermediate in heme oxygenases. We conclude that this mode most likely arises from the symmetric stretch of a formally Fe(IV)-oxo intermediate which abstracts a hydrogen atom from taurine. Additional modes were identified at  $555 \text{ cm}^{-1}$  and  $859 \text{ cm}^{-1}$  which were not assigned, but could arise from either a Fe(II)- $\text{O}_2$  or Fe(III)-superoxo, intermediates that are proposed to precede formation of the Fe(IV)-oxo. Experiments to discriminate among these possibilities are currently in progress.

## *AlkB as an Fe(II)/ $\alpha$ -ketoglutarate Dioxygenase*

The observation that AlkB repairs methylated lesions in DNA and the possibility that it may adopt the fold of an Fe(II)/ $\alpha$ -KG dioxygenase led us to hypothesize that it may repair methylated DNA by hydroxylating the aberrant methyl group (Scheme I.12). This hydroxymethyl intermediate would spontaneously decompose to yield formaldehyde and the unmodified base in an oxidative N-demethylation mechanism. If correct, this mechanism would explain the experimental observations that had been obtained over two decades. Such a mechanism has precedent in heme systems and would account for previous unsuccessful attempts to identify an enzymatic activity for AlkB, as iron and  $\alpha$ -ketoglutarate are not common additions to enzyme activity screens. In fact, such a mechanism would be anathema to the DNA repair community, as one most often thinks of “oxidative DNA *damage*,” not “oxidative DNA *repair*.” Chapter V presents experiments designed to test this mechanism.



**Scheme I.12 Proposed Fe(II)/ $\alpha$ -KG dependent AlkB mechanism: “oxidative DNA repair”**

## References

1. Bird, A., *Genes Dev*, **2002**, *16*, 6-21.
2. Frey, P. A. and Magnusson, O. T., *Chemical Reviews*, **2003**, *103*, 2129-2148.
3. Knappe, J., Schacht, J., Mockel, W., Hopner, T., Vetter, H., Jr., and Edenharder, R., *Eur J Biochem*, **1969**, *11*, 316-27.
4. Wagner, A. F. V., Frey, M., Neugebauer, F. A., Schafer, W., and Knappe, J., *Proceedings of the National Academy of Sciences of the United States of America*, **1992**, *89*, 996-1000.
5. Knappe, J., Neugebauer, F. A., Blaschkowski, H. P., and Ganzler, M., *Proceedings of the National Academy of Sciences of the United States of America-Biological Sciences*, **1984**, *81*, 1332-1335.
6. Unkrig, V., Neugebauer, F. A., and Knappe, J., *European Journal of Biochemistry*, **1989**, *184*, 723-728.
7. Conradt, H., Hohmannberger, M., Hohmann, H. P., Blaschkowski, H. P., and Knappe, J., *Archives of Biochemistry and Biophysics*, **1984**, *228*, 133-142.
8. Knappe, J. and Schmitt, T., *Biochemical and Biophysical Research Communications*, **1976**, *71*, 1110-1117.
9. Frey, M., Rothe, M., Wagner, A. F. V., and Knappe, J., *Journal of Biological Chemistry*, **1994**, *269*, 12432-12437.
10. Wagner, A. F. V., Demand, J., Schilling, G., Pils, T., and Knappe, J., *Biochemical and Biophysical Research Communications*, **1999**, *254*, 306-310.
11. Frey, P. A., *Faseb Journal*, **1993**, *7*, 662-670.
12. Wong, K. K., Murray, B. W., Lewisch, S. A., Baxter, M. K., Ridky, T. W., Ulissidemario, L., and Kozarich, J. W., *Biochemistry*, **1993**, *32*, 14102-14110.
13. Broderick, J. B., Duderstadt, R. E., Fernandez, D. C., Wojtuszewski, K., Henshaw, T. F., and Johnson, M. K., *Journal of the American Chemical Society*, **1997**, *119*, 7396-7397.
14. Kulzer, R., Pils, T., Kappl, R., Huttermann, J., and Knappe, J., *Journal of Biological Chemistry*, **1998**, *273*, 4897-4903.

15. Sofia, H. J., Chen, G., Hetzler, B. G., Reyes-Spindola, J. F., and Miller, N. E., *Nucleic Acids Res*, **2001**, *29*, 1097-106.
16. Stubbe, J. and van der Donk, W. A., *Chemical Reviews*, **1998**, *98*, 705-762.
17. Harder, J., Eliasson, R., Pontis, E., Ballinger, M. D., and Reichard, P., *Journal of Biological Chemistry*, **1992**, *267*, 25548-25552.
18. Bianchi, V., Eliasson, R., Fontecave, M., Mulliez, E., Hoover, D. M., Matthews, R. G., and Reichard, P., *Biochemical and Biophysical Research Communications*, **1993**, *197*, 792-797.
19. Sun, X., Eliasson, R., Pontis, E., Andersson, J., Buist, G., Sjöberg, B.-M., and Reichard, P., *J. Biol. Chem.*, **1995**, *270*, 2443-2446.
20. Mulliez, E., Fontecave, M., Gaillard, J., and Reichard, P., *Journal of Biological Chemistry*, **1993**, *268*, 2296-2299.
21. Ollagnier, S., Mulliez, E., Gaillard, J., Eliasson, R., Fontecave, M., and Reichard, P., *Journal of Biological Chemistry*, **1996**, *271*, 9410-9416.
22. Ollagnier, S., Mulliez, E., Schmidt, P. P., Eliasson, R., Gaillard, J., Deronzier, C., Bergman, T., Graslund, A., Reichard, P., and Fontecave, M., *Journal of Biological Chemistry*, **1997**, *272*, 24216-24223.
23. Padovani, D., Thomas, F., Trautwein, A. X., Mulliez, E., and Fontecave, M., *Biochemistry*, **2001**, *40*, 6713-6719.
24. Chirpich, T. P., Zappia, V., Costilow, R. N., and Barker, H. A., *J. Biol. Chem.*, **1970**, *245*, 1778-1789.
25. Moss, M. and Frey, P. A., *Journal of Biological Chemistry*, **1987**, *262*, 14859-14862.
26. Petrovich, R. M., Ruzicka, F. J., Reed, G. H., and Frey, P. A., *Biochemistry*, **1992**, *31*, 10774-10781.
27. Lieder, K. W., Booker, S., Ruzicka, F. J., Beinert, H., Reed, G. H., and Frey, P. A., *Biochemistry*, **1998**, *37*, 2578-2585.
28. Magnusson, O. T., Reed, G. H., and Frey, P. A., *Journal of the American Chemical Society*, **1999**, *121*, 9764-9765.
29. Magnusson, O. T., Reed, G. H., and Frey, P. A., *Biochemistry*, **2001**, *40*, 7773-7782.
30. Cospers, N. J., Booker, S. J., Ruzicka, F., Frey, P. A., and Scott, R. A., *Biochemistry*, **2000**, *39*, 15668-15673.

31. Chen, D. W., Walsby, C., Hoffman, B. M., and Frey, P. A., *Journal of the American Chemical Society*, **2003**, *125*, 11788-11789.
32. Walsby, C. J., Hong, W., Broderick, W. E., Cheek, J., Ortillo, D., Broderick, J. B., and Hoffman, B. M., *Journal of the American Chemical Society*, **2002**, *124*, 3143-3151.
33. Walsby, C. J., Ortillo, D., Broderick, W. E., Broderick, J. B., and Hoffman, B. M., *Journal of the American Chemical Society*, **2002**, *124*, 11270-11271.
34. Fontecave, M., Ollagnier-de-Choudens, S., and Mulliez, E., *Chem Rev*, **2003**, *103*, 2149-66.
35. Ugulava, N. B., Gibney, B. R., and Jarrett, J. T., *Biochemistry*, **2001**, *40*, 8343-51.
36. Ugulava, N. B., Surerus, K. K., and Jarrett, J. T., *J Am Chem Soc*, **2002**, *124*, 9050-1.
37. Ugulava, N. B., Sacanell, C. J., and Jarrett, J. T., *Biochemistry*, **2001**, *40*, 8352-8.
38. Ollagnier-De-Choudens, S., Mulliez, E., Hewitson, K. S., and Fontecave, M., *Biochemistry*, **2002**, *41*, 9145-52.
39. Berkovitch, F., Nicolet, Y., Wan, J. T., Jarrett, J. T., and Drennan, C. L., *Science*, **2004**, *303*, 76-9.
40. Layer, G., Moser, J., Heinz, D. W., Jahn, D., and Schubert, W. D., *Embo J*, **2003**, *22*, 6214-24.
41. Varghese, A. J., *Biochemical and Biophysical Research Communications*, **1970**, *38*, 484-&.
42. Munakata, N. and Rupert, C. S., *Molecular & General Genetics*, **1974**, *130*, 239-250.
43. Rebeil, R., Sun, Y. B., Chooback, L., Pedraza-Reyes, M., Kinsland, C., Begley, T. P., and Nicholson, W. L., *Journal of Bacteriology*, **1998**, *180*, 4879-4885.
44. Rebeil, R. and Nicholson, W. L., *Proceedings of the National Academy of Sciences of the United States of America*, **2001**, *98*, 9038-9043.
45. Cheek, J. and Broderick, J. B., *J Am Chem Soc*, **2002**, *124*, 2860-1.
46. Mehl, R. A. and Begley, T. P., *Organic Letters*, **1999**, *1*, 1065-1066.
47. Wood RD, M. M., Sgouros J, Lindahl T, *Science*, **2001**, *291*, 1284-1289.

48. Singer, B. and D., G., *Molecular Biology of Mutagens and Carcinogens: Reactions of Directly Acting Agents with Nucleic Acids*. 1983, New York: Plenum Press.
49. Demple, B., Sedgwick, B., Robins, P., Totty, N., Waterfield, M. D., and Lindahl, T., *Proc Natl Acad Sci U S A*, **1985**, *82*, 2688-92.
50. He, C., Wei, H., and Verdine, G. L., *J Am Chem Soc*, **2003**, *125*, 1450-1.
51. Sedgwick, B., Robins, P., Totty, N., and Lindahl, T., *J Biol Chem*, **1988**, *263*, 4430-3.
52. Nakabeppu, Y., Kondo, H., and Sekiguchi, M., *J Biol Chem*, **1984**, *259*, 13723-9.
53. Nakabeppu, Y., Miyata, T., Kondo, H., Iwanaga, S., and Sekiguchi, M., *J Biol Chem*, **1984**, *259*, 13730-6.
54. Margison, G. P., Cooper, D. P., and Potter, P. M., *Mutat Res*, **1990**, *233*, 15-21.
55. Steinum, A. L. and Seeberg, E., *Nucleic Acids Res*, **1986**, *14*, 3763-72.
56. Kataoka, H., Yamamoto, Y., and Sekiguchi, M., *Journal of Bacteriology*, **1983**, *153*, 1301-1307.
57. Kataoka, H. and Sekiguchi, M., *Molecular and General Genetics*, **1985**, *198*, 263-269.
58. Kondo, H., Nakabeppu, Y., Kataoka, H., Kuhara, S., Kawabata, S., and Sekiguchi, M., *Journal of Biological Chemistry*, **1986**, *261*, 15772-15777.
59. Dinglay, S., Gold, B., and Sedgwick, B., *Mutation Research-DNA Repair*, **1998**, *407*, 109-116.
60. Chen, B. R. J., Carroll, P., and Samson, L., *Journal of Bacteriology*, **1994**, *176*, 6255-6261.
61. Dinglay, S., Trewick, S. C., Lindahl, T., and Sedgwick, B., *Genes & Development*, **2000**, *14*, 2097-2105.
62. Aravind, L. and Koonin, E. V., *Genome Biol*, **2001**, *2*, RESEARCH0007.
63. Kivirikko, K. I. and Pihlajaniemi, T., *Adv Enzymol Relat Areas Mol Biol*, **1998**, *72*, 325-98.
64. Hewitson, K. S., McNeill, L. A., and Schofield, C. J., *Current Pharmaceutical Design*, **2004**, *10*, 821-833.
65. Bruick, R. K. and McKnight, S. L., *Science*, **2001**, *294*, 1337-1340.

66. Epstein, A. C. R., Gleadle, J. M., McNeill, L. A., Hewitson, K. S., O'Rourke, J., Mole, D. R., Mukherji, M., Metzen, E., Wilson, M. I., Dhanda, A., Tian, Y. M., Masson, N., Hamilton, D. L., Jaakkola, P., Barstead, R., Hodgkin, J., Maxwell, P. H., Pugh, C. W., Schofield, C. J., and Ratcliffe, P. J., *Cell*, **2001**, *107*, 43-54.
67. Ivan, M., Kondo, K., Yang, H. F., Kim, W., Valiando, J., Ohh, M., Salic, A., Asara, J. M., Lane, W. S., and Kaelin, W. G., *Science*, **2001**, *292*, 464-468.
68. Jaakkola, P., Mole, D. R., Tian, Y. M., Wilson, M. I., Gielbert, J., Gaskell, S. J., von Kriegsheim, A., Hebestreit, H. F., Mukherji, M., Schofield, C. J., Maxwell, P. H., Pugh, C. W., and Ratcliffe, P. J., *Science*, **2001**, *292*, 468-472.
69. Hewitson, K. S., McNeill, L. A., Riordan, M. V., Tian, Y. M., Bullock, A. N., Welford, R. W., Elkins, J. M., Oldham, N. J., Bhattacharya, S., Gleadle, J. M., Ratcliffe, P. J., Pugh, C. W., and Schofield, C. J., *Journal of Biological Chemistry*, **2002**, *277*, 26351-26355.
70. Lloyd, M. D., Merritt, K. D., Lee, V., Sewell, T. J., Wha-Son, B., Baldwin, J. E., Schofield, C. J., Elson, S. W., Baggaley, K. H., and Nicholson, N. H., *Tetrahedron*, **1999**, *55*, 10201-10220.
71. Dotzlaf, J. E. and Yeh, W.-K., *Journal of Bacteriology*, **1987**, *169*, 1611-1618.
72. Baldwin, J. E., Adlington, R. M., Coates, J. B., Crabbe, M. J. C., Crouch, N. P., Keeping, J. W., Knight, G. C., Schofield, C. J., Ting, H. H., Vallejo, C. A., Thorniley, M., and Abraham, E. P., *Biochemical Journal*, **1987**, *245*, 831-841.
73. Samson, S. M., Belagaje, R., Blankenship, D. T., Chapman, J. L., Perry, D., Skatrud, P. L., Vanfrank, R. M., Abraham, E. P., Baldwin, J. E., Queener, S. W., and Ingolia, T. D., *Nature*, **1985**, *318*, 191-194.
74. Thornburg, L. D., Lai, M. T., Wishnok, J. S., and Stubbe, J., *Biochemistry*, **1993**, *32*, 14023-33.
75. Solomon, E. I., Brunold, T. C., Davis, M. I., Kemsley, J. N., Lee, S. K., Lehnert, N., Neese, F., Skulan, A. J., Yang, Y. S., and Zhou, J., *Chemical Reviews*, **2000**, *100*, 235-349.
76. Hausinger, R. P., *Crit Rev Biochem Mol Biol*, **2004**, *39*, 21-68.
77. Ryle, M. J., Liu, A., Muthukumaran, R. B., Ho, R. Y., Koehntop, K. D., McCracken, J., Que, L., Jr., and Hausinger, R. P., *Biochemistry*, **2003**, *42*, 1854-62.
78. Liu, A., Ho, R. Y., Que, L., Jr., Ryle, M. J., Phinney, B. S., and Hausinger, R. P., *J Am Chem Soc*, **2001**, *123*, 5126-7.

79. Mehn, M. P., Fujisawa, K., Hegg, E. L., and Que, L., Jr., *J Am Chem Soc*, **2003**, *125*, 7828-42.
80. Rohde, J. U., In, J. H., Lim, M. H., Brennessel, W. W., Bukowski, M. R., Stubna, A., Munck, E., Nam, W., and Que, L., *Science*, **2003**, *299*, 1037-1039.
81. Price, J. C., Barr, E. W., Tirupati, B., Bollinger, J. M., Jr., and Krebs, C., *Biochemistry*, **2003**, *42*, 7497-508.
82. Price, J. C., Barr, E. W., Glass, T. E., Krebs, C., and Bollinger, J. M., Jr., *J Am Chem Soc*, **2003**, *125*, 13008-9.
83. Proshlyakov, D. A., Henshaw, T. F., Monterosso, G. R., Ryle, M. J., and Hausinger, R. P., *J Am Chem Soc*, **2004**, *126*, 1022-3.

## CHAPTER II

### CHARACTERIZATION OF THE IRON-SULFUR CENTER OF PYRUVATE FORMATE-LYASE ACTIVATING ENZYME

The results presented in this chapter have been published in Broderick, J. B., Henshaw, T. F., Cheek, J., Wojtuszewski, K., Smith, S. R., Trojan, M. R., McGhan, R. M., Kopf, A., Kibbey, M., and Broderick, W. E., *Biochemical and Biophysical Research Communications*, **2000**, *269*, 451-456 and Krebs, C., Henshaw, T. F., Cheek, J., Huynh, B. H., and Broderick, J. B., *Journal of the American Chemical Society*, **2000**, *122*, 12497-12506.

My contribution to this work did not include acquisition or analysis of Mössbauer spectra

## II.1 Introduction

Pyruvate formate-lyase is a pivotal enzyme in the anaerobic glucose metabolism of *Escherichia coli* and other facultative anaerobes. It catalyzes the reversible non-oxidative cleavage of pyruvate to formate and acetyl-CoA, the determinate step in anaerobic glucose metabolism. PFL is a member of a class of enzymes that contain a catalytically essential glycyl radical which is generated in a post-translational modification; in the case of PFL this modification is catalyzed by pyruvate formate-lyase activating enzyme (1, 2). This modification is dependent on S-adenosylmethionine, which is reductively cleaved to methionine and 5'-deoxyadenosine (3). When the glycine residue is labeled with deuterium, the label is incorporated into 5'-deoxyadenosine, implicating a 5'-deoxyadenosyl radical as the direct hydrogen-abstracting species (4). A major interest in the Broderick lab is the mechanism by which this putative radical is generated.

The first detailed studies of PFL-AE suggested the presence of an organic cofactor, as indicated by a broad absorbance in the visible region, but further characterization was hampered by the low availability of the enzyme (1). These problems were overcome with the cloning (5) and overexpression of the gene which yielded large quantities of enzyme for detailed study (6). Unfortunately, most of this protein was found in insoluble inclusion bodies, and the researchers resorted to purifying the enzyme under denaturing conditions followed by refolding and reconstitution with a variety of metal ions. The activity was found to be dependent on Fe(II), which could be incorporated into the enzyme in an approximate 1:1 ratio, and was inhibited by other

thiophilic metals, suggesting that the metal was coordinated by cysteine residues. The activity exhibited by the refolded protein was much lower than the native enzyme purified previously and showed no appreciable visible chromophore, observations that indicate a fundamental difference between the native and refolded protein (1, 6).

The first work to identify an iron-sulfur cluster in PFL-AE was done by the Broderick lab at Amherst College in collaboration with Professor Michael Johnson at the University of Georgia (7). The evidence that PFL-AE contained an iron-sulfur cluster was obtained using enzyme that had been purified using nitrogen-filled glove bags and argon-purged buffers. Resonance Raman spectroscopy indicated the presence of a mixture of  $[4\text{Fe-4S}]^{2+}$  and  $[2\text{Fe-2S}]^{2+}$  clusters. Then the sample was reduced with excess dithionite, only the  $[4\text{Fe-4S}]^{2+}$  clusters remained, as indicated by resonance Raman and the lack of an EPR signal. When the enzyme was reduced in the presence of AdoMet, a fast-relaxing EPR signal was observed that was attributed to a  $[4\text{Fe-4S}]^{1+}$  cluster which was not observed in the absence of substrate. While the method of purification used in these studies allowed for the isolation of enzyme containing intact clusters, they could hardly be considered strictly anaerobic conditions. In addition, the plasmid used to overexpress *pflA* (the gene that encodes PFL-AE) used a heat-inducible promoter, requiring growth at 42 °C. This elevated temperature could contribute to degradation of the cluster.

The work described in this chapter presents a detailed characterization of the iron-sulfur cluster of PFL-AE, a necessary prerequisite for determining the role, if any, this cluster plays in the radical-generating reaction. The work in this chapter also represents a major step forward in the evolution of our methods of purifying and handling the

enzyme. Two improvements in particular have facilitated the characterization of the enzyme. The first is the subcloning of *pflA* into a pET-based vector that allows IPTG-induced expression of the gene. The second is the much more rigorous anaerobic conditions used in the purification and manipulation of the enzyme using anaerobic chambers.

## II.2 Experimental Methods

### *Growth and expression of PFL*

pKK-PFL (gift from John Kozarich) was used to transform BL21(DE3)pLysS. A single colony of transformed cells was used to inoculate 5 to 50 mL of LB media containing 50 mg/mL ampicillin (LB/Amp). This culture was grown to saturation and then used to inoculate LB/Amp in 2.8 L Fernbach flasks or in a 10-L bench-top fermentor (New Brunswick). The cultures were grown at 37°C with vigorous shaking (flasks) or continuous air purge and vigorous agitation (fermentor) to early log phase (OD<sub>600</sub> ~ 0.6-0.8), and then induced by addition of isopropyl-β-D-thiogalactopyranoside (IPTG) to 1 mM. The cultures were grown for 2 more h before harvesting by centrifugation (8000 rpm, Sorvall GS3 rotor). The supernatant was decanted and the cells stored at -80°.

### *Subcloning, growth, and expression of PFL-AE*

The *pflA* gene, which encodes PFL-AE, was digested from pMG-AE (gift from John Kozarich) using NdeI/HindIII and ligated to pCAL-n-EK that had been cut with the same enzymes. The resultant vector (pCalnAE) was used to transform BL21(DE3)pLysS. A single colony of the resulting overexpressing strain was used to inoculate 50 mL of LB

containing 50 µg/mL ampicillin (LB/Amp). This culture was grown to saturation at 37 °C and then used to inoculate 10 L of LB/Amp. The 10 L culture was grown at 37 °C in a bench-top fermentor (New Brunswick) with a continuous air purge and vigorous agitation. When the culture reached an optical density of 0.6 to 0.8, isopropyl-β-D-thiogalactopyranoside (IPTG) was added to 1 mM final concentration, and the medium was supplemented with 150 mg Fe(NH<sub>4</sub>)<sub>2</sub>(SO<sub>4</sub>)<sub>2</sub> per liter of culture. The culture was allowed to grow for an additional 2 h, at which time the temperature was reduced to 4 °C and the culture was purged with nitrogen. The culture was incubated for 14–24 h at 4 °C under nitrogen before harvesting under anaerobic conditions. The harvested cells were stored under nitrogen at -80 °C until used for purification.

In order to prepare PFL-AE for Mössbauer studies, the pCalnAE/BL21(DE3)*pLysS* strain described above was grown in a defined MOPS medium (8) that was modified to include 0.5 mM CaCl<sub>2</sub>, 1% (w/v) casamino acids, and 0.001% each of pyroxidine, riboflavin, niacinamide, folic acid, cyanocobalamin, pantothenic acid, and thiocitic acid. <sup>57</sup>Fe was added to a final concentration of 20 µM from a concentrated stock that was prepared by dissolving the metal in a minimal volume of 2:3:1 H<sub>2</sub>O:HCl (concentrated):HNO<sub>3</sub> (concentrated).

#### *Purification of pyruvate formate-lyase-activating enzyme (PFL-AE)*

PFL-AE was purified from *E. coli* BL21(DE3)*pLysS* transformed with pCAL-n-AE3, prepared as described above. All steps in the purification were performed in a single day under strictly anaerobic conditions in a Coy anaerobic chamber (Coy Laboratories, Grass Lake, MI) at ambient temperature except where noted. Solutions and buffers used in the purification were thoroughly degassed prior to bringing them in to the

Coy chamber. Approximately 4 to 6 g of cell paste was suspended in 5 to 10 mL of enzymatic lysis buffer containing 50 mM Tris–sulfate, pH 7.5, 200 mM NaCl, 1% Triton X-100, 5% glycerol, 10mM MgCl<sub>2</sub>, 1mM DTT, 40 mM dithionite, 1 mM PMSF, 8 mg lysozyme, and trace amounts (approximately 0.1 mg each) of DNase I and RNase A. This suspension was incubated at ambient temperature for 1 h, and then centrifuged at 15,000 rpm (SS34) for 15 min at 4°C. The extract was decanted and used directly in purification. Up to 10 mL of the crude extract was loaded onto a Sephacryl S-200 HR column (5 x 60 cm) equilibrated with 50 mM Hepes, 200 mM NaCl, pH 7.2. The protein was eluted with this same buffer at 3 mL/min. AE eluted from the column in a relatively sharp peak at approximately 750 mL after injection. The fractions were analyzed by SDS-PAGE, and those determined to be >95% pure were pooled and concentrated using an Amicon concentrator with YM10 filter membranes. If additional purification was required, the protein was chromatographed on a Superdex 75 column (1.6 x 60 cm) using the same buffers. The concentrated, purified protein was flash-frozen and stored in O-ring-sealed tubes at -80 °C.

#### *Activity, protein and iron assays*

PFL-AE activity was determined by the direct detection of the PFL glycyl radical by EPR spectroscopy. A 1 ml reaction mix contained 0.1 M Tris-HCl, pH 7.6, 0.1 M KCl, 10 mM DTT, 10 mM oxamate (allosteric effector), 10 mg/ml PFL, 200 μM 5-deazariboflavin, 0.2 mM AdoMet and catalytic amounts of PFL-AE. This mix was prepared in an Mbraun glove box from anaerobic stocks. The mix was divided into EPR tubes and illuminated with a 500 W halogen lamp for varying times. The samples were maintained at ambient temperature (20-25 °C) by immersion in a water bath, which was

cooled with ice as necessary. The amount of glycy radical generated was determined by EPR spectroscopy.

Protein concentrations were determined using the method of Bradford using a kit purchased from Bio-Rad. For PFL-AE, these results were calibrated by amino acid hydrolysis of the purified enzyme done at the MCB core facility at the University of Massachusetts.

Iron concentrations were determined according to the method of Beinert (9).

### *EPR and Mössbauer Spectroscopy*

Mössbauer spectroscopy was done in collaboration with Professor Boi Hanh (Vincent) Huynh and Dr. Carsten Krebs at Emory University.

First derivative EPR spectra were recorded on a Bruker ER-200D-SRC or ESP300E spectrometer equipped with a continuous-flow helium cryostat. Details of conditions are given in figure legends. Mössbauer spectra were recorded in either a weak-field spectrometer equipped with a Janis 8DT variable-temperature cryostat or a strong-field spectrometer furnished with a Janis CNDT/SC SuperVaritemp cryostat encasing an 8-T superconducting magnet. Both spectrometers operate in a constant acceleration mode in a transmission geometry. The zero velocity of the spectra refers to the centroid of a room-temperature spectrum of a metallic iron foil.

## II.3 Results

### *Enzyme Activity*

The preparations of PFL-AE prepared as described above exhibit specific activities that are higher than those previously published, presumably as a result of the direct detection of the glycy radical by EPR spectroscopy rather than the coupled assay used previously (1, 6, 10). A preparation AE from cells grown in enriched media exhibits a specific activity of 95 U/mg and AE purified from cells grown in media exhibits a specific activity of 48 U/mg. As discussed below, these specific activities correlate directly with iron content.

### *Characterization of purified PFL-AE*

Purified PFL-AE contains iron ( $2.8 \pm 0.3$  mol/mol PFL-AE). The UV-visible spectrum of purified PFL-AE is indicative of the presence of an iron sulfur cluster (Figure II.1), with a maximum at 412 nm ( $\epsilon = 3.0 \text{ mM}^{-1}\text{cm}^{-1}$ ), and shoulders at 320 nm ( $\epsilon = 4.4 \text{ mM}^{-1}\text{cm}^{-1}$ ), 455 nm ( $\epsilon = 2.6 \text{ mM}^{-1}\text{cm}^{-1}$ ), and 550 nm ( $\epsilon = 0.94 \text{ mM}^{-1}\text{cm}^{-1}$ ). The energies and extinction coefficients of these absorption bands are similar to those observed for the cuboidal [3Fe-4S] form of aconitase (11). PFL-AE exhibits a strong, nearly isotropic electron paramagnetic resonance (EPR) signal, which is centered at  $g = 2.02$  and observable only below approximately 30 K (Figure II.2). The  $g$  value and low anisotropy of this fast-relaxing signal are consistent with its assignment to a [3Fe-4S]<sup>+</sup> cluster. The signal, quantified by using a Cu(II)edta standard and the method outlined by Aasa and Vänngård (12), accounts for 62% of the total iron in the sample, with the remainder of the iron being present in an EPR-silent form.

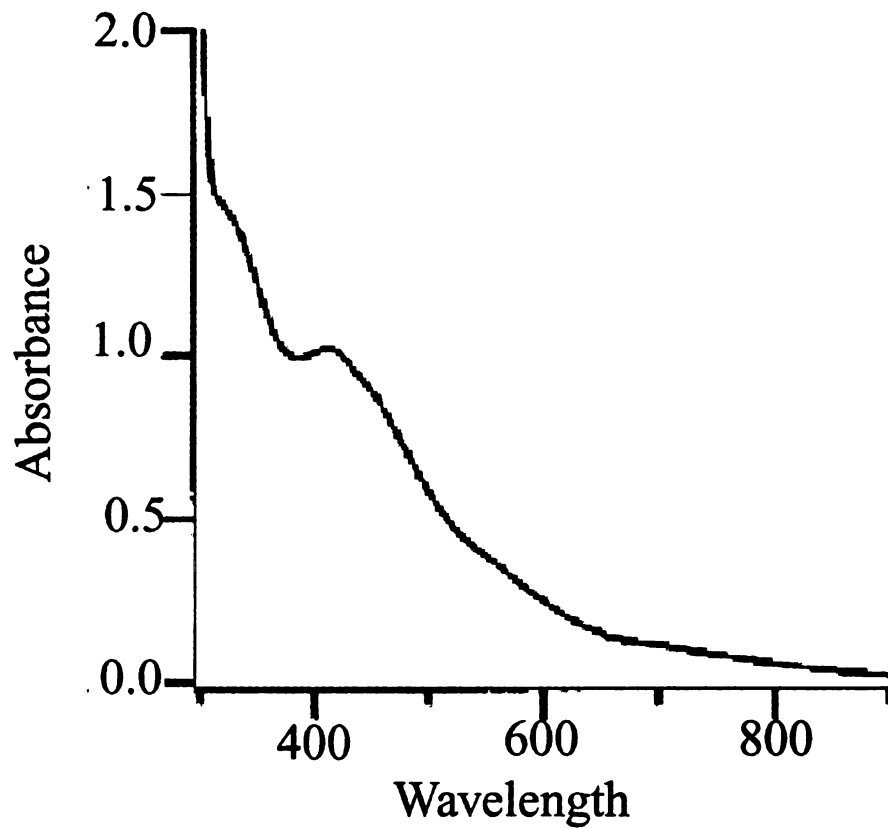


**Figure II.1 UV-visible absorption spectrum of pyruvate formate-lyase activating enzyme as isolated.**

The protein was 0.34 mM in 50 mM Hepes/200 mM NaCl, pH 7.2, and the spectra were recorded in a 1 mm pathlength cuvette under anaerobic conditions at 4°C. Reproduced with permission from (13).

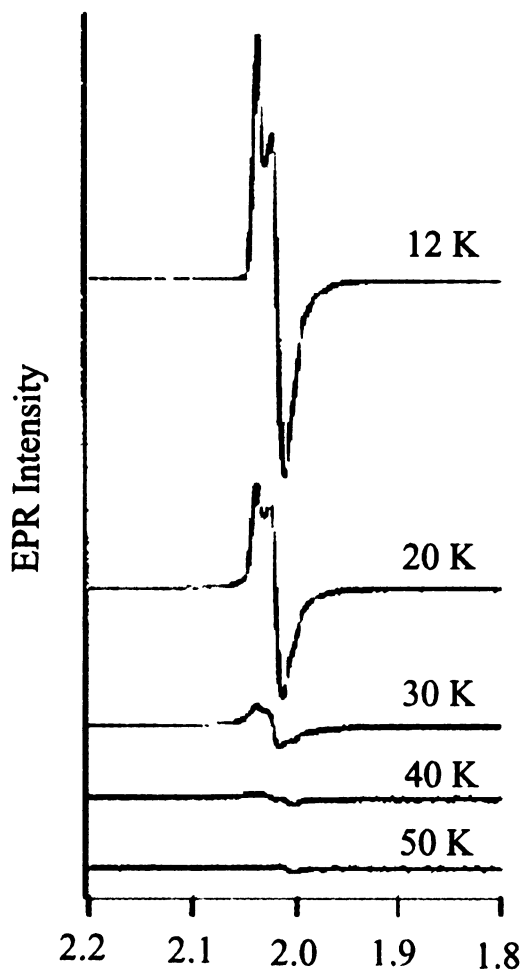


**Figure II.2 X-band EPR spectra of pyruvate formate-lyase-activating enzyme as a function of temperature.**

PFL-AE is 1.26 mM in 50 mM HEPES/200 mM NaCl, pH 7.2. Conditions of measurement, T as indicated, microwave power, 0.02 mW, microwave frequency, 9.4792 GHz, modulation amplitude, 10.084, and receiver gain,  $2 \times 10^4$ , 5 scans accumulated for each spectrum. Reproduced with permission from (13).

Preparations of the  $^{57}\text{Fe}$ -enriched PFL-AE were analyzed for iron and protein content. The results show an iron to protein monomer ratio of  $1.3 \pm 0.1$ . This value is lower than the 2.8 Fe/protein monomer for the enzyme purified from bacteria grown in enriched medium with naturally available Fe. Since the  $^{57}\text{Fe}$ -enriched PFL-AE was isolated from bacteria grown in defined medium, this observed difference in Fe content may suggest inefficient incorporation of the Fe cluster under suboptimal growth conditions. Two observations, however, indicate that the only difference between  $^{57}\text{Fe}$ -enriched and unenriched PFL-AE is the absolute quantity of iron incorporated, not the form in which it is incorporated. First, the EPR and UV-visible spectroscopic properties of  $^{57}\text{Fe}$ -enriched PFL-AE are essentially identical to those of PFL-AE isolated from bacteria grown with naturally available Fe. Second, the specific activity of the  $^{57}\text{Fe}$ -enriched PFL-AE containing 1.3 Fe per protein monomer (48 U/mg) is approximately half that for unenriched PFL-AE containing 2.65 Fe per protein monomer (95 U/mg). The specific activities reported here are higher than any previously published for PFL-AE, a difference that is likely a result of the direct detection of the glycy radical rather than the coupled assay previously used (1, 6).

Figure II.3 shows a Mössbauer spectrum of the as-isolated PFL-AE recorded at 4.2 K in a parallel applied field of 50 mT. At least three spectral components are discernible from this spectrum. The major component, which accounts for 66% of the Fe absorption, displays magnetic hyperfine interactions with absorption extending from -2 to 3 mm/s (solid line plotted above the data). This component is composed of three equal-intensity subspectral components and exhibits field-orientation and field-strength dependence consistent with an  $S = 1/2$  electronic system. At temperatures

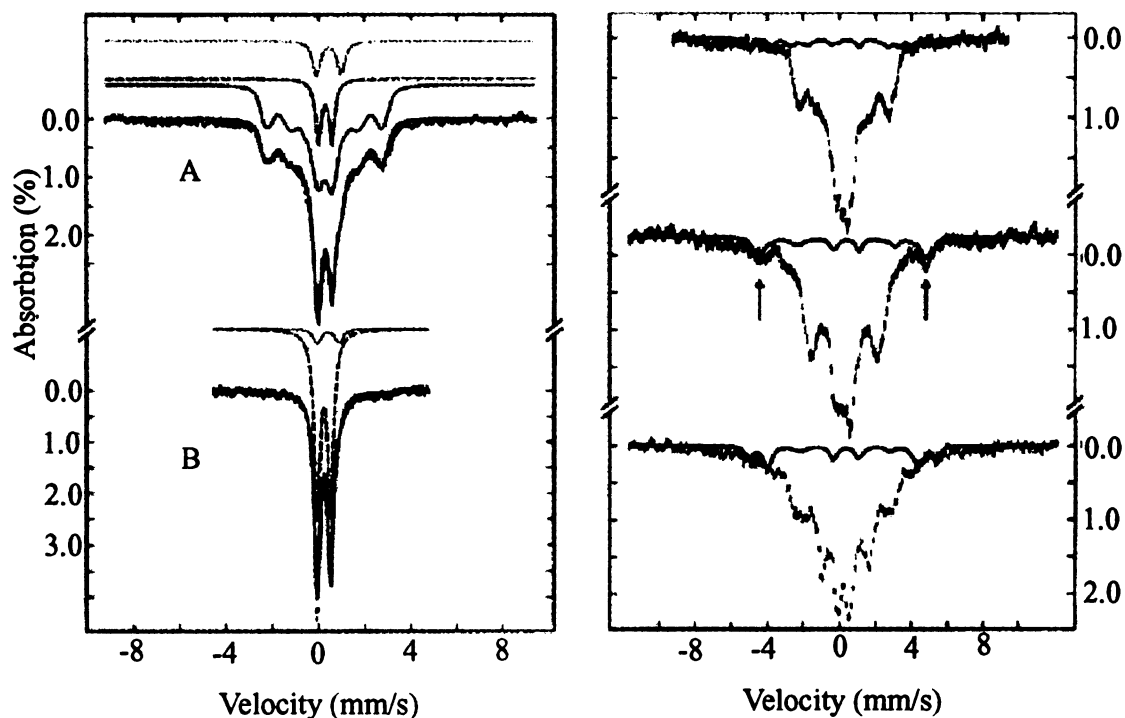


**Figure II.3 Mössbauer spectra of anaerobically purified native PFL-AE.**

The spectra were recorded at 4.2 K in a parallel field of 0.05 T (A and C), 170 K in zero field (B), 4.2 K in a parallel field of 4 T (D), or 8 T (E). For the spectra shown in C, D, and E, contributions from the  $[4\text{Fe-4S}]^{2+}$  (8%) and  $[2\text{Fe-2S}]^{2+}$  (12%) clusters have been removed. The solid line overlaid with the experimental spectrum in A is the sum of the theoretical simulations of the cuboidal  $[3\text{Fe-4S}]^+$  (solid line above the experimental spectrum, 66%),  $[2\text{Fe-2S}]^{2+}$  (dashed line, 12%), and  $[4\text{Fe-4S}]^{2+}$  (dotted line, 8%) clusters. The solid line in B is the sum of the quadrupole doublets arising from the  $[4\text{Fe-4S}]^{2+}$  cluster (dotted line above the experimental spectrum) and from the cuboidal  $[3\text{Fe-4S}]^+$  and  $[2\text{Fe-2S}]^{2+}$  (dashed line) clusters. The solid lines shown in C, D, and E are theoretical simulations of the linear  $[3\text{Fe-4S}]^+$  cluster using the parameters given in (11). The arrows in D indicate the positions at which the outermost lines of the three Fe sites of the linear  $[3\text{Fe-4S}]^+$  cluster overlap at 4 T (see text). Reproduced with permission from (14). Copyright 2000 American Chemical Society.

above 77 K, this magnetic component collapses into a quadrupole doublet (Figure II.3B) with parameters ( $\delta = 0.23$  mm/s and  $\Delta E_Q = 0.58$  mm/s at 170 K) typical of tetrahedral sulfur-coordinated high-spin Fe(III). All these features are characteristic of the all-ferric cuboidal  $[3\text{Fe-4S}]^+$  cluster. This magnetic component is thus assigned to such a cluster. This assignment is consistent with the EPR finding that the majority of the Fe-S cluster in the as-isolated PFL-AE is in an  $S = 1/2$   $[3\text{Fe-4S}]^+$  state.

A second spectral component accounting for 12% of the total Fe absorption is a sharp quadrupole doublet observed at 4.2 K (dashed line plotted above the data in Figure 4A) with parameters (listed in Table 1) characteristic of  $[2\text{Fe-2S}]^{2+}$  clusters (15, 16). Spectra recorded at strong applied field indicate that this component originates from a diamagnetic species. On the basis of this observed diamagnetism and the characteristic parameters, this component is assigned to a  $[2\text{Fe-2S}]^{2+}$  cluster. Removal of the contributions of the  $[3\text{Fe-4S}]^+$  and  $[2\text{Fe-2S}]^{2+}$  clusters from the raw data reveals a third component identical to that of the  $[4\text{Fe-4S}]^{2+}$  cluster observed in the dithionite-reduced PFL-AE (discussed below and dotted line plotted above the data in Figure II.3A). The high-energy line of this doublet can be seen as a shoulder at  $\sim 1$  mm/s in the raw data. This component is estimated to account for  $\sim 8\%$  of the total Fe absorption. A sum of the three components (the  $[3\text{Fe-4S}]^+$ ,  $[2\text{Fe-2S}]^{2+}$ , and  $[4\text{Fe-4S}]^{2+}$ ) yields the solid line plotted over the data in Figure II.3A. Although the agreement between the experiment and the simulated spectrum is reasonable, approximately 14% of the Fe absorption remains not accounted for. Spectra recorded at strong applied field reveal the presence of a fourth component.

The complexity of the above-discussed low-temperature spectrum is greatly reduced when data are collected at high temperatures. This is due to the fact that, at high temperature, the  $[3\text{Fe-4S}]^+$  cluster exhibits a single quadrupole doublet, and this doublet is similar to that of a  $[2\text{Fe-2S}]^{2+}$  cluster since both clusters are composed of only  $\text{Fe(III)S}_4$  units. As expected, the 170 K spectrum of the as-isolated PFL-AE (Figure II.3B) shows predominantly a quadrupole doublet arising from both the  $[3\text{Fe-4S}]^+$  and  $[2\text{Fe-2S}]^{2+}$  clusters (dashed line in Figure II.3B). This central doublet accounts for 80% of the total Fe absorption, consistent with the sum of the amounts of these two types of clusters determined at 4.2 K. The presence of a small quantity of the  $[4\text{Fe-4S}]^{2+}$  cluster is supported by the appearance of a shoulder at the high-energy line of the central doublet. To illustrate this point, we plot in Figure II.3B a simulated spectrum (dotted line in Figure II.3B) of the  $[4\text{Fe-4S}]^{2+}$  cluster using the parameters determined from the dithionite-reduced sample (Table II.1). The plotted spectrum is normalized to 8% of the total Fe absorption. Addition of the simulated central quadrupole doublet with the simulated  $[4\text{Fe-4S}]^{2+}$  doublet yields the solid line overlaid with the experimental data. Again, reasonable agreement between experiment and simulation is observed.

The fourth spectral component is readily observed in a spectrum recorded at 4.2 K in a parallel field of 4 T (Figure II.3D). This component is seen as a magnetic spectrum with its outermost lines appearing at approximately -5 and 5 mm/s (indicated by arrows). In a much weaker (0.05 T) or stronger (8 T) applied field (Figure II.3, spectra C and E, respectively), however, this magnetic component becomes broad and is difficult to detect. This field-strength dependence and the observed magnetic splitting are consistent with those of a linear  $[3\text{Fe-4S}]^+$  cluster (11, 17). In the following, we use the results obtained

**Table II.1 Temperature-Dependent Mössbauer Parameters of the Fe-S Clusters in Native PFL-AE**

|                               |                     | T(K)     |          |          |
|-------------------------------|---------------------|----------|----------|----------|
|                               |                     | 4.2      | 113      | 170      |
| [4Fe-4S] <sup>2+</sup> site 1 | $\delta$ (mm/s)     | 0.45 (2) | 0.44 (2) | 0.44 (2) |
|                               | $\Delta E_Q$ (mm/s) | 1.15 (4) | 1.13 (4) | 1.10 (4) |
|                               | $\eta$              | 0.3      |          |          |
| [4Fe-4S] <sup>2+</sup> site 2 | $\delta$ (mm/s)     | 0.45 (2) | 0.44 (2) | 0.42 (2) |
|                               | $\Delta E_Q$ (mm/s) | 1.00 (4) | 0.83 (4) | 0.80 (4) |
|                               | $\eta$              | 0.7      |          |          |
| [2Fe-2S] <sup>2+</sup>        | $\delta$ (mm/s)     | 0.29 (2) | 0.26 (2) | 0.23 (2) |
|                               | $\Delta E_Q$ (mm/s) | 0.58 (4) | 0.58 (4) | 0.58 (4) |
|                               | $\eta$              | 0        |          |          |

for the linear  $[3\text{Fe-4S}]^+$  cluster in aconitase (11) as an example to illustrate this point and to compare with the PFL-AE spectra. For a linear  $[3\text{Fe-4S}]^+$  cluster, the three  $S = 5/2$  Fe(III) sites are spin-coupled to form an  $S = 5/2$  ground state. The spin of the middle Fe site (site 3) is antiparallel to those of the two terminal Fe sites (sites 1 and 2). Consequently, the internal field of site 3 is parallel to the applied field, while those of the other two sites oppose the applied field. For the linear  $[3\text{Fe-4S}]^+$  cluster in aconitase, (11) the observed internal fields for sites 1, 2, and 3 are -33.6, -31.9, and 24.2 T, respectively. The signs indicate the direction of the internal field in relation to that of the applied field. At 0.05 T, since all three internal fields are different in magnitude, the spectra arising from the three Fe sites show different magnetic splittings. Superposition of these three spectra results in a relatively broad spectrum (solid line overlaid with the experimental spectrum in Figure II.3C). At 4 T, to a good approximation, the magnitudes of the effective fields at sites 1 and 2 are reduced by 4 T to 29.6 and 27.9 T, respectively, while that of site 3 is increased to 28.2 T. These values are quite similar, and thus, all three sites show similar magnetic spectra, superposition of which results in a "single" magnetic spectrum with its intensity tripled (solid line in Figure II.3D). At 8 T, the magnitudes of the effective fields at sites 1, 2, and 3 are again different, and a broad magnetic spectrum is again observed (solid line in Figure II.3E). On the basis of the above analysis, it is concluded that the as-isolated PFL-AE contains linear  $[3\text{Fe-4S}]^+$  clusters, accounting for approximately 10% of the total iron absorption.

In summary, analysis of the Mössbauer data of the as-isolated PFL-AE shows the presence of mixtures of Fe-S clusters. A majority of the clusters are present in the cuboidal  $[3\text{Fe-4S}]^+$  state ( $\sim 0.29$  cluster/protein monomer), while minor portions are in the

$[2\text{Fe-2S}]^{2+}$  ( $\sim 0.08$  cluster/monomer),  $[4\text{Fe-4S}]^{2+}$  ( $\sim 0.03$  cluster/monomer), and linear  $[3\text{Fe-4S}]^+$  ( $\sim 0.04$  cluster/monomer) states.

#### *Characterization of the dithionite-reduced enzyme*

The 4.2 K Mossbauer spectrum of a dithionite-reduced PFL-AE sample (Figure II.4), recorded in a magnetic field of 50 mT oriented parallel to the  $\gamma$ -beam, displays an intense central quadrupole doublet (marked by a bracket), a broad absorption peak at  $\sim 2.8$  mm/s, and weak absorptions between -2 and +2.5 mm/s. These features are associated with three spectral components and thus represent three different Fe species. The broad absorption peak at  $\sim 2.8$  mm/s is the high-energy line of a quadrupole doublet (shown as a solid line in Figure II.4), of which the parameters (see legend of Figure II.4) and shape are indicative of adventitiously bound high-spin Fe(II). Removal of the contribution of the adventitious Fe(II) (25% of the total Fe absorption) from the raw data reveals the spectrum arising from the Fe-S clusters (Figure II.5A). The central quadrupole doublet, accounting for 66% of the total Fe absorption, is best simulated with two overlapping quadrupole doublets (dashed line in Figure II.5A). The parameters used in the simulation are listed in Table II.1 and are typical for  $[4\text{Fe-4S}]^{2+}$  clusters (18, 19). Without exception,  $[4\text{Fe-4S}]^{2+}$  clusters have an  $S = 0$  ground state, resulting from antiferromagnetic coupling of the two valence-delocalized Fe(II)Fe(III) units. To examine the spin state of the species associated with the central doublet, a spectrum of the dithionite-reduced PFL-AE was recorded in a strong external field of 8 T at 4.2 K (Figure II.5C). The solid line plotted over the data in Figure 2C is a simulation using the parameters obtained for the central doublet from the weak-field spectrum and assuming diamagnetism. The agreement between the simulation and the central portion of

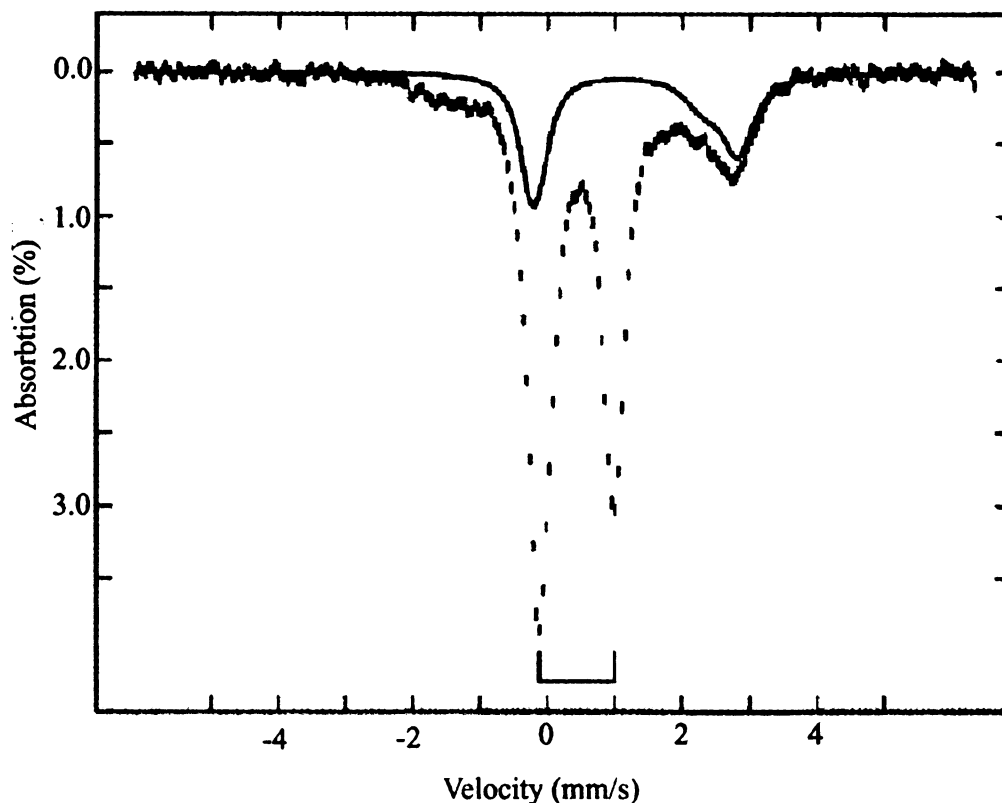


**Figure II.4 Mössbauer spectrum of dithionite-reduced native PFL-AE recorded at 4.2 K in a magnetic field of 0.05 T applied parallel to the  $\gamma$ -beam.**

The bracket indicates the positions of the quadrupole doublet arising from the  $[4\text{Fe-4S}]^{2+}$  cluster. The solid line is the theoretical simulation of the adventitiously bound Fe(II) assuming two quadrupole doublets with  $\delta(1) = 1.28$  mm/s,  $\Delta E_Q(1) = 3.07$  mm/s,  $\delta(2) = 1.10$  mm/s, and  $\Delta E_Q = 2.42$  mm/s. Doublet 1 contributes 17% of the total Fe absorption, and doublet 2 contributes 8%. Reproduced with permission from (14). Copyright 2000 American Chemical Society.

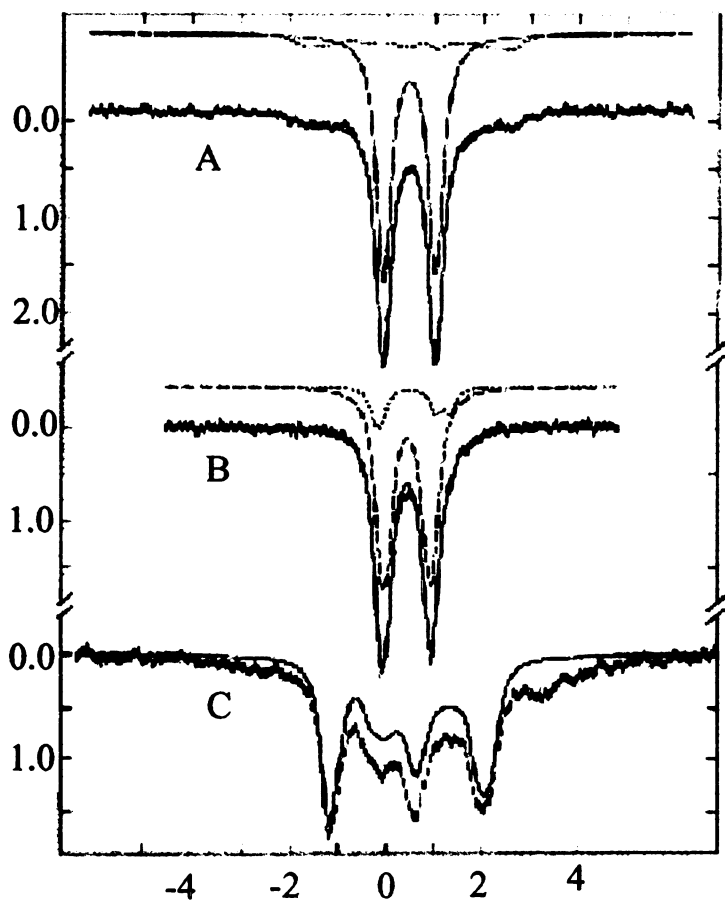


**Figure II.5 Mössbauer spectra of dithionite-reduced PFL-AE**

Spectra were recorded at 4.2 K in a parallel field of 0.05 T (A), 170 K in the absence of applied field (B), and 4.2 K in a parallel field of 8 T (C). The contributions from the adventitiously bound Fe(II) have been removed for the spectra shown in A and B. The solid lines in A and B are summations of theoretical simulations of the  $[4\text{Fe-4S}]^{2+}$  (dashed lines, 66% of total Fe absorption) and the  $[4\text{Fe-4S}]^+$  (dotted lines, 12%) clusters. The solid line in C is the theoretical simulation of the  $[4\text{Fe-4S}]^{2+}$  cluster, assuming diamagnetism. Reproduced with permission from (14). Copyright 2000 American Chemical Society.

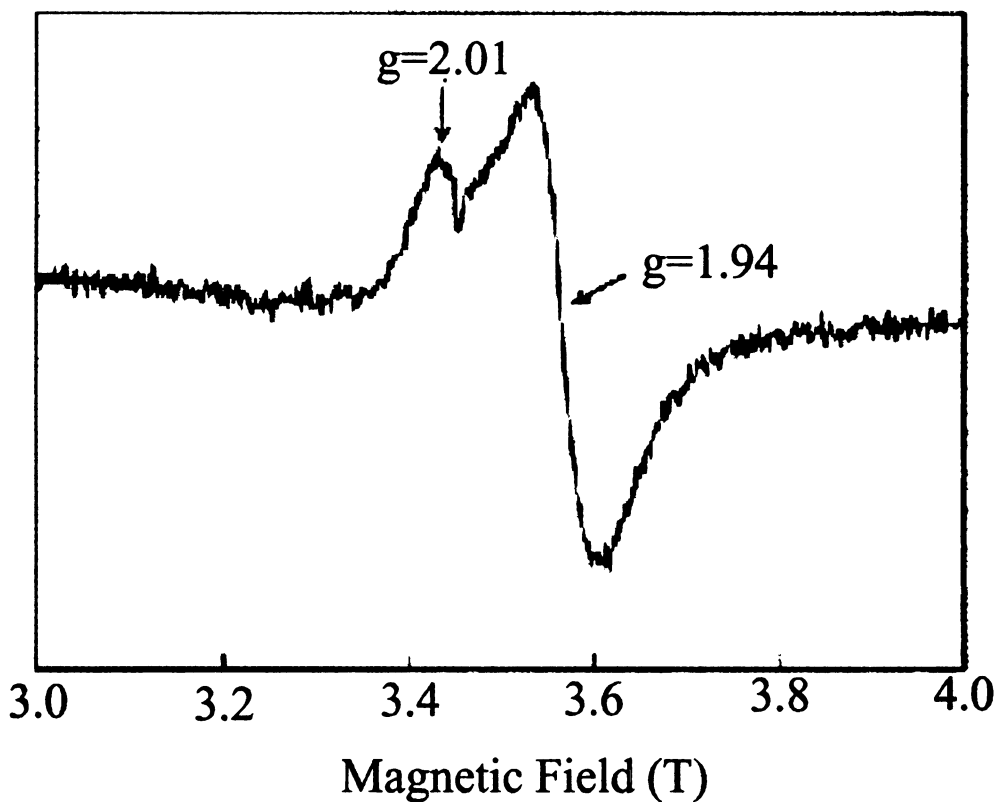


**Figure II.6 EPR spectrum of dithionite-reduced PFL-AE showing a weak signal originating from the  $[4\text{Fe-4S}]^+$  cluster.**

The spectrum was recorded with the following instrumental settings: temperature, 12 K; microwave power, 2 mW; microwave frequency, 9.65 GHz; modulation amplitude, 1 mT; modulation frequency, 100 kHz. Reproduced with permission from (14). Copyright 2000 American Chemical Society.

the experimental spectrum confirms that the central doublet is arising from a diamagnetic species. Thus, this component is assigned to a  $[4\text{Fe-4S}]^{2+}$  cluster.

The component having absorption extending from -2 to 2.5 mm/s, which accounts for 12% of the total Fe absorption, is originating from a paramagnetic species and can be attributed to a  $[4\text{Fe-4S}]^+$  cluster with an  $S = 1/2$  ground state. Mössbauer spectra of such clusters consist of two equal intensity subspectra representing a valence-delocalized Fe(II)Fe(III) pair and a diferrous pair (15, 18). Because of the weak intensity and because the number of variables required for spectral simulation of a  $[4\text{Fe-4S}]^+$  cluster is large, we did not attempt to determine the specific parameters for the  $[4\text{Fe-4S}]^+$  cluster in the dithionite-reduced PFL-AE by fitting this paramagnetic component. Instead, to show that this paramagnetic component is consistent with that of a  $[4\text{Fe-4S}]^+$  cluster, we have used the parameters obtained for the  $[4\text{Fe-4S}]^+$  cluster of *Bacillus stearothermophilus* ferredoxin (18) to simulate a spectrum for comparison with this component. The simulation is plotted in Figure II.5A as a dotted line. It can be seen that the magnetic splitting and shape of the paramagnetic component in PFL-AE agree well with the simulation. Addition of the simulated  $[4\text{Fe-4S}]^+$  spectrum (12%) with the least-squares fit spectrum for the  $[4\text{Fe-4S}]^{2+}$  cluster (66%) generates the solid line overlaid with the experimental spectrum shown in Figure II.5A. The agreement observed between the theory and the experimental spectrum supports the above assignment.

At high temperatures the electronic relaxation of a  $[4\text{Fe-4S}]^+$  cluster is fast in comparison with the Larmor frequency of the  $^{57}\text{Fe}$  nucleus, resulting in cancellation of the internal field and collapse of the low-temperature magnetic spectrum into two quadrupole doublets associated with the Fe(II)Fe(III) and the diferrous pairs. (15, 18)

Figure II.5B shows a spectrum of the dithionite-reduced PFL-AE recorded at 170 K in the absence of an applied field (the contribution of the adventitiously bound Fe(II) has been removed from the spectrum shown). As expected, the paramagnetic component observed at 4.2 K has collapsed into quadrupole doublets at this temperature. A small shoulder at  $\sim 1.3$  mm/s is observed. A comparison with the simulated spectrum of the *B. stearothermophilus* [4Fe-4S]<sup>+</sup> cluster (18) at this temperature (dotted line in Figure II.5B) indicates that this shoulder is at the position of the high-energy line of the quadrupole doublet of the diferrous pair. The intensity of this shoulder is also consistent with the percent absorption (12% of total Fe absorption) determined for the [4Fe-4S]<sup>+</sup> cluster from the low-temperature data. To demonstrate that the high-temperature spectrum is in agreement with the assignment made from analyzing the low-temperature data, we have again added the simulated central doublet (long-dashed line in Figure II.5B for the [4Fe-4S]<sup>2+</sup> cluster) and the simulated *B. stearothermophilus* [4Fe-4S]<sup>+</sup> spectrum (dotted line) according to the intensities determined from the low-temperature spectra (66% for the [4Fe-4S]<sup>2+</sup> and 12% for the [4Fe-4S]<sup>+</sup>) and plotted the sum (solid line) over the experimental spectrum. The agreement between the simulation and experiment indicates that both the high-temperature and low-temperature Mossbauer data are consistent with the conclusion that, except for the adventitiously bound Fe(II), only [4Fe-4S] clusters are present in the dithionite-reduced PFL-AE. The percent absorption of the [4Fe-4S] cluster determined from the Mössbauer measurement, together with the iron and protein determinations, yields a stoichiometry of  $\sim 0.25$  [4Fe-4S] cluster per protein monomer, of which 85% are in the diamagnetic [4Fe-4S]<sup>2+</sup> state and the remainder are in the paramagnetic [4Fe-4S]<sup>+</sup> state.

The presence of a small quantity of  $[4\text{Fe-4S}]^+$  cluster in the dithionite-reduced PFL-AE is also supported by EPR measurements. An X-band EPR spectrum of a dithionite-reduced PFL-AE prepared in parallel with the Mössbauer sample displays an axial  $S = 1/2$  signal with  $g$  values at 2.01 and 1.94 (Figure II.6). This signal is very similar to that reported for the dithionite-reduced reconstituted PFL-AE (10). Double integration of this signal yields a spin quantitation of 0.03-0.04 spin/protein monomer, a value that is consistent with the Mössbauer finding of  $\sim 0.04$   $[4\text{Fe-4S}]^+$  cluster per protein monomer.

## II.4 Discussion

The results presented in this chapter show that native PFL-AE may be isolated under anaerobic conditions and may be isolated with nearly a full complement of iron-sulfur cluster. In addition these preparations exhibit high specific activities in the absence of Fe(II) in the assay mix. Previous studies on PFL-AE included 0.2 mM Fe(II) in the assay and this added iron was thought to be an absolute requirement for activity (1, 6). In addition, the specific activities of different enzyme preparations correlate directly with the iron content of the preparation. For example, the enzyme that was isolated for Mössbauer studies showed an iron content of 1.3 Fe/monomer and a specific activity of 48 U/mg. A preparation isolated from cells grown in enriched media had an iron content of 2.65 Fe/monomer and a specific activity of 95 U/mg. The direct correlation between the iron content, in the form of an FeS cluster, indicate that this cluster is required for enzyme activity.

The detailed spectroscopic studies presented in this chapter show that AE has the ability to coordinate a plethora of cluster types, including the  $[2\text{Fe-2S}]^{2+}$ , the  $[4\text{Fe-4S}]^{2+}$

and the cuboidal  $[3\text{Fe-4S}]^+$  with the latter being the predominant cluster type. In addition, a small amount of linear  $[3\text{Fe-4S}]^+$  cluster was identified by Mössbauer spectroscopy. Under reducing conditions, these cluster types are converted to a mixture of  $[4\text{Fe-4S}]^{2+/1+}$  clusters. This finding is consistent with the expectation that the  $[3\text{Fe-4S}]$  cluster represents an inactive form of the enzyme and that the  $[4\text{Fe-4S}]$  clusters are generated under the reducing conditions of the activity assay. The results presented in Chapter IV explicitly demonstrate that the  $[4\text{Fe-4S}]^{1+}$  is the catalytically relevant form of the cluster.

The ready accessibility of the  $[3\text{Fe-4S}]$  and  $[4\text{Fe-4S}]$  cluster types invites a comparison with aconitase and suggests that there may be a unique iron site in PFL-AE. In addition, aconitase is the only other enzyme system in which a linear  $[3\text{Fe-4S}]$  cluster has been identified (11). A  $\text{CX}_3\text{CX}_2\text{C}$  cluster binding motif has been identified in the FeS/AdoMet enzyme family (20), but the identity of the fourth ligand to the cluster has not been identified. The results presented in Chapter III demonstrate that there is a unique iron site in PFL-AE and that AdoMet is a ligand to this site.

## References

1. Conradt, H., Hohmannberger, M., Hohmann, H. P., Blaschkowski, H. P., and Knappe, J., *Archives of Biochemistry and Biophysics*, **1984**, 228, 133-142.
2. Knappe, J., Neugebauer, F. A., Blaschkowski, H. P., and Ganzler, M., *Proceedings of the National Academy of Sciences of the United States of America-Biological Sciences*, **1984**, 81, 1332-1335.
3. Knappe, J. and Schmitt, T., *Biochemical and Biophysical Research Communications*, **1976**, 71, 1110-1117.
4. Frey, M., Rothe, M., Wagner, A. F. V., and Knappe, J., *Journal of Biological Chemistry*, **1994**, 269, 12432-12437.
5. Rodel, W., Plaga, W., Frank, R., and Knappe, J., *European Journal of Biochemistry*, **1988**, 177, 153-158.
6. Wong, K. K., Murray, B. W., Lewisch, S. A., Baxter, M. K., Ridky, T. W., Ulissidemario, L., and Kozarich, J. W., *Biochemistry*, **1993**, 32, 14102-14110.
7. Broderick, J. B., Duderstadt, R. E., Fernandez, D. C., Wojtuszewski, K., Henshaw, T. F., and Johnson, M. K., *Journal of the American Chemical Society*, **1997**, 119, 7396-7397.
8. Garboczi, D., Hullihen, J., and Pedersen, P., *J. Biol. Chem.*, **1988**, 263, 15694-15698.
9. Beinert, H., *Methods Enzymol*, **1978**, 54, 435-45.
10. Kulzer, R., Pils, T., Kappl, R., Huttermann, J., and Knappe, J., *Journal of Biological Chemistry*, **1998**, 273, 4897-4903.
11. Kennedy, M., Kent, T., Emptage, M., Merkle, H., Beinert, H., and Munck, E., *J. Biol. Chem.*, **1984**, 259, 14463-14471.
12. Aasa, R. and Vanngard, T., *Journal of Magnetic Resonance*, **1975**, 19, 308-315.
13. Broderick, J. B., Henshaw, T. F., Cheek, J., Wojtuszewski, K., Smith, S. R., Trojan, M. R., McGhan, R. M., Kopf, A., Kibbey, M., and Broderick, W. E., *Biochemical and Biophysical Research Communications*, **2000**, 269, 451-456.
14. Krebs, C., Henshaw, T. F., Cheek, J., Huynh, B. H., and Broderick, J. B., *Journal of the American Chemical Society*, **2000**, 122, 12497-12506.

15. Trautwein, A. X., Bill, E., Bominaar, E. L., and Winkler, H., *Structure and Bonding*, **1991**, *78*, 1-95.
16. Ferreira, G. C., Franco, R., Lloyd, S. G., Pereira, A. S., Moura, I., Moura, J. J. G., and Huynh, B. H., *Journal of Biological Chemistry*, **1994**, *269*, 7062-7065.
17. Girerd, J. J., Papaefthymiou, G. C., Watson, A. D., Gamp, E., Hagen, K. S., Edelstein, N., Frankel, R. B., and Holm, R. H., *Journal of the American Chemical Society*, **1984**, *106*, 5941-5947.
18. Middleton, P., Dickson, D. P. E., Johnson, C. E., and Rush, J. D., *European Journal of Biochemistry*, **1978**, *88*, 135-141.
19. Middleton, P., Dickson, D. P. E., Johnson, C. E., and Rush, J. D., *European Journal of Biochemistry*, **1980**, *104*, 289-296.
20. Sofia, H. J., Chen, G., Hetzler, B. G., Reyes-Spindola, J. F., and Miller, N. E., *Nucleic Acids Res*, **2001**, *29*, 1097-106.

## CHAPTER III

### IDENTIFICATION OF A UNIQUE IRON SITE

The results presented in this chapter have been published in: Krebs, C., Broderick, W. E., Henshaw, T. F., Broderick, J. B., and Huynh, B. H., *Journal of the American Chemical Society*, **2002**, *124*, 912-913.

### III.1 Introduction

Pyruvate formate-lyase activating enzyme is a member of a growing class of enzymes that use AdoMet and iron-sulfur clusters in radical generating roles. These enzymes have been shown to participate in the generation of stable protein radicals, sulfur insertion, DNA repair, and tRNA modification. PFL-AE catalyzes the reductive cleavage of AdoMet to methionine and a putative 5'-deoxyadenosyl radical which abstracts a hydrogen atom from Gly-734 of PFL to generate a stable glycy radical.

A conserved feature of the "Radical SAM" (1) or "AdoMet radical" (2) enzymes is a -C-X<sub>3</sub>-C-X<sub>2</sub>-C- cluster-binding motif. However, [4Fe-4S] clusters are typically coordinated to the protein by four ligands, and other conserved cluster-binding residues have not been identified. In addition, [3Fe-4S] clusters have been identified in several of the FeS/AdoMet enzymes (3-7), suggesting that there is a unique iron site in these systems, one that is not ligated by a cysteine residue. AdoMet itself has several functional groups that could bind the cluster and is an appealing ligand candidate from a mechanistic perspective. It could ligate the cluster through the ribose hydroxyl groups, the amino and carboxylate moieties, or the sulfonium center. Direct binding of AdoMet to the cluster would position it for reductive cleavage and generation of the 5'-dAdo radical. All of these observations suggest that AdoMet binds directly to the cluster, but other experiments are necessary to define the nature of the interaction.

Aconitase catalyzes the interconversion citrate and isocitrate in the Krebs cycle and is an iron-sulfur cluster protein that contains a [3Fe-4S] cluster in the inactive form and a [4Fe-4S] cluster in the active form. The [4Fe-4S] cluster is ligated by three cysteines and water in the absence of substrate. Mössbauer spectroscopy is a powerful

technique in the elucidation of the roles of iron sulfur clusters. It allows the investigation of the oxidation state and coordination environment of all forms of iron in the sample. Beinert, Munck and coworkers took advantage of the isotope selective nature of Mössbauer in characterizing the iron-sulfur cluster in aconitase and its role as a Lewis acid in catalysis (8). When isolated under aerobic conditions, aconitase contains an inactive  $[3\text{Fe-4S}]^{1+}$  cluster and may be activated with iron and reductant to generate an active  $[4\text{Fe-4S}]^{2+}$  cluster. During this activation, the iron is incorporated into a unique iron site,  $\text{Fe}_a$ . By activating aconitase with  $^{57}\text{Fe}$ , the researchers obtained clusters with a powerful spectroscopic probe at the unique iron and showed that the Mössbauer and parameters were dramatically altered when bound to the substrate, isocitrate (9).

In the experiments presented in this chapter, a similar dual-isotope approach was used in combination with Mössbauer spectroscopy to show the existence of a unique iron site in PFL-AE and provide evidence that AdoMet directly binds to this site in the  $[4\text{Fe-4S}]^{2+}$  cluster.

### **III.2 Experimental Methods**

PFL-AE was expressed and purified as described in Chapter II with the inclusion of 1 mM DTT in all purification buffers. In addition, the ratio of absorbance of each PFL-AE-containing fraction was measured at 280 and 426 nm. Fractions with the highest  $A_{426}/A_{280}$  ratios (an indirect measure of iron content) that did not show a blue shift of the  $A_{280}$  peak (an indication of nucleic acid contamination) were pooled and concentrated.

### *Preparation of Specifically Labeled Samples*

The  $[3\text{Fe-4S}]^+$  cluster state was generated by exposing PFL-AE (isolated in the  $[4\text{Fe-4S}]^{2+}$  state) to air for 30 minutes on ice followed by gel filtration through a 5 ml HiTrap desalting column (Pharmacia) with 50 mM Tris, 200 mM NaCl, pH 8.5 as eluant. The red protein was collected and the amount of  $[3\text{Fe-4S}]^+$  was quantified by EPR. The iron content was determined by the method of Fish (10) and the protein concentration determined as described in Chapter II. Reconstitution with  $^{57}\text{Fe}$  was accomplished by addition of 1.4 equiv (relative to  $[3\text{Fe-4S}]^+$ ) of  $^{57}\text{FeSO}_4$  to the  $[3\text{Fe-4S}]^+$ , under an inert atmosphere, followed by addition of DTT (10 mM). The  $^{57}\text{FeSO}_4$  solution was prepared by dissolving the metal in dilute  $\text{H}_2\text{SO}_4$  followed by neutralization with hydroxide.

### **III.3 Results and Discussion**

The nature of the  $^{57}\text{Fe}$  that was incorporated into the  $[4\text{Fe-4S}]$  cluster was investigated by Mössbauer spectroscopy. A 4.2 K Mössbauer spectrum (Figure III.1A, hashed marks) of the reconstituted enzyme shows that 70% of the added  $^{57}\text{Fe}$  appears as a quadrupole doublet typical of a  $[4\text{Fe-4S}]^{2+}$  in PFL-AE, as determined in Chapter II (solid line, Figure III.1A). We estimate the amount of  $^{57}\text{Fe}$  incorporated in  $[4\text{Fe-4S}]$  clusters (365  $\mu\text{M}$ ) is comparable to the amount of  $[3\text{Fe-4S}]^+$  (380  $\mu\text{M}$ , from EPR) present prior to addition of  $^{57}\text{Fe}$  and DTT. Taken together, these data strongly suggest that under the reconstitution conditions the  $[3\text{Fe-4S}]^+$  cluster is converted into a  $[4\text{Fe-4S}]^{2+}$  cluster by selective incorporation of the  $^{57}\text{Fe}$  into the fourth, unique Fe site, a process also observed in aconitase (9). Addition of AdoMet (10 equiv) to the reconstituted enzyme yields the Mössbauer spectrum shown in Figure III.1B. The quadrupole doublet arising from the

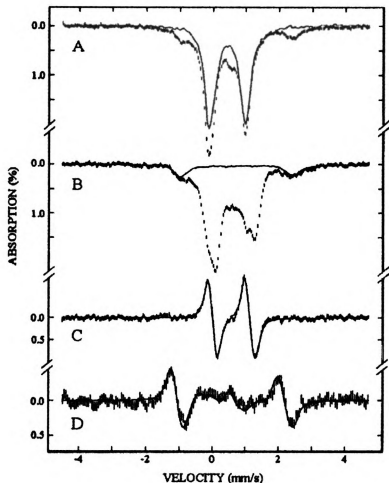


**Figure III.1** Mossbauer spectra of  $^{56}\text{Fe}$  PFL-AE reconstituted with  $^{57}\text{Fe}$  and DTT in the absence (A) and presence (B) of AdoMet.

The data (hashed marks) were recorded at 4.2 K in a magnetic field of 50 mT applied parallel to the  $\gamma$  rays. The solid line in A is the experimental spectrum of  $[\text{4Fe-4S}]^{2+}$  clusters in PFL-AE normalized to 70% of the total Fe absorption of A. The solid line in B is the spectrum of a control sample containing only the reconstitution ingredients and AdoMet but without PFL-AE and is normalized to 15% of the total Fe absorption of B. A difference spectrum of B minus A is shown in C. Spectrum D is a difference spectrum of the spectra of samples A and B recorded in a parallel field of 8 T. The solid lines in C and D are difference spectra of theoretical simulations of the unique Fe site with and without AdoMet using the parameters given in the text and assuming diamagnetism. Reproduced with permission from (11). Copyright 2002 American Chemical Society.

unique Fe site has reduced in intensity while a new quadrupole doublet appears, indicating that a portion of the unique Fe site has converted into a new Fe species. This conversion is best illustrated by a difference spectrum between A and B to eliminate contributions from Fe species that are common to both samples (Figure III.1C, B minus A, hashed marks). The amount of the unique Fe site that converts to the new Fe species appears as a doublet pointing upward and accounts for 32% of the total  $^{57}\text{Fe}$  in the sample, while the new Fe species accounting for the same portion appears as a doublet pointing downward. In the absence of AdoMet, as expected, the quadrupole splitting ( $\Delta E_Q = 1.12$  mm/s) and isomer shift ( $\delta = 0.42$  mm/s) are typical for Fe sites in a  $[\text{4Fe-4S}]^{2+}$  cluster. In the presence of AdoMet, however, the parameters ( $\Delta E_Q = 1.15$  mm/s,  $\delta = 0.72$  mm/s) are distinct, with the unusually large isomer shift signaling an increase of coordination number and/or binding of more ionic ligands, suggesting coordination of the substrate AdoMet to the unique Fe site. The solid line shown in Figure III.1C is a theoretical difference spectrum of the two doublets mentioned above.

To show that the doublets in A and B originate from Fe associated with PFL-AE and not from Fe in solution, we obtained the Mössbauer spectrum of a sample containing  $^{57}\text{Fe(II)}$ , DTT, and AdoMet but without PFL-AE. The spectrum, shown as a solid line in Figure III.1B and normalized to 15% of the Fe absorption, exhibits a broad quadrupole doublet with parameters ( $\Delta E_Q = 3.38$  mm/s,  $\delta = 0.73$  mm/s) typical of a tetracoordinate  $\text{Fe(II)S}_4$  complex. The quadrupole doublets assigned to iron-sulfur clusters of PFL-AE are not observed in the control sample.

To demonstrate that both quadrupole doublets are due to an Fe site that is part of a diamagnetic  $[\text{4Fe-4S}]^{2+}$  cluster, we have recorded the spectra of the reconstituted PFL-

AE with and without AdoMet in a parallel applied field of 8 T. A difference spectrum of the two 8-T spectra is shown in Figure 1D. The solid line overlaid with the experimental data is a theoretical difference spectrum using the parameters obtained for the two doublets mentioned above and assuming diamagnetism. The excellent agreement between theory and experiment establishes unambiguously that the two doublets are indeed arising from an iron site associated with a diamagnetic system. This observation also indicates that upon binding of the substrate, the unique Fe site remains exchange coupled to the other 3 Fe atoms in the cluster.

Analogous experiments were also done using  $^{57}\text{Fe}$ -containing PFL-AE that had been reconstituted with natural abundance iron. The Mössbauer spectra of these samples were similar to those of the specifically labeled samples, but were insensitive to the presence of AdoMet.

While the existence of a unique iron site in several Fe/S AdoMet enzymes has long been postulated, the results presented in this chapter provide the first direct evidence for such a site and suggest that AdoMet binds to this iron in a catalytically relevant manner. The observation that AdoMet binds before reduction to the catalytically active  $[4\text{Fe-4S}]^{1+}$  suggests that the bound form of the oxidized cluster represents an ES complex that is a prerequisite for radical generation. The strict conservation of the C-XXX-C-XX-C motif also suggests that such a site-differentiated cluster may be a common feature of the Fe/S-AdoMet enzymes. These three cysteine residues have been repeatedly implicated as cluster ligands, but the fourth ligand had not been identified in any AdoMet radical system. The results presented here show that AdoMet itself is a ligand to the cluster of PFL-AE.

It has been proposed that the sulfonium center of AdoMet interacts with an iron site in the reaction catalyzed by LAM (12). Using seleno-substituted AdoMet (Se-AdoMet), a Se X-ray absorption study detected 2.7 Å interaction between Se-Met (the cleavage product of Se-AdoMet). It is important to note that no such interaction was detected between AdoMet and the cluster prior to cleavage. The large Mössbauer shift observed here disfavors coordination of the sulfonium center to the cluster, however AdoMet has several other functionalities that could coordinate the cluster, specifically the amino and carboxylate groups of the methionine moiety, and the ribose hydroxyls. The change in isomer shift observed upon addition of AdoMet is insufficient to differentiate among these possibilities.

## References

1. Sofia, H. J., Chen, G., Hetzler, B. G., Reyes-Spindola, J. F., and Miller, N. E., *Nucleic Acids Res*, **2001**, *29*, 1097-106.
2. Jarrett, J. T., *Curr Opin Chem Biol*, **2003**, *7*, 174-82.
3. Petrovich, R. M., Ruzicka, F. J., Reed, G. H., and Frey, P. A., *Biochemistry*, **1992**, *31*, 10774-10781.
4. Miller, J. R., Busby, R. W., Jordan, S. W., Cheek, J., Henshaw, T. F., Ashley, G. W., Broderick, J. B., Cronan, J. E., and Marletta, M. A., *Biochemistry*, **2000**, *39*, 15166-15178.
5. Krebs, C., Henshaw, T. F., Cheek, J., Huynh, B. H., and Broderick, J. B., *J Am Chem Soc*, **2000**, *122*, 12497-12506.
6. Pierrel, F., Bjork, G. R., Fontecave, M., and Atta, M., *J Biol Chem*, **2002**, *277*, 13367-70.
7. Mulliez, E., Fontecave, M., Gaillard, J., and Reichard, P., *J Biol Chem*, **1993**, *268*, 2296-9.
8. Kent, T. A., Dreyer, J. L., Kennedy, M. C., Huynh, B. H., Emptage, M. H., Beinert, H., and Munck, E., *Proc Natl Acad Sci U S A*, **1982**, *79*, 1096-100.
9. Emptage, M. H., Kent, T. A., Kennedy, M. C., Beinert, H., and Munck, E., *Proc Natl Acad Sci U S A*, **1983**, *80*, 4674-4678.
10. Fish, W. W., *Methods in Enzymology*, **1988**, *158*, 357-364.
11. Krebs, C., Broderick, W. E., Henshaw, T. F., Broderick, J. B., and Huynh, B. H., *J Am Chem Soc*, **2002**, *124*, 912-913.
12. Cosper, N. J., Booker, S. J., Ruzicka, F., Frey, P. A., and Scott, R. A., *Biochemistry*, **2000**, *39*, 15668-15673.

## CHAPTER IV

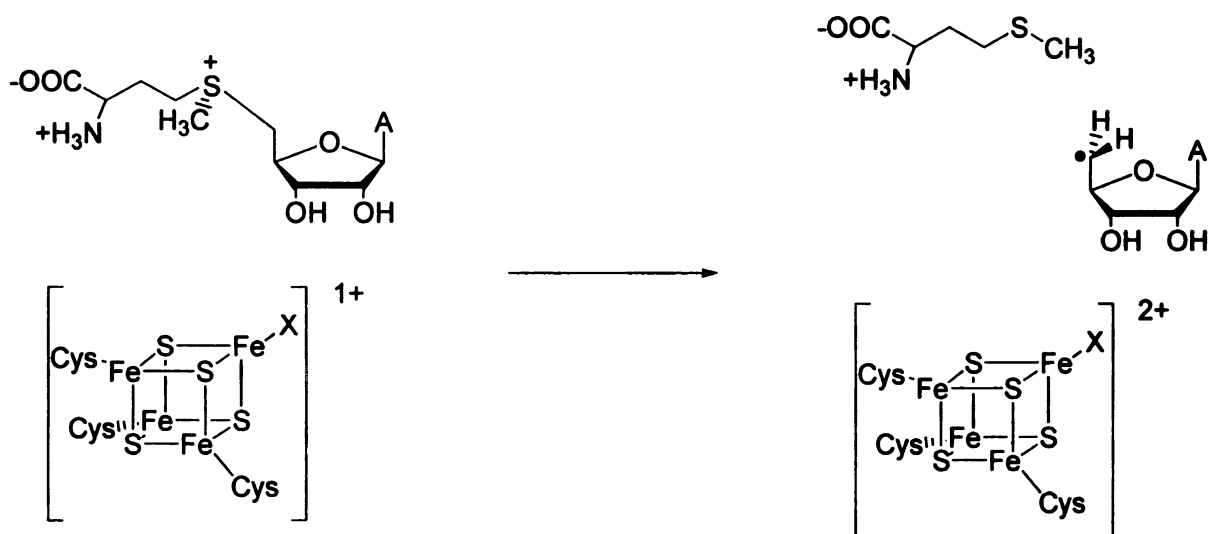
### THE ACTIVE FORM OF THE CLUSTER: SINGLE TURNOVER EXPERIMENTS

The results presented in this chapter have been published in Henshaw, T. F.; Cheek, J.;  
Broderick, J. B. *J. Am. Chem. Soc.* **2000**, *122*, 8331

## IV.1 Introduction

The work in Chapter II detailed the ability of PFL-AE to coordinate a plethora of iron-sulfur clusters and the work presented in Chapter III demonstrated that AdoMet binds to a unique iron site in the [4Fe-4S] cluster. The work in this chapter determines which cluster type is relevant in catalysis and identifies a redox role for the cluster. The reductive cleavage of AdoMet represents a two-electron reduction, one of which is supplied as a hydrogen atom that is abstracted from Gly-734 of PFL to generate the glycy radical. The source of the second electron has been difficult to conclusively identify. Since iron-sulfur clusters are well known to play redox roles, it is reasonable to propose that the cluster provides the additional electron. A primary goal of my graduate research was to determine whether this is the case by allowing PFL-AE to complete a well-characterized single turnover (1). This includes determination of the oxidation state of the cluster before turnover, confirmation of the production of a stoichiometric amount of product (the glycy radical of PFL), and characterization of the oxidation state after turnover. A reasonable proposal is that the [4Fe-4S]<sup>1+</sup> cluster provides the reducing equivalents for the generation of the putative 5'-deoxyadenosyl radical and is oxidized to the [4Fe-4S]<sup>2+</sup> state during turnover (Scheme IV.1). At the time these results were published, there were few reports that implicated the [4Fe-4S]<sup>1+</sup> cluster in FeS/AdoMet catalysis. Fontecave and coworkers had published a report that the rate of methionine production was comparable to the rate of oxidation of the [4Fe-4S]<sup>1+</sup> cluster of the ARR activating enzyme, however, the stoichiometry they observed was inconsistent with the reaction scheme (2). They observed three methionines produced for each cluster

oxidized or glycy radical produced, calling their results into question. In addition, they did not report any data that characterized the oxidation state of the cluster after turnover (2). Work with LAM showed that reduction to the  $[4\text{Fe-4S}]^{1+}$  oxidation state is required for activity (3), but AdoMet is used as a cofactor rather than a substrate in the LAM reaction and so stoichiometric cluster oxidation could not be demonstrated.



**Scheme IV.1 Proposed redox role for the iron-sulfur cluster of PFL-AE**

There were significant challenges to rigorously testing the hypothesis shown in Scheme IV.1. Even in the presence of a large excess of dithionite, EPR quantitation of the signal from the reduced cluster accounted for only a fraction of the iron in the sample, indicating that most of the cluster was not in the  $[4\text{Fe-4S}]^{1+}$  oxidation state. In addition, excess dithionite could rereduce the cluster after turnover, making characterization of the cluster after a single turnover impossible. Various attempts to remove excess reductant resulted in loss of the  $[4\text{Fe-4S}]^{1+}$  EPR signal. Ti(III) was used as a reductant, and while preliminary Mössbauer results showed that the yield of  $[4\text{Fe-4S}]^{1+}$  increased, the  $S = \frac{1}{2}$  EPR signal from excess reductant made characterization by EPR difficult.

The solution to these problems was twofold. First, the inclusion of 1 mM DTT in all purification buffers allowed for the isolation of PFL-AE that contained primarily [4Fe-4S]<sup>2+</sup> clusters rather than [3Fe-4S]<sup>+</sup> clusters. The second was the use of 5-deazariboflavin and light as reductant. I found that this method allowed for the quantitative reduction to the [4Fe-4S]<sup>1+</sup> oxidation state. In addition, since photoreduction may be used to reduce the cluster to the [4Fe-4S]<sup>1+</sup>, removal of excess reductant becomes a trivial matter, as the samples may simply be stored in the dark.

## **IV.2 Methods**

PFL-AE was expressed and purified as described in Chapter II with modifications. DTT was included at a concentration of 1 mM in all purification buffers. In addition, cells used for purification were grown in the modified MOPS medium containing natural abundance iron. PFL was purified as described. Protein and iron assays were performed as described in Chapter II.

### *Preparation of single turnover samples*

Samples were prepared in an anaerobic chamber at 0 °C using 200 μM PFL-AE (2.65 Fe/monomer) in 50 mM Hepes, 50 mM Tris (pH 7.4). 5-Deazariboflavin was added in the dark to a final concentration of 100 μM. The samples were illuminated by a 500 W halogen lamp for various times, followed by addition of AdoMet to 2 mM. In the dark, each sample was split into two, and to one an equal volume of PFL solution (200 μM PFL, 20 mM oxamate (allosteric effector), 100 μM 5-deazariboflavin) was added. Samples were stored frozen in the dark until EPR spectra were recorded.

## *EPR Spectroscopy*

EPR first-derivative spectra were obtained at X-band on a Bruker ESP300E spectrometer equipped with a liquid He cryostat and a temperature controller from Oxford Instruments. The sample spin concentrations were estimated by comparing the double integral of the sample spectrum to that of a 1.04 mM  $\text{K}_2(\text{SO}_3)_2\text{NO}$  solution (for the radical signals) or a 0.1 mM Cu(II) 1 mM EDTA solution (for the cluster signals) recorded under identical conditions.

### **IV.2 Results and Discussion**

As indicated by Scheme IV.1, single turnover conditions for PFL-AE can be achieved by limiting the amount of reductant. The clean conversion to  $[\text{4Fe-4S}]^{1+}$  provided by photoreduction has allowed us to carry out single turnover experiments for glycy radical production, since removing illumination eliminates the exogenous reductant. PFL-AE was photoreduced for various times, after which a 10-fold excess of AdoMet was added and the sample was wrapped in aluminum foil to prevent further reduction. Each sample was then split into two halves and equimolar PFL was added to one-half in the dark. EPR spectra were recorded to detect formation of  $[\text{4Fe-4S}]^{1+}$  and glycy radical in these samples. Figure 1A shows, from bottom to top, the 12 K EPR spectra of PFL-AE photoreduced in the presence of 5-deazariboflavin for 0, 1, 2, 5, 10, and 30 min. Quantitation of these EPR signals results in 0, 2.8( $\pm$ 0.5), 17( $\pm$ 2), 28( $\pm$ 3),

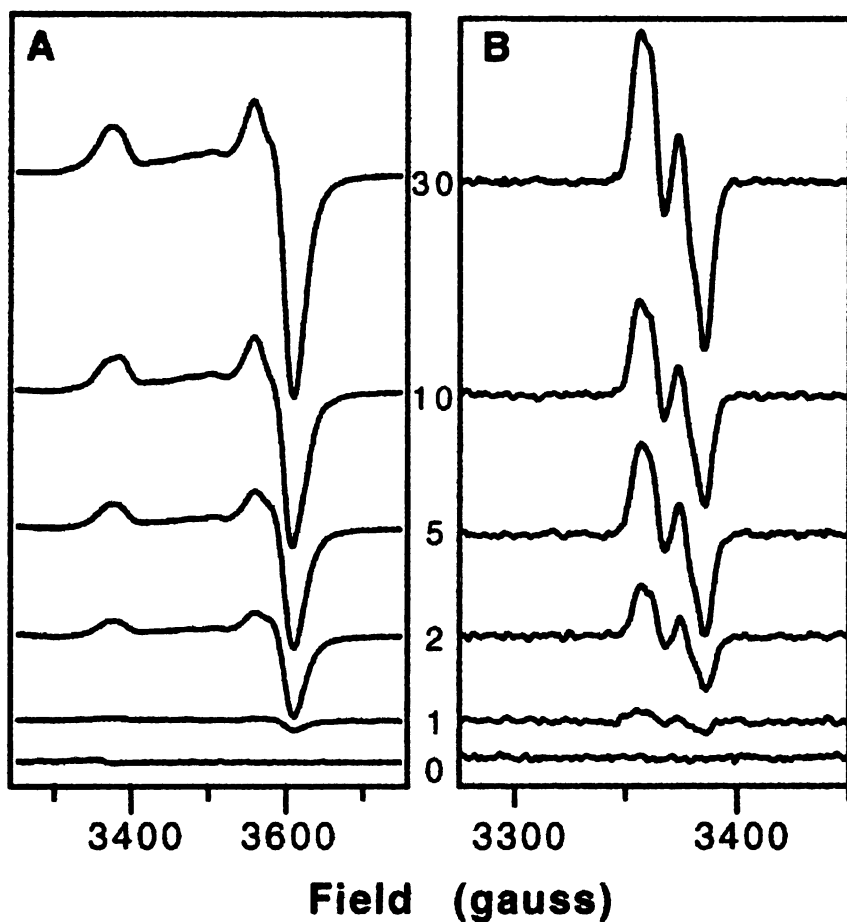


**Figure IV.1 X-band EPR spectra of photoreduced PFL-AE before and after addition of PFL.**

Panel A: EPR spectra recorded after photoreduction of PFL-AE in the presence of 5-deazariboflavin for the times indicated. Panel B: EPR spectra of the photoreduced PFL-AE samples after addition of PFL. Conditions of measurement:  $T = 12$  (A) or 60 K (B); microwave power, 2 mW (A) or 20  $\mu$ W (B); microwave frequency, 9.48 GHz; modulation amplitude, 10.084 (A) or 5.054 G (B); single scan. Protein concentrations are 200 (A) or 100  $\mu$ M (B). Reproduced with permission from (1). Copyright 2000 American Chemical Society.

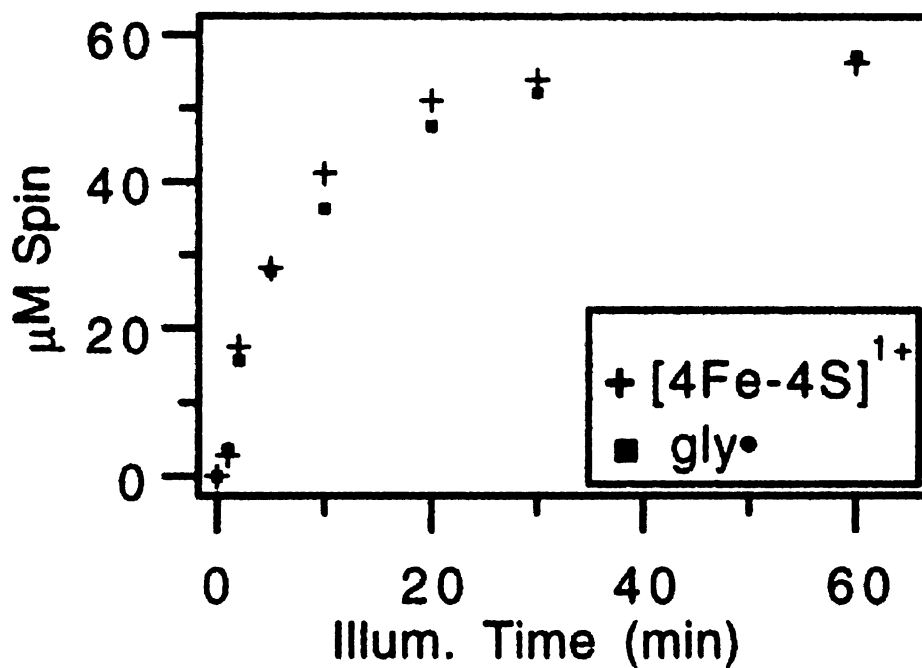


**Figure IV.2 Spin quantitation of the EPR spectra shown in Figure IV.1A ([4Fe-4S]<sup>1+</sup>) and 1B (gly•) as a function of illumination time.**

Included are additional data points for 20 min ( $51 \pm 5 \mu\text{M}$  [4Fe-4S]<sup>1+</sup> and  $48 \pm 5 \mu\text{M}$  gly•) and 60 min ( $56 \pm 6$  [4Fe-4S]<sup>1+</sup> and  $57 \pm 6 \mu\text{M}$  gly•) illumination. Reproduced with permission from (1). Copyright 2000 American Chemical Society.

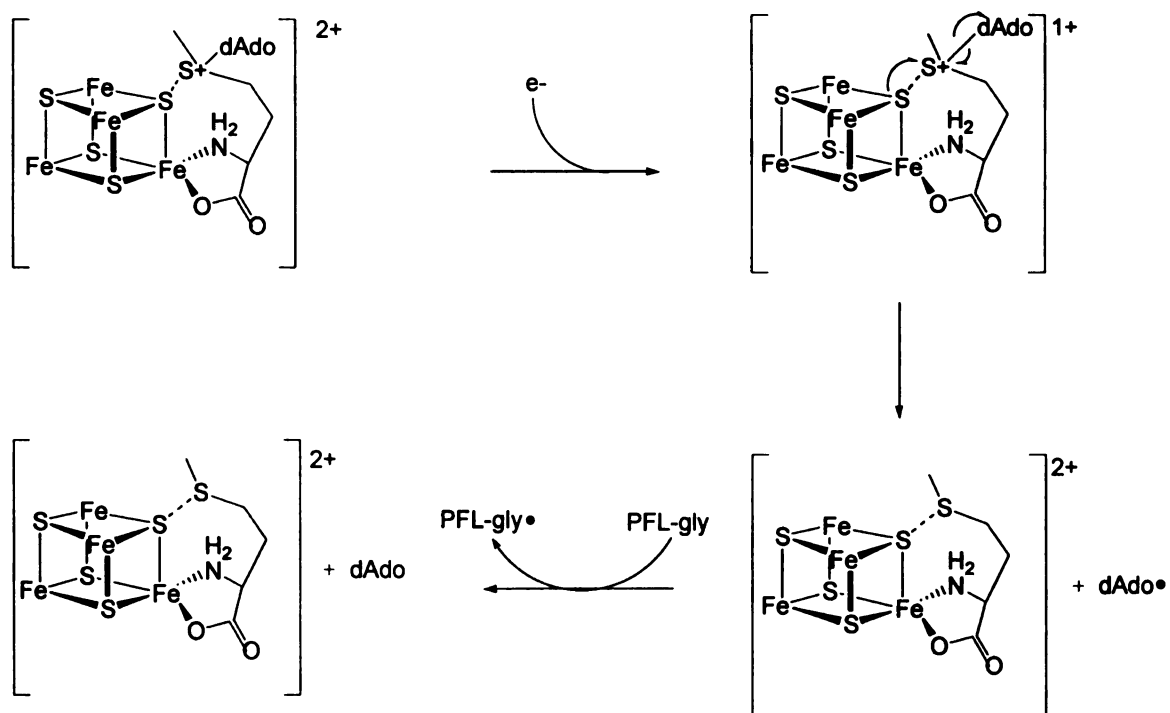
41( $\pm$ 4), and 54( $\pm$ 5)  $\mu$ M spins, respectively. The nearly axial EPR signals shown in Figure IV.1A are characteristic of a  $[4\text{Fe-4S}]^{1+}$  cluster, and are essentially identical to the EPR signal previously reported for dithionite-reduced PFL-AE in the presence of AdoMet (4). After 60 min of illumination, 85% of the cluster in PFL-AE is in the reduced  $[4\text{Fe-4S}]^{1+}$  state. Saturation of cluster reduction is indicated by the illumination time course shown in Figure 2.

EPR spectra (60 K) for samples with PFL added are shown in Figure IV.1B. Increasing amounts of a multiplet EPR signal characteristic of the PFL glycy radical are observed with increasing time. Spin quantitation of the glycy radical EPR signals at each time point show a 1:1 correspondence between the amount of glycy radical observed and the amount of  $[4\text{Fe-4S}]^{1+}$  cluster present prior to addition of PFL, as shown in Figure IV.2. The glycy radical spin quantitations are 3.6( $\pm$ 0.5), 16( $\pm$ 2), 28( $\pm$ 3), 36( $\pm$ 4), and 52( $\pm$ 5)  $\mu$ M for 1, 2, 5, 10, and 30 min illumination, respectively.

The glycy radical spectra were recorded at 60 K, a temperature at which the  $[4\text{Fe-4S}]^{1+}$  signal of PFL-AE is not observable. However, EPR spectra recorded at 12 K for the same samples also showed no  $[4\text{Fe-4S}]^{1+}$  signal. This observation demonstrates that the  $[4\text{Fe-4S}]^{1+}$  cluster has been converted to an EPR-silent state upon addition of PFL to the  $[4\text{Fe-4S}]^{1+}$ /PFL-AE/AdoMet and subsequent generation of the glycy radical. Cleavage of AdoMet is stoichiometric with PFL glycy radical generation, and requires a source of electrons. Our results strongly suggest that the required electrons come from the  $[4\text{Fe-4S}]^{1+}$  cluster, thereby converting it to an EPR-silent  $[4\text{Fe-4S}]^{2+}$  cluster. This conclusion is supported by the observation of a UV-vis spectrum which is typical of a

$[4\text{Fe-4S}]^{2+}$  cluster. In addition, the increase in  $\epsilon_{400}$  upon addition of PFL is consistent with oxidation of the  $[4\text{Fe-4S}]^{1+}$  to a  $[4\text{Fe-4S}]^{2+}$  cluster. Furthermore, re-illumination of samples containing the EPR-silent cluster can regenerate the  $[4\text{Fe-4S}]^{1+}$  EPR signal (data not shown), indicating an ability to cycle readily between the  $[4\text{Fe-4S}]^{1+}$  and  $[4\text{Fe-4S}]^{2+}$  states.

The results presented in this chapter demonstrate that the  $[4\text{Fe-4S}]^{1+}$  cluster of PFL-AE generated in the presence of AdoMet is sufficient to generate the glycy radical of PFL and is oxidized during turnover to the  $[4\text{Fe-4S}]^{2+}$  oxidation state. The results presented in Chapter III demonstrate that AdoMet binds directly to the cluster. As such, we are now prepared to propose a mechanism of radical generation that is consistent with the results presented in this dissertation (Scheme IV.2). In this mechanism AdoMet chelates the unique iron site of the  $[4\text{Fe-4S}]^{2+}$  cluster, accounting for the observed changes in the Mössbauer parameters of the unique site and positioning the sulfonium group in close proximity to one of the bridging sulfides. This binding mode was demonstrated by later ENDOR experiments (5, 6). Following reduction to the  $[4\text{Fe-4S}]^{1+}$  state, the sulfide-sulfonium interaction facilitates an inner-sphere electron transfer promoting homolytic cleavage of the sulfonium-carbon bond. This generates the 5'-deoxyadenosyl radical, which abstracts a hydrogen atom from gly-734 of PFL to generate the glycy radical.



**Scheme IV.2 Proposed Mechanism of PFL-AE**

## **CHAPTER V**

### **OXIDITAVE DNA REPAIR**

The results presented in this chapter have been published in Trewick, S. C., Henshaw, T. F., Hausinger, R. P., Lindahl, T., and Sedgwick, B., *Nature*, **2002**, *419*, 174-178.

My contribution to this work did not include radioactivity or HPLC-based assays.

## V.1 Introduction

DNA alkylating agents occur endogenously, are present in the environment and are used in chemotherapy (1, 2). *Escherichia coli* exposed to these compounds respond by inducing the expression of four genes, *ada*, *alkA*, *aidB* and *alkB*. *Ada* is an O<sup>6</sup>-methylguanine-DNA methyltransferase and regulates this adaptive response. *AlkA* is a 3-methyladenine-DNA glycosylase, and *AidB* is proposed to destroy certain alkylating agents (3). *AlkB* is conserved from bacteria to mammals, but its role has not been resolved despite the early isolation of an *E. coli alkB* mutant (4). Expression of *E. coli alkB* confers alkylation resistance to human cells (5), and conversely, a human homologue has been reported to convey methyl methanesulphonate (MMS) resistance to the *E. coli* mutant (6). *AlkB* processes the cytotoxic DNA damage generated in single-stranded DNA by S<sub>N</sub>2 methylating agents, such as MMS, dimethylsulphate (DMS) and methyl iodide (7). 1-Methyladenine (1me-A) and 3-methylcytosine (3-meC) are predominant forms of base damage in single-stranded DNA because the sites of methylation are normally protected by base pairing (8, 9). These lesions are cytotoxic because they stall DNA replication, and are not removed by known DNA repair pathways. 1-Methyladenine and 3-methylcytosine in DNA were previously proposed as candidate substrates of *AlkB*, nevertheless, many attempts to develop assays for this enzyme were unsuccessful (10). Theoretical sequence profile and fold recognition searches suggested that *AlkB* an  $\alpha$ -ketoglutarate- and Fe(II)-dependent dioxygenase (11). The results in this chapter demonstrate DNA repair activity for *AlkB* using DNA substrates containing 1-methyladenine or 3-methylcytosine,  $\alpha$ -ketoglutarate as a co-substrate, and Fe(II) as a cofactor.

## V.2 Experimental Methods

### *Expression and purification of AlkB*

AlkB with an N-terminal was purified as previously described (10) with the inclusion of 1 mM EDTA in purification buffers. EDTA was removed following purification by extensive dialysis against 50 mM HEPES, 100 mM NaCl, 5 % glycerol (w/v) pH 8.

### *Radioactive substrates and assays*

A total of 0.6 mg poly(dA) (average length 310 residues; Amersham Biosciences) was treated with 1 mCi [<sup>14</sup>C]methyl iodide (58 mCi mmol<sup>-1</sup>) (Amersham Biosciences) in 0.8 ml of 10 mM sodium cacodylate, pH 7, at 30 °C for 6 h. The methylated polymer was precipitated in ethanol, dissolved in 10 mM Tris-HCl, pH 8, and had a specific activity of 1,860 counts per min (c.p.m.) per μg. To prepare a double-stranded substrate, [<sup>14</sup>C]-labelled methylated poly(dA) was annealed to poly(dT) at 20 °C. A total of 1.2 mg poly(dC) (average length 370 residues) in 1.3 ml of 50 mM HEPES-KOH, pH 8, was similarly treated with [<sup>14</sup>C]methyl iodide to yield a specific activity of 700 c.p.m. μg<sup>-1</sup>. A plasmid coding for Flag-tagged AlkB was constructed by digestion of pBAR54 (10) with *NdeI* and *NcoI* to remove DNA coding for the His tag. This DNA fragment was replaced by a double-stranded oligonucleotide coding for the Flag tag. The Flag-tagged protein was purified by immunoaffinity chromatography (Sigma). Purified AlkB was incubated with the [<sup>14</sup>C]methyl iodide-treated substrates in 50 mM HEPES-KOH, pH 8, 75 μM

$\text{Fe}(\text{NH}_4)_2(\text{SO}_4)_2 \cdot 6\text{H}_2\text{O}$ , 1 mM  $\alpha$ -ketoglutarate, 2 mM ascorbate, and  $50 \mu\text{g ml}^{-1}$  BSA for 15 min at 37 °C. The reaction was stopped by adding 11 mM EDTA, and the substrate was precipitated in ethanol in the presence of carrier calf thymus DNA. Ethanol-soluble radioactive material was monitored by scintillation counting.

#### *HPLC assays*

Methylated adenine residues were released from [ $^{14}\text{C}$ ]-methylated poly(dA) by hydrolysis in 0.1 M HCl at 95°C for 1 h, and 3-meC from methylated poly(dC) by treatment with 90% formic acid at 180°C for 20 min. Methylated bases were analyzed by HPLC on a Whatman Partisil 10 cation exchange column in 0.1 M ammonium formate, pH 3.6. A gradient of MeOH from 20 to 40% was applied to separate the methylated adenine derivatives, and a gradient from 5 to 40% MeOH was used to analyze 3-meC.

#### *High-level methylation of an oligonucleotide*

A 41-mer oligonucleotide, TTTTTT(ATTTTTT)<sub>5</sub>, was treated with 50 mM DMS in 75 mM sodium cacodylate, pH 7.4, at 30°C, 2 times for 2 h and then 4 times for 1 h. Between each treatment the DMS was removed by centrifugation through a G25 Sephadex mini-column equilibrated in the same buffer. The level of methylation of adenine residues was examined by acid hydrolysis, HPLC and  $A_{260}$  measurements. The  $A_{260}$  ratio of adenine to 1-meA was 1.04 which was determined by monitoring known amounts of these purines in the same conditions.

### *UV-visible spectroscopy*

Samples containing AlkB (0.35 mM) and  $\alpha$ -KG (1.2 mM) in 50 mM HEPES, 100 mM NaCl, 5 % glycerol (w/v) pH 8 were sealed with a rubber septum in a 1 cm pathlength quartz cuvette. The enzyme was made anaerobic by several rounds of evacuating and refilling the cuvette with argon. A background spectrum was recorded and ferrous ammonium sulfate was added (using a gas-tight Hamilton syringe) to a final concentration of 0.3 mM from an anaerobic stock and the UV-vis spectrum was again recorded.

### *Gas chromatography/mass spectrometry*

Oligo(dA) (25-mer) was treated with 500 mM MMS at 30°C for 30 min and, after removal of the MMS, annealed to oligo(dT). AlkB (38  $\mu$ M) was incubated with this substrate (50  $\mu$ M) in 50 mM HEPES-KOH, pH 8, containing 1 mM  $\alpha$ KG, 75  $\mu$ M  $\text{Fe}(\text{NH}_4)_2(\text{SO}_4)_2 \cdot 6\text{H}_2\text{O}$ , and 2 mM ascorbate in a final volume of 200  $\mu$ l. After 10 min at 30°C, 200  $\mu$ l 15 mM PFPH in 1.2 M phosphoric acid was added, and incubation continued at 50°C for 2 h. The reaction mixtures were extracted with 100  $\mu$ l of 85:15 hexane:dichloromethane, and 20  $\mu$ l was analyzed by GC/MS as described (12).

### *Oxygen consumption*

50 mM HEPES, pH 8, with 1 mM  $\alpha$ KG, 75  $\mu$ M  $\text{Fe}(\text{NH}_4)_2(\text{SO}_4)_2 \cdot 6\text{H}_2\text{O}$ , 100  $\mu$ M ascorbate, and 50  $\mu$ M oligonucleotide substrate, prepared as described for GC/MS, were mixed for 3 min in a YSI 5300 oxygen electrode at 30°C to allow equilibration with

atmospheric oxygen. The electrode was precalibrated with air saturated water (236  $\mu\text{M}$   $\text{O}_2$ ). AlkB was added through a gas tight syringe to a final concentration of 9  $\mu\text{M}$ .

### V.3 Results and Discussion

#### *Release of ethanol-soluble radioactivity*

A substrate containing  $^{14}\text{C}$ -labelled methylated adenine residues was prepared by treating poly(dA) with [ $^{14}\text{C}$ ]methyl iodide. In the presence of  $\alpha$ -ketoglutarate and Fe(II), purified His-tagged AlkB protein released ethanol-soluble radioactive material from this methylated substrate (Figure V.1A). Similar activity was also observed with Flag-tagged AlkB protein (data not shown). The activity was dependent on  $\alpha$ -ketoglutarate, inhibited by EDTA and stimulated by ascorbate (Figure V.1B). Inhibition by EDTA was overcome by adding an excess of  $\text{Fe}(\text{NH}_4)_2(\text{SO}_4)_2 \cdot 6\text{H}_2\text{O}$ , thus demonstrating a requirement for Fe(II). At 100-fold higher AlkB concentrations, the effect of ascorbate was reduced. To determine whether AlkB could also act on double-stranded DNA, the [ $^{14}\text{C}$ ]-labelled methylated poly(dA) was annealed to poly(dT). AlkB was approximately threefold more active on the double- compared with the single-stranded substrate (Figure V.1C).

#### *UV-visible spectroscopy*

Figure V.1D shows the visible difference spectrum of an anaerobic AlkB sample in the presence of Fe(II) and  $\alpha$ -KG which exhibits a weak chromophore at 500 nm and is attributed to a metal to ligand charge transfer transition that is characteristic of the Fe(II)/ $\alpha$ KG dioxygenases (13-15). This chromophore was not observed in the absence of

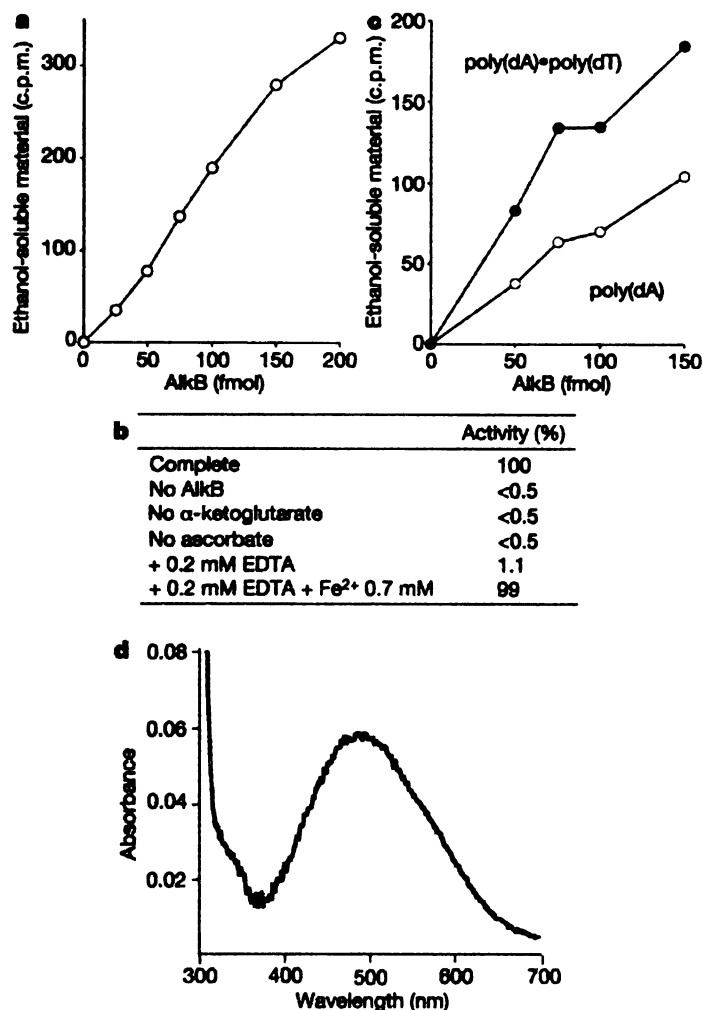
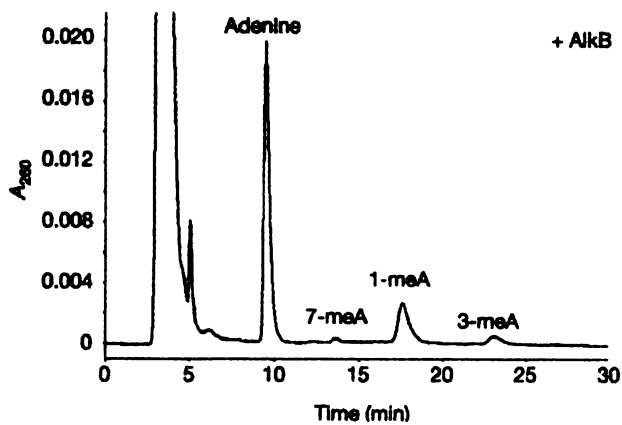
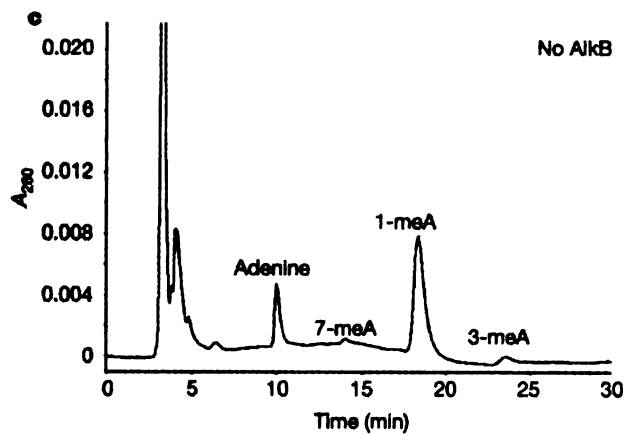
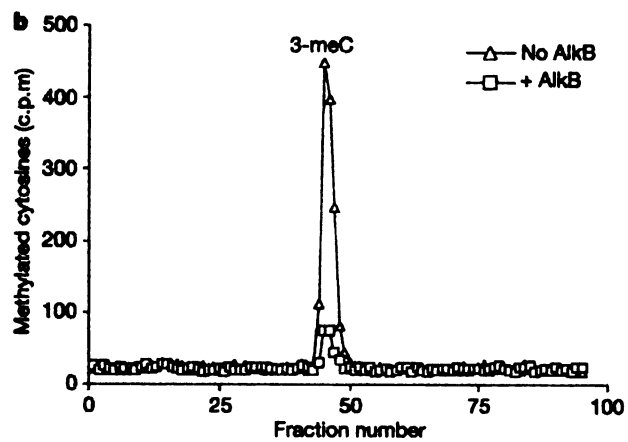
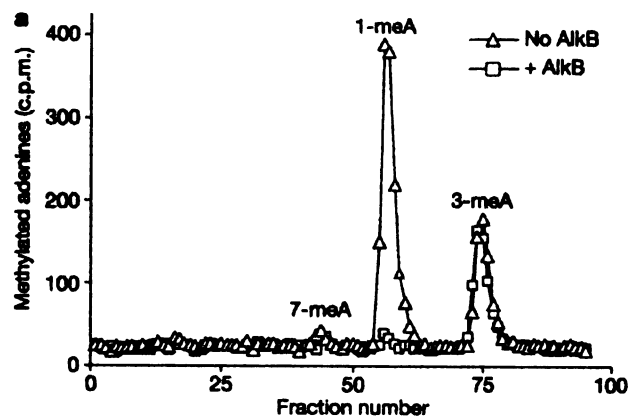


**Figure V.1 Release of ethanol-soluble material from methylated poly(dA) by AlkB in the presence of Fe(II) and  $\alpha$ -ketoglutarate.**

**a**, [<sup>14</sup>C]Methyl iodide-treated poly(dA) (1,200 c.p.m.) was incubated with AlkB in the complete reaction mixture, and the release of radioactive material was monitored. **b**, Requirements for AlkB activity (2 pmol AlkB). **c**, Comparison of AlkB activity on [<sup>14</sup>C]-labelled methylated poly(dA) (1,200 c.p.m.) (open circles) and after annealing to poly(dT) (filled circles), assayed at 20 °C for 30 min to maintain stable duplexes. **d**, Difference absorption spectrum of anaerobic AlkB (0.35 mM) in the presence of  $\alpha$ -ketoglutarate (1 mM) and Fe(II) (0.3 mM) minus the spectrum without Fe(II).

**Figure V.2 Repair of 1-methyladenine (1-meA) and 3-methylcytosine (3-meC) by AlkB.**

**a, b,** [<sup>14</sup>C]Methyl iodide-treated poly(dA) (**a**) or poly(dC) (**b**) were incubated without AlkB (triangles) or with 2.5 pmol AlkB (squares). The [<sup>14</sup>C]-labelled methylated bases remaining in the substrates were analysed by HPLC and scintillation counting. 3-meA and 7-meA, 3- and 7-methyladenine, respectively. **c,** Direct reversion of 1-methyladenine to adenine by AlkB. A thymine-rich oligodeoxynucleotide containing five adenine residues was heavily methylated and then incubated without (top) or with (bottom) 920 pmol AlkB at 37 °C for 30 min. The bases present in the oligonucleotide were analysed by HPLC and *A*<sub>260</sub> measurements. The early eluting peaks were oligo(dT) fragments.



$\alpha$ -KG or iron and provides strong evidence that AlkB coordinates Fe(II) in a 2-His-1-Asp facial triad (16) and that  $\alpha$ -KG chelates the iron.

#### *Identification of 1-meA and 3-meC as AlkB substrates*

To examine which methylated adenines were processed by AlkB, the poly(dA) substrate was incubated with AlkB, acid hydrolysed, and analysed by high-performance liquid chromatography (HPLC). In the poly(dA) polymer treated with [ $^{14}$ C]methyl iodide, 1-methyladenine was the principal methylated base, 3-methyladenine was also abundant, but 7-methyladenine was a minor product. After incubation with AlkB, the levels of 1-methyladenine were reduced whereas the amounts of 3-methyladenine and 7-methyladenine remained unchanged (Figure V.2A). Thus, AlkB specifically catalyzed removal of 1-methyladenine from methylated poly(dA). From the data in Figure V.1A, 0.1 pmol AlkB protein removed 1.7 pmol 1-methyladenine from methylated poly(dA) in 15 min, indicating that AlkB acts enzymatically and is not consumed during the reaction. This distinguishes its mode of action from O<sup>6</sup>-methylguanine-DNA methyltransferase.

A second modification that is formed to a greater extent in single- compared with double-stranded DNA is 3-methylcytosine. This lesion was also considered as a candidate substrate of AlkB. AlkB protein released radioactive material from poly(dC) treated with [ $^{14}$ C]methyl iodide (data not shown). HPLC analysis showed that 3-methylcytosine was the only detectable modified base in this substrate, and that it disappeared on incubation with AlkB (Figure V.2B). We have therefore identified two substrates of AlkB, 1-methyladenine and 3-methylcytosine, that are both generated in single-stranded DNA on treatment with S<sub>N</sub>2 methylating agents.

It is proposed that AlkB repairs 1-meA and 3-meC in DNA by oxidative demethylation. In such a mechanism, the lesions would be reverted to adenine and cytosine, formaldehyde would be generated and O<sub>2</sub> consumed. To demonstrate that AlkB directly reverts 1-meA in DNA to adenine residues, a non-radioactive substrate was prepared in which 76% of the adenine residues were methylated to form 1-meA. This was achieved by repeated treatments with DMS of an oligonucleotide containing adenine residues interspersed between inefficiently methylated thymine residues. Only 4% of the adenines were recovered as 3-meA, and 2% were 7-meA (Figure V.2C). The low amount of 3-meA might be caused by instability of the glycosyl bond and loss of this modification during the extensive DMS treatments. The heavily methylated substrate was incubated with AlkB in the optimized assay conditions, the DNA hydrolyzed and individual bases quantified by HPLC and A<sub>260</sub> measurements. In the presence of AlkB, a decrease in the amount of 1-meA correlated with a stoichiometric increase in the amount of adenine recovered (Figure V.2C). It is concluded that AlkB converts 1-meA directly to adenine in DNA.

#### *Formaldehyde release and oxygen consumption*

To determine whether formaldehyde was a reaction product, AlkB was incubated with MMS-treated poly(dA) annealed to poly(dT), the products were derivatised with pentafluorophenylhydrazine (PFPH) and analysed by gas chromatography (GC). One derivatised product, as indicated by the arrow in Figure V.3A, arose only when the DNA substrate was methylated and Fe(II) and  $\alpha$ KG were present (Figure V.3B), and had a mass spectrum (MS) identical to that previously described for the HCHO-PFPH adduct (12)(Figure V.3C). The release of HCHO was also monitored by a coupled

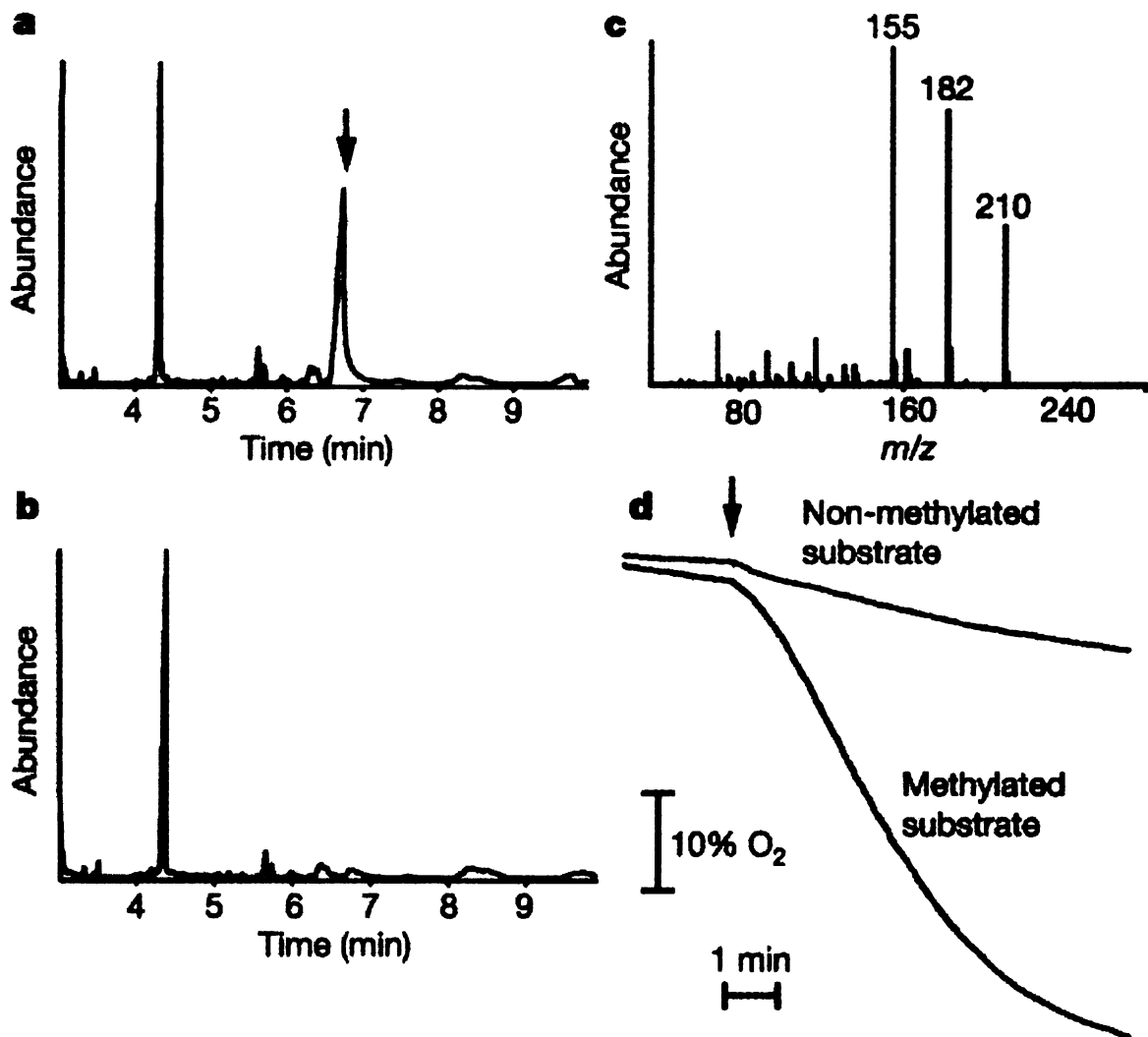


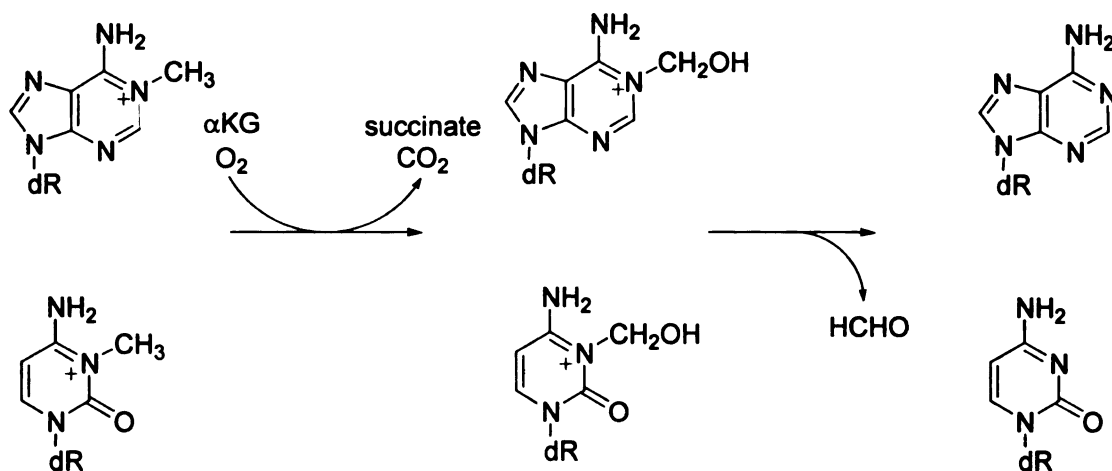
**Figure V.3 Production of formaldehyde and consumption of O<sub>2</sub> by AlkB.**

Methylated oligo(dA)•oligo(dT) was incubated with AlkB. The products were derivatized with PFPH and analysed by gas chromatography mass spectrometry. Gas chromatography traces are shown of derivatized products generated when the DNA was methylated (a) or not methylated (b). c, Mass spectrum of the product indicated by the arrow in a. d, Consumption of O<sub>2</sub> during incubation of AlkB with either methylated or non-methylated oligo(dA)•oligo(dT) was determined by using an oxygen electrode. AlkB (9 μM) was added at the point indicated by the arrow.

spectrophotometric assay using formaldehyde dehydrogenase (17), and again was detected only in complete assay conditions with the heavily methylated DNA substrate (turnover number  $1.5 \text{ s}^{-1}$ , data not shown). A yield of  $140 \text{ }\mu\text{M}$  HCHO correlated stoichiometrically with the amount of 1-meA in the DNA substrate (7-10% of the adenines), the amount of  $\text{O}_2$  consumed (Figure V.3D) and the succinate generated (data not shown). This stoichiometric relationship further verifies the proposal that AlkB is an  $\alpha\text{KG}$ -dependent dioxygenase. In the absence of methylated DNA, an observed slow consumption of oxygen (Figure V.3D) and  $\alpha\text{KG}$  was consistent with a partial uncoupling of  $\alpha\text{KG}$  decomposition and hydroxylation of the methylated DNA bases. Such uncoupling is a well-known property of this family of enzymes (18, 19).

Oxidative demethylation is an unprecedented mechanism of DNA repair. The proposed reaction mechanism by which AlkB repairs 1-meA and 3-meC in DNA is shown in Scheme V.1. Due to the stability of the N-C bond in 1-meA and 3-meC, demethylation by hydrolysis would be energetically unfavorable; consequently oxidative demethylation by reactive iron-oxygen species is required. Direct reversal of this base damage to unsubstituted parent residues would be a highly accurate form of DNA repair and agrees with *in vivo* observations that repair by AlkB is non-mutagenic (10). *E. coli alkB* mutants are more sensitive to alkylating agents during active growth than in stationary phase probably because 1-meA and 3-meC are produced in single-stranded regions of DNA in replication forks and transcription bubbles (10). DNA unfolds only transiently during replication and transcription, so it is beneficial that AlkB repairs its substrates not only in single-strands but also, and even more efficiently, after DNA

reannealing (Figure V.1). Interestingly, *Caulobacter crescentus alkB* expression is cell cycle regulated with a pattern similar to activities required for DNA replication (20).



**Scheme V.1 Oxidative DNA repair mechanism catalyzed by AlkB**

We have extended the family of  $\alpha$ KG-Fe(II) dependent dioxygenases to include AlkB, as recently proposed on theoretical grounds (11). These enzymes catalyse a variety of reactions including hydroxylations, desaturations and oxidative ring closures, and account for oxidation of proline in collagen, steps in the biosynthesis of several antibiotics and cellular metabolites, as well as biodegradation of selected compounds (21). No other members of this family are presently known to act on DNA, but it is notable that a fungal enzyme, thymine-7-hydroxylase, oxidises the methyl group of free thymine (22, 23).

## References

1. Rebeck, G. W. and Samson, L., *Journal of Bacteriology*, **1991**, *173*, 2068-2076.
2. Vaughan, P., Sedgwick, B., Hall, J., Gannon, J., and Lindahl, T., *Carcinogenesis*, **1991**, *12*, 263-268.
3. Lindahl, T., Sedgwick, B., Sekiguchi, M., and Nakabeppu, Y., *Annu Rev Biochem*, **1988**, *57*, 133-57.
4. Kataoka, H., Yamamoto, Y., and Sekiguchi, M., *Journal of Bacteriology*, **1983**, *153*, 1301-1307.
5. Chen, B. R. J., Carroll, P., and Samson, L., *Journal of Bacteriology*, **1994**, *176*, 6255-6261.
6. Wei, Y. F., Carter, K. C., Wang, R. P., and Shell, B. K., *Nucleic Acids Research*, **1996**, *24*, 931-937.
7. Dingley, S., Gold, B., and Sedgwick, B., *Mutation Research-DNA Repair*, **1998**, *407*, 109-116.
8. Singer, B. and D., G., *Molecular Biology of Mutagens and Carcinogens: Reactions of Directly Acting Agents with Nucleic Acids*. 1983, New York: Plenum Press.
9. Bodell, W. J. and Singer, B., *Biochemistry*, **1979**, *18*, 2860-2863.
10. Dingley, S., Trewick, S. C., Lindahl, T., and Sedgwick, B., *Genes & Development*, **2000**, *14*, 2097-2105.
11. Aravind, L. and Koonin, E. V., *Genome Biol*, **2001**, *2*, RESEARCH0007.
12. Heck, H. D., White, E. L., and Casanovaschmitz, M., *Biomedical Mass Spectrometry*, **1982**, *9*, 347-353.
13. Ryle, M. J., Padmakumar, R., and Hausinger, R. P., *Biochemistry*, **1999**, *38*, 15278-86.
14. Hegg, E. R., Ho, R. Y. N., and Que, L., Jr., *Journal of the American Chemical Society*, **1999**, *121*, 1972-1973.
15. Pavel, E. G., Zhou, J., Busby, R. W., Gunsior, M., Townsend, C. A., and Solomon, E. I., *Journal of the American Chemical Society*, **1998**, *120*, 743-753.
16. Hegg, E. L. and Que, L., Jr., *Eur J Biochem*, **1997**, *250*, 625-9.
17. Lizcano, J. M., Unzeta, M., and Tipton, K. F., *Anal Biochem*, **2000**, *286*, 75-9.

18. Myllyla, R., Majamaa, K., Gunzler, V., Hanauske-Abel, H. M., and Kivirikko, K. I., *J Biol Chem*, **1984**, *259*, 5403-5.
19. de Jong, L., Albracht, S. P., and Kemp, A., *Biochim Biophys Acta*, **1982**, *704*, 326-32.
20. Colombi, D. and Gomes, S. L., *Journal of Bacteriology*, **1997**, *179*, 3139-3145.
21. Hausinger, R. P., *Crit Rev Biochem Mol Biol*, **2004**, *39*, 21-68.
22. Thornburg, L. D. and Stubbe, J., *Biochemistry*, **1993**, *32*, 14034-42.
23. Thornburg, L. D., Lai, M. T., Wishnok, J. S., and Stubbe, J., *Biochemistry*, **1993**, *32*, 14023-33.

## CHAPTER VI

### ABBERANT ACTIVITY OF THE DNA REPAIR ENZYME ALKB

The results presented in this chapter have been published in Henshaw, T. F., Feig, M., and Hausinger, R. P., *J Inorg Biochem*, **2004**, 98, 856-61.

## VI.1 Introduction

AlkB and its human homologues belong to a family of enzymes known as the iron(II)- and alpha-ketoglutarate ( $\alpha$ KG)-dependent dioxygenases (1). Like other family members, they activate dioxygen at a redox-active mononuclear center and abstract a hydrogen atom from a chemically non-reactive C-H bond to initiate transformations that can include hydroxylations, ring closures, desaturations, and other reactions. An additional key feature of most of these enzymes is their ability to couple the oxidative decarboxylation of  $\alpha$ KG to oxygen reduction; thus generating a putative Fe(IV)-oxo intermediate. Evidence for the production of an Fe(IV) intermediate was obtained in another family member, taurine/ $\alpha$ KG dioxygenase (TauD) (2-4), and model studies have demonstrated that Fe(IV)-oxo species can be generated at a mononuclear site (5). Also consistent with the intermediacy of an Fe(IV)-oxo species is the finding of enzyme self-hydroxylation reactions in other family members (6-8). For example, in the presence of  $\alpha$ KG, but absence of taurine, TauD oxidizes Tyr 73 located near the active site to form a tyrosyl radical that converts to a catechol (8). Coordination of the catechol side chain to the oxidized metal site creates greenish-brown ( $\lambda_{\max}$  550 nm;  $\epsilon_{550} \sim 700 \text{ M}^{-1}\text{cm}^{-1}$ ) or green ( $\lambda_{\max}$  700 nm;  $\epsilon_{700} \sim 380 \text{ M}^{-1}\text{cm}^{-1}$ ) ligand-to-metal charge-transfer (LMCT) chromophores, depending on whether bicarbonate is present (6). Similarly, in the absence of its primary substrate 2,4-dichlorophenoxyacetic acid (2,4-D), but presence of  $\alpha$ KG, the 2,4-D/ $\alpha$ KG dioxygenase TfdA hydroxylates Trp 113, a residue located adjacent to a metal ligand of this protein (7). Coordination of the hydroxytryptophan (OH-Trp) to the oxidized metal center yields a blue chromophore ( $\lambda_{\max}$  580 nm;  $\epsilon_{580}$

$\sim 1000 \text{ M}^{-1} \text{ cm}^{-1}$ ). These self-hydroxylation reactions are likely to arise from side reactions of the highly activated Fe(IV)-oxo species.

In this chapter, I provide evidence that AlkB also catalyzes self-oxidation of an amino acid side chain when incubated with Fe(II),  $\alpha$ KG, and oxygen in the absence of its primary substrate, methylated DNA/RNA. This hydroxylated residue coordinates the oxidized metal site to produce a blue chromophore, analogous to that observed in TfdA. On the basis of mass spectrometric evidence, we identify the modification as hydroxylated Trp 178. Modeling of the AlkB structure provided evidence that Trp 178 is appropriately positioned near the metallocenter to undergo the observed oxidation chemistry.

## **VI.2 Experimental**

### *Sample Preparation*

His-tagged AlkB was overproduced in *E. coli* BL21(DE3) [pBAR54] and purified as described in Chapter VI. Significantly, cell disruption was carried out in buffers containing ethylenediaminetetraacetic acid (EDTA) to chelate the Fe(II) that is weakly bound to the enzyme and minimize any oxidative damage to the protein sample during purification.

### *UV-visible (UV-vis) spectroscopy*

A cuvette containing 500  $\mu\text{l}$  of AlkB (240  $\mu\text{M}$  protein in 50 mM Hepes buffer, pH 8.0, with 300 mM NaCl) was made anaerobic by several rounds of vacuum and argon on an anaerobic Schlenk line. Ferrous ammonium sulfate was added from an anaerobic

stock (10 mM) to a final concentration of 200  $\mu$ M.  $\alpha$ KG was added to a concentration of 1 mM. The enzyme was oxidized at room temperature ( $\sim$ 23 $^{\circ}$  C) by the addition of 300  $\mu$ L of water that had been saturated with O<sub>2</sub> at atmospheric pressure. The headspace of the cuvette was replaced with pure O<sub>2</sub>. UV-vis spectra were recorded at times indicated in the figure using a Beckman DU 7500 diode array spectrophotometer.

### *Mass Spectrometry (MS)*

MS samples were run by Brett Phinney of the MSU Mass Spectrometry Facility.

AlkB samples were extensively dialyzed, diluted to a concentration of 1 nmole in 50  $\mu$ l of 100 mM ammonium bicarbonate buffer (pH 8.0), digested overnight with sequencing-grade modified trypsin (Promega) (1:40 molar ratio) at 37 $^{\circ}$ C, and analyzed by nanoscale liquid chromatography mass spectrometry/mass spectrometry (LC/MS/MS). 500 fmole aliquots were applied to a picofrit column (75  $\mu$ m i.d. x 5 cm) packed with 3  $\mu$ m Magic C-18 material (Micron Bioresources). Mobile phase A consisted of 0.1% formic acid while mobile phase B consisted of 0.1% formic acid in 90/10 acetonitrile/water. Peptides were eluted during a 25 min gradient extending from 2% B to 60% B. The picofrit column made electrical contact through a pre-column ZDV titanium union, terminating in a 8  $\mu$ m tip i.d. outlet spray needle. Mass spectra were acquired by data dependent analysis in a Micromass Q-TOF Ultima mass spectrometer, where peptide ions detected in the MS survey scans triggered MS/MS fragmentation for obtaining product ion spectra. In order to identify peptides in the digest, the Mascot search engine was used to search the AlkB sequence.

## *Structural Modeling*

Structural modeling was done by Michael Feig of the MSU Physics Department.

The structure for *E. coli* AlkB was predicted based on fold recognition in a functionally related oxidoreductase (deacetoxycephalosporin C synthase from *Streptomyces clavuligerus*) where the structure is available from crystallography (PDB codes: 1DCS and 1RXG). This structure was identified as the best template with the Bioinfo Meta Server (<http://bioinfo.pl/Meta>) (9). The alignment of secondary structure elements, as generated with the ORFeus method (10), was used to generate a structure scaffold by comparative modeling, where side chains in the template structure are replaced with the corresponding amino acids in *E. coli* AlkB. Connecting loops and other missing fragments were then added with the MMTSB Tool Set (11) by sampling conformational space with a low-resolution lattice model (12) and selecting the most favorable conformation based on clustering and an all-atom energy scoring function (13). The position of the  $\alpha$ KG ligand and Fe(II) were copied from the 1RXG crystal structure where the ligands were present. The complete structure including the ligand and iron was then minimized for 1000 steps with the molecular mechanics program CHARMM (14) under harmonic restraints to keep backbone and C $\beta$  atoms near their initial positions. The ligand and iron were fixed during the minimization.

## VI.3 Results and Discussion

### *Chromophore Formation*

The addition of  $\alpha$ KG and Fe(II) to AlkB under anaerobic conditions generates a weak metal-to-ligand charge-transfer (MLCT) absorption at 450-500 nm (Chapter V and (15)). When mixed with oxygen-saturated water, the pink color associated with this species disappeared and was replaced by a more intense blue chromophore ( $\epsilon_{590}$  960 M<sup>-1</sup>cm<sup>-1</sup> on the basis of iron concentration) with an absorption centered at 595 nm (Figure VI.1). The slow color transformation occurred in two phases, with the relatively rapid disappearance of the  $\alpha$ KG/Fe(II) chromophore (note the decrease in absorption at ~500 nm) preceding the increase of the 595 nm absorption. Full development of the blue chromophore required more than 10 min and followed an approximate first-order process ( $0.36 \pm 0.05$  min<sup>-1</sup> when measured starting at 2 min). Incubation of the sample under vacuum and exchange with an anaerobic atmosphere did not affect the blue color. Addition of dithionite to reduce the sample led to protein precipitation. In contrast to the situation for  $\alpha$ KG/Fe(II)AlkB, no color was generated when Fe(II)AlkB lacking  $\alpha$ -keto acid was mixed with oxygen-saturated water. The behavior observed here for AlkB and the resulting 595 nm spectrum are very similar to what was previously reported for TfdA, where the chromophore was attributed to the development of a LMCT transition involving OH-Trp coordinated to Fe(III) (7).

### *Mass spectrometric analysis*

A hydroxylated Trp side chain of AlkB was identified by nanoscale capillary LC/MS/MS analysis. In this analysis, AlkB samples were first extensively dialyzed, diluted into ammonium bicarbonate (a volatile buffer), and digested with trypsin before injection. This method allows for very accurate and sensitive determinations of post-translationally modified amino acids within a protein. Using this approach, clear evidence was obtained for hydroxylation of a Trp side chain at position 178 (with numbering on the basis of the translated gene sequence). Product ion spectra revealed

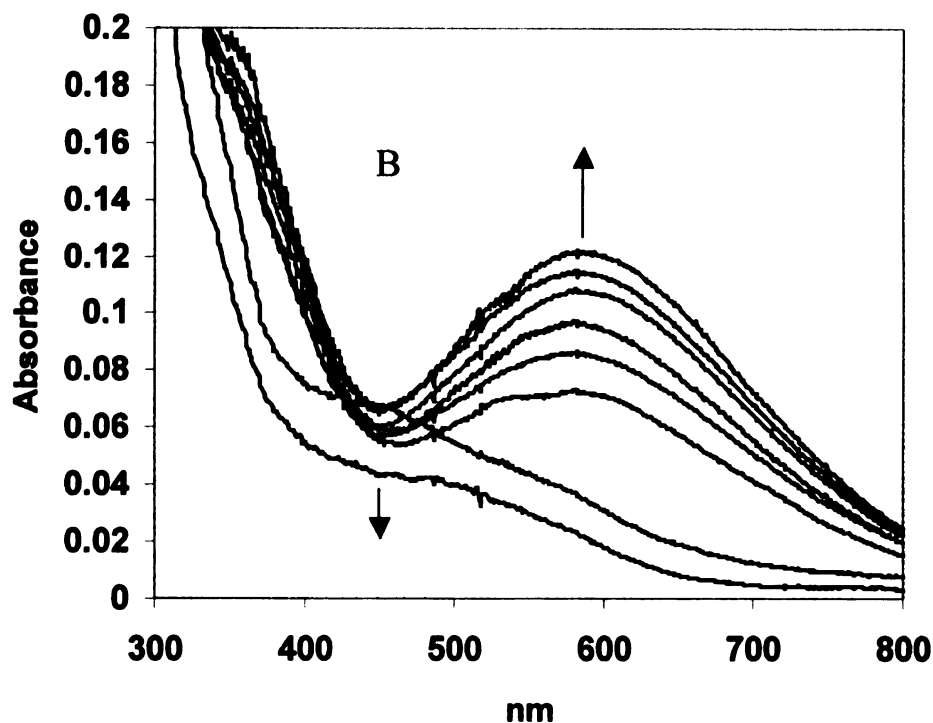
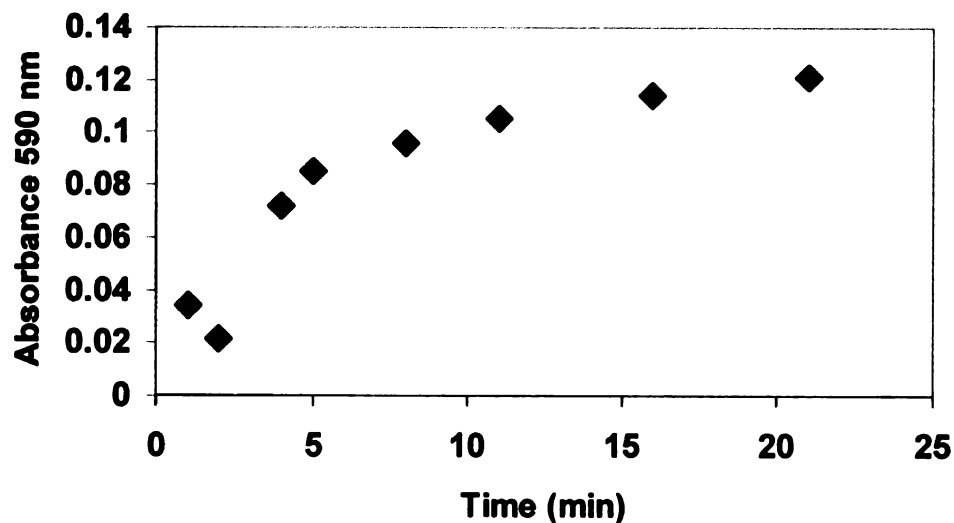


**Figure VI.1 UV-visible spectroscopic analysis of the reaction of  $\alpha$ KG-Fe(II)AlkB with oxygen.**

The Fe(II)- and  $\alpha$ KG-bound form of AlkB was mixed with O<sub>2</sub>-saturated water and spectra were recorded as a function of time. Panel A shows the loss of the MLCT absorption near 500 nm associated with the Fe(II)/ $\alpha$ KG center and the development of an intense visible chromophore centered at 595 nm. The kinetics of the spectral changes at 590 nm are illustrated in Panel B.

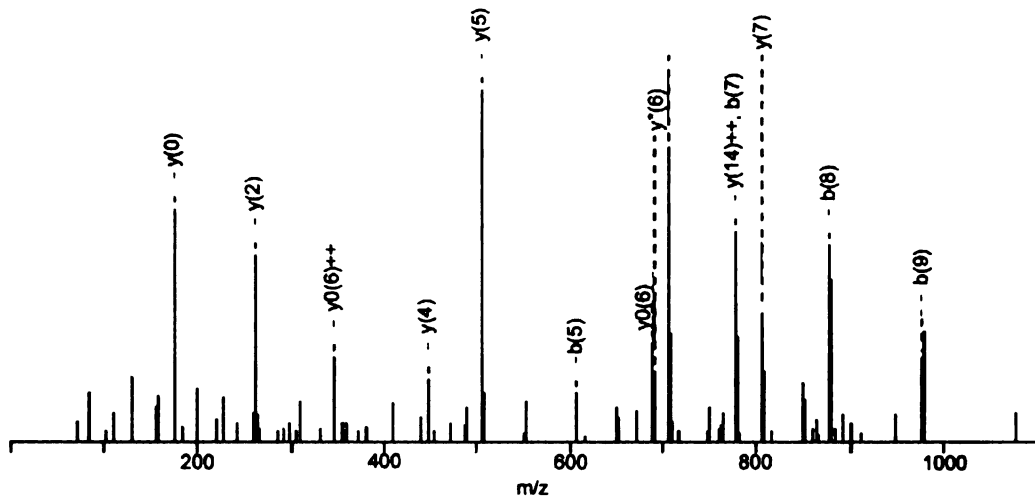


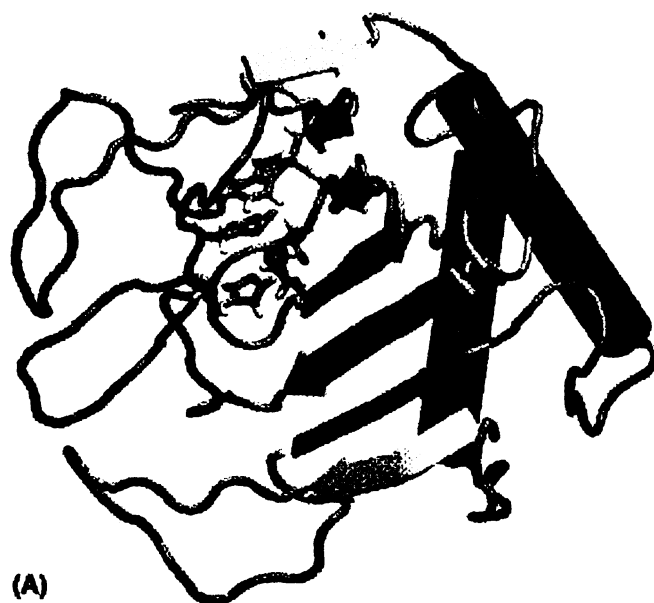
**Figure VI.2 LC/MS/MS identification of hydroxy-Trp 178 in AlkB.**

Tryptic peptides derived from oxygen-exposed  $\alpha$ KG-Fe(II)AlkB were resolved by HPLC and analyzed by tandem MS/MS. The figure depicts the observed secondary MS product ions (mono- and di-protonated) derived from fragmentation of a parent ion (mass of 1780.91) associated with a single tryptic peptide. B ions are amino-terminal fragments and Y ions include the carboxyl terminal fragments. The parent ion and product ion masses match the sequence LLEHGDVVVWGGESR (residues 168-183 of AlkB) with a mass addition of 16 Da starting on the B11 and Y6 product ions. This 16 Da mass addition was consistent with the presence of hydroxy-Trp at residue 178.

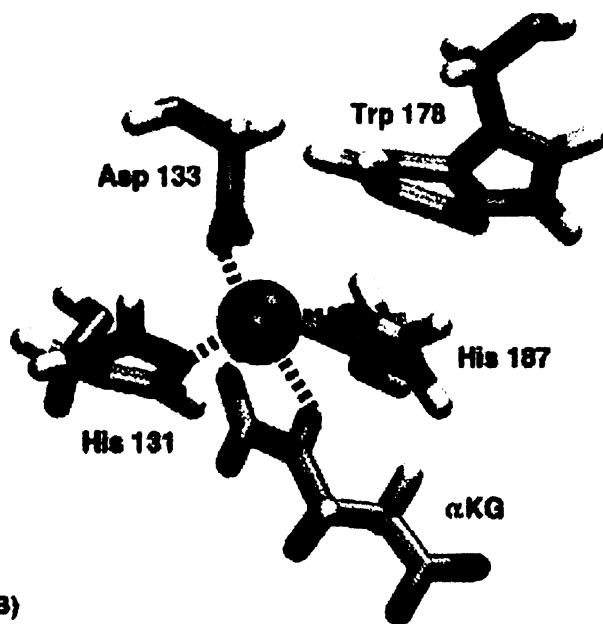
that all fragments containing Trp 178 were shifted by 16 Da and fragments not containing Trp 178 were unshifted (Figure VI.2). Surprisingly, similar analyses revealed the presence of the same modification in a tryptic peptide of the control sample. This result is consistent with at least a portion of the overproduced AlkB undergoing modification during cell growth. We interpret the finding of Trp 178 hydroxylation as evidence that an Fe(IV)-oxo, or similarly reactive species, is generated in the reaction of  $\alpha$ KG-Fe(II)AlkB with O<sub>2</sub> in the absence of methylated DNA substrate. Oxidation of the nearby Trp initiates the eventual formation of the hydroxy-Trp feature observed in the mass spectral analysis.

### *Protein Modeling*

An overview of the predicted structure for *E. coli* AlkB is shown in Figure VI.3A. It features the same double-stranded beta-helix and jelly-roll topology as the deacetoxycephalosporin C synthase templates used to build the model. Residues 1-15 are not shown since the prediction of the amino terminus is considered less reliable for the lack of a suitable template. The closeup view shown in Figure VI.3B focuses on the immediate environment of the Fe(II) binding site. As expected, His 131, Asp 133, and His 187 are in direct interaction with the Fe(II). The model also shows Trp 178 located above His 187 and in the immediate vicinity. In fact, the distance between the Trp carbon at the 5 position, where hydroxylation is most likely, and the Fe(II) ion is only 4.7 Å in the predicted model after force-field based minimization. This compares favorably with the geometry in TauD where the distance between Fe(II) to Tyr 73, the tyrosine that becomes hydroxylated, is 6.5 Å (8).



(A)



(B)

**Figure VI.3 Structure of AlkB determined by protein modeling.**

Panel A depicts the predicted fold of the monomer and reveals a  $\beta$ -jellyroll structure as found in other family members. Residues 1-15 are not included since their positions could not be reliably predicted. Panel B focuses on the region near the metal center and shows the three amino acid side chains that serve as ligands, the  $\alpha$ KG, and the nearby Trp 178 that undergoes hydroxylation.

## *Conclusions*

When exposed to oxygen,  $\alpha$ KG-Fe(II)AlkB forms a blue chromophore that closely resembles the spectrum of oxygen-exposed  $\alpha$ KG-Fe(II)TfdA. On the basis of resonance Raman and mass spectrometric evidence, the TfdA chromophore previously was assigned to a LMCT band associated with OH-Trp coordination to Fe(III) (7). LC/MS/MS evidence confirms that OH-Trp also is produced in AlkB and we propose that the spectrum similarly derives from a OH-Trp/Fe(III) LMCT transition. Whereas the modified Trp in TfdA (Trp 113) immediately precedes a metal ligand (His 114), the AlkB modification (OH-Trp 178) is more distant from the closest ligand (His 187) in the sequence. Structure prediction efforts provide a robust three-dimensional model of AlkB that is consistent with Trp 178 being close to the metal center and capable of becoming hydroxylated.

Of interest, OH-Trp 178 also was identified in a control AlkB sample. We attribute this finding as indicating that self-hydroxylation can occur within the cell, where  $\alpha$ KG, Fe(II), and oxygen are present, at least in the case of an overexpressing strain. Because oxygen exposure of Fe(II)AlkB does not yield a detectable blue chromophore, either the amount of OH-Trp is quite small in the sample or the chromophore only can be generated from unmodified AlkB, i.e., OH-Trp does not coordinate Fe(III) when previously modified protein is amended with Fe(II) and the metal is oxidized. These results suggest that anaerobic growth conditions could be used to help insure the production of fully active, unmodified protein.

The phenomenon of enzyme self-hydroxylation appears to be widespread in non-heme Fe(II) oxygenases. In addition to the hydroxylation of a Trp side chain noted above

for AlkB and previously described for TfdA (7), a tyrosine residue is hydroxylated to form a catecholate derivative in TauD (6, 8) and phenylalanine hydroxylation has been noted in both tyrosine hydroxylase (16, 17) and the Y325F variant of phenylalanine hydroxylase (18). Furthermore, both tyrosine and phenylalanine hydroxylation have been observed in various mutants of the R2 subunit of ribonucleotide reductase, a dinuclear iron protein (19-22). The blue oxidized form of 4-hydroxyphenylpyruvate dioxygenase (23), assigned to a species possessing tyrosinate-Fe(III) LMCT transitions (24), might derive from analogous hydroxylation of an active site phenylalanine (as proposed in (25)) on the basis of the enzyme crystal structure which shows the absence of tyrosines, but presence of phenylalanines, in the vicinity of the metallocenter (26). Biomimetic complexes designed to mimic the reactivity of  $\alpha$ KG-dependent dioxygenases also undergo self-hydroxylation chemistry involving a ligand phenyl group (27, 28). In summary, the hydroxylation chemistry of several enzymes and model compounds is consistent with the generation of a highly reactive intermediate that oxidizes an aromatic substituent when the primary substrate is absent. It remains unclear whether the aberrant enzymatic reactions of AlkB and these other systems may benefit the proteins by protecting them from more harmful oxidative reactions such as backbone cleavage reactions (as observed in aminocyclopropane carboxylate oxidase (29)).

## References

1. Prescott, A. G. and Lloyd, M. D., *Natural Products Reports*, **2000**, *17*, 367-383.
2. Price, J. C., Barr, E. W., Glass, T. E., Krebs, C., and Bollinger, J. M., Jr., *J Am Chem Soc*, **2003**, *125*, 13008-9.
3. Price, J. C., Barr, E. W., Tirupati, B., Bollinger, J. M., Jr., and Krebs, C., *Biochemistry*, **2003**, *42*, 7497-508.
4. Proshlyakov, D. A., Henshaw, T. F., Monterosso, G. R., Ryle, M. J., and Hausinger, R. P., *J Am Chem Soc*, **2004**, *126*, 1022-3.
5. Rohde, J. U., In, J. H., Lim, M. H., Brennessel, W. W., Bukowski, M. R., Stubna, A., Munck, E., Nam, W., and Que, L., *Science*, **2003**, *299*, 1037-1039.
6. Ryle, M. J., Koehntop, K. D., Liu, A., Que, L., Jr., and Hausinger, R. P., *Proc Natl Acad Sci U S A*, **2003**, *100*, 3790-5.
7. Liu, A., Ho, R. Y., Que, L., Jr., Ryle, M. J., Phinney, B. S., and Hausinger, R. P., *J Am Chem Soc*, **2001**, *123*, 5126-7.
8. Ryle, M. J., Liu, A., Muthukumaran, R. B., Ho, R. Y., Koehntop, K. D., McCracken, J., Que, L., Jr., and Hausinger, R. P., *Biochemistry*, **2003**, *42*, 1854-62.
9. Ginalski, K., Elofsson, A., Fisher, D., and Rychlewski, L., *Bioinformatics*, **2003**, *19*, 1015-1018.
10. Ginalski, K., Pas, J., Wyrwicz, L. S., von Grotthuss, M., Bujnicki, J. M., and Rychlewski, L., *Nucleic Acids Research*, **2003**, *31*, 3804-3807.
11. Feig, M., Karanicolas, J., and Brooks, C. L., 3rd, *J Mol Graph Model*, **2004**, *22*, 377-95.
12. Skolnick, J., Kolinski, A., and Ortiz, A. R., *Journal of Molecular Biology*, **1997**, *265*, 217-241.
13. Feig, M. and Brooks, C. L., 3rd, *Proteins*, **2002**, *49*, 232-45.
14. Brooks, B. R., Brucoleri, R. E., Olafson, B. D., States, D. J., Swaminathan, S., and Karplus, M., *Journal of Computational Chemistry*, **1983**, *4*, 187-217.
15. Trewick, S. C., Henshaw, T. F., Hausinger, R. P., Lindahl, T., and Sedgwick, B., *Nature*, **2002**, *419*, 174-178.
16. Ellis, H. R., Daubner, S. C., McCulloch, R. I., and Fitzpatrick, P. F., *Biochemistry*, **1999**, *38*, 10909-14.

17. Goodwill, K. E., Sabatier, C., and Stevens, R. C., *Biochemistry*, **1998**, *37*, 13437-45.
18. Kinzie, S. D., Thevis, M., Ngo, K., Whitelegge, J., Loo, J. A., and Abu-Omar, M. M., *J Am Chem Soc*, **2003**, *125*, 4710-1.
19. Baldwin, J., Voegtli, W. C., Khidekel, N., Moenne-Loccoz, P., Krebs, C., Pereira, A. S., Ley, B. A., Huynh, B. H., Loehr, T. M., Riggs-Gelasco, P. J., Rosenzweig, A. C., and Bollinger, J. M., Jr., *J Am Chem Soc*, **2001**, *123*, 7017-30.
20. Ormo, M., deMare, F., Regnstrom, K., Aberg, A., Sahlin, M., Ling, J., Loehr, T. M., Sanders-Loehr, J., and Sjoberg, B. M., *J Biol Chem*, **1992**, *267*, 8711-4.
21. Ormo, M., Regnstrom, K., Wang, Z., Que, L., Jr., Sahlin, M., and Sjoberg, B. M., *J Biol Chem*, **1995**, *270*, 6570-6.
22. Logan, D. T., deMare, F., Persson, B. O., Slaby, A., Sjoberg, B. M., and Nordlund, P., *Biochemistry*, **1998**, *37*, 10798-807.
23. Lindstedt, S. and Rundgren, M., *J Biol Chem*, **1982**, *257*, 11922-31.
24. Bradley, F. C., Lindstedt, S., Lipscomb, J. D., Que, L., Jr., Roe, A. L., and Rundgren, M., *J Biol Chem*, **1986**, *261*, 11693-6.
25. Ryle, M. J. and Hausinger, R. P., *Curr Opin Chem Biol*, **2002**, *6*, 193-201.
26. Serre, L., Sailland, A., Sy, D., Boudec, P., Rolland, A., Pebay-Peyroula, E., and Cohen-Addad, C., *Structure Fold Des*, **1999**, *7*, 977-88.
27. Hegg, E. R., Ho, R. Y. N., and Que, L., Jr., *Journal of the American Chemical Society*, **1999**, *121*, 1972-1973.
28. Mehn, M. P., Fujisawa, K., Hegg, E. L., and Que, L., Jr., *J Am Chem Soc*, **2003**, *125*, 7828-42.
29. Zhang, Z., Barlow, J. N., Baldwin, J. E., and Schofield, C. J., *Biochemistry*, **1997**, *36*, 15999-6007.

## **CHAPTER VII**

### **CONCLUSIONS AND FUTURE DIRECTIONS**

The results presented in this dissertation represent a significant advance in our understanding of the FeS/AdoMet enzymes. When I first started work on AE, the existence of an iron sulfur cluster was a hypothesis. Now the role of the cluster in radical generation has been identified and the interaction with AdoMet established. Chapter II demonstrated the exceptional flexibility of the cluster-binding site of PFL-AE to accommodate a wide variety of cluster types. The work presented in Chapter IV differentiated among the various types and demonstrated that the  $[4\text{Fe-4S}]^{1+/2+}$  redox couple is catalytically relevant.

The work presented in Chapter III demonstrated the existence of a unique iron site in the iron-sulfur cluster of PFL-AE and the binding of AdoMet to this site, however the results were unable to differentiate between various potential binding modes. The sulfonium center was deemed unlikely to be a ligand, since the large change in isomer shift observed was more consistent with coordination of the amino, carboxylate, or hydroxyl groups. Since these results were reported, further work with PFL-AE and other systems has clarified our understanding of the interaction between AdoMet and the iron-sulfur cluster. ENDOR studies of PFL-AE using specifically labeled AdoMet have provided strong evidence that AdoMet indeed chelates the unique iron site of PFL-AE through the amino and carboxylate groups, perhaps positioning the sulfonium group for an inner-sphere electron transfer or attack by one of the bridging sulfides (1, 2). Using  $^{17}\text{O}$  and  $^{15}\text{N}$  labeled AdoMet the Broderick and Hoffman groups clearly showed that both the amino and carboxylate groups coordinate an iron of the cluster. This coordination mode is consistent with the data presented in Chapter III of this dissertation.

Mössbauer studies of BioB show that the isomer shift of one of the mixed-valence pairs of the  $[4\text{Fe-4S}]^{2+}$  cluster increases from 0.47 to 0.64 mm/s in the presence of AdoMet, a similar shift to that observed in PFL-AE. In addition, the symmetric breathing mode of the cluster shifts from 338 to 342  $\text{cm}^{-1}$  upon addition of AdoMet, a shift that is consistent with the ligation of an O/N ligand to the cluster (3). Significantly, the crystal structures of two FeS/AdoMet enzymes have been reported. The structure of BioB shows AdoMet bound to a unique site in the  $[4\text{Fe-4S}]$  cluster through the amino and carboxylate groups (4), in a manner similar to that of PFL-AE based on the available spectroscopic data (1, 2, 5). The crystal structure of HemN, another FeS/AdoMet enzyme, also shows AdoMet chelated to a unique iron site of the  $[4\text{Fe-4S}]$  cluster with the sulfonium group approximately equidistant from the nearest iron and bridging sulfide (6). In the absence of any structural information on PFL-AE, it might be possible to build a useful model using the structures of BioB and HemN as templates. An interesting aspect of these structures is that they are both built around a TIM barrel fold, perhaps the most common fold known. The authors of the BioB structure paper suggest that this would be a favorable architecture for an enzyme with a small-molecule substrate but raises questions about how other FeS/AdoMet enzymes could gain access to large-molecule substrates, such as other proteins. The answer might come from observing the HemN structure, which is built around an incomplete TIM barrel (6). Perhaps the substrate completes the TIM barrel, providing a basis for protein docking in the enzyme-substrate complex. The crystal structure of PFL is known (7-9), and with a model of PFL-AE, it might be possible to dock the structures such that PFL completes an  $\alpha/\beta$

barrel in PFL-AE and Gly-734 is positioned close to the 5' carbon of the adenosyl moiety of AdoMet.

The chelation of a unique iron site of the [4Fe-4S] cluster by the amino and carboxylate groups of AdoMet will likely be a common theme in this group of enzymes. The exact mechanism by which this complex generates a 5'dAdo radical remains uncertain. Although an inner sphere electron transfer may generate the adenosyl radical, it is also possible that there are cluster bound AdoMet derived intermediates. The PFL-AE system represents an excellent opportunity to investigate this question using pre-steady state methods, such as freeze-quench and stopped-flow spectroscopy. To my knowledge, the single turnover conditions described in Chapter IV are more precisely defined than those generated for other FeS/AdoMet enzymes.

The function and mechanism of AlkB in protecting cells from the toxic effects of methylating agents has been an open question for decades. The results presented in Chapter V establish that AlkB functions as an Fe(II)/ $\alpha$ -KG dioxygenase by a novel mechanism of oxidative DNA repair. It is assumed that the enzyme utilizes the same mechanism as other Fe(II)/ $\alpha$ -KG dioxygenases in generating an Fe(IV)=O intermediate (10-12), however, there are several interesting questions that are unique to AlkB. The first is how does it bind DNA. The model presented in Chapter VI could be used to identify potential DNA-interacting residues and mutagenesis targets. It is also unknown how AlkB recognizes the 1-meA and 3-meC substrates. Our lab, in collaboration with Professor John McCracken, is currently investigating this question by EPR, ESEEM, and ENDOR spectroscopy using NO-bound AlkB. Using deuterium-labeled methylated DNA, we hope to obtain information on the distance and orientation of the methyl group

with respect to the metal center. The crystal structure of AlkB bound to substrates would answer many of these questions and is being actively pursued in multiple crystallography labs.

A human homolog of AlkB was identified in 1996 (hABH1 for human AlkB homolog) and was reported to complement an *E. coli alkB* mutant, but more recent studies have been unable to reproduce these findings and have not identified an enzymatic activity for this homolog (13, 14). As such, the function of hABH1 remains a mystery. Two recently identified human homologs of AlkB (hABH2 and 3) have been shown to demethylate 1-meA and 3-meC (13, 14). In addition to their activities with methylated DNA, AlkB and hABH3 have been shown to repair 1-meA and 3-meC in RNA (14). In order to ascertain the role of these different AlkB homologs, interference RNA knockdown cell lines and knockout mice are being generated (15). In addition to the AlkB homologs that have been characterized by biochemical means, bioinformatic work has identified an additional five putative homologs in the human genome (16). These additional homologs should be investigated by biochemical and genetic approaches.

## References

1. Walsby, C. J., Hong, W., Broderick, W. E., Cheek, J., Ortillo, D., Broderick, J. B., and Hoffman, B. M., *Journal of the American Chemical Society*, **2002**, *124*, 3143-3151.
2. Walsby, C. J., Ortillo, D., Broderick, W. E., Broderick, J. B., and Hoffman, B. M., *Journal of the American Chemical Society*, **2002**, *124*, 11270-11271.
3. Cosper, M. M., Jameson, G. N. L., Hernandez, H. L., Krebs, C., Huynh, B. H., and Johnson, M. K., *Biochemistry*, **2004**, *43*, 2007-2021.
4. Berkovitch, F., Nicolet, Y., Wan, J. T., Jarrett, J. T., and Drennan, C. L., *Science*, **2004**, *303*, 76-9.
5. Krebs, C., Broderick, W. E., Henshaw, T. F., Broderick, J. B., and Huynh, B. H., *Journal of the American Chemical Society*, **2002**, *124*, 912-913.
6. Layer, G., Moser, J., Heinz, D. W., Jahn, D., and Schubert, W. D., *Embo J*, **2003**, *22*, 6214-24.
7. Leppanen, V. M., Merckel, M. C., Ollis, D. L., Wong, K. K., Kozarich, J. W., and Goldman, A., *Structure Fold Des*, **1999**, *7*, 733-44.
8. Becker, A. and Kabsch, W., *J Biol Chem*, **2002**, *277*, 40036-42.
9. Becker, A., Fritz-Wolf, K., Kabsch, W., Knappe, J., Schultz, S., and Volker Wagner, A. F., *Nat Struct Biol*, **1999**, *6*, 969-75.
10. Price, J. C., Barr, E. W., Glass, T. E., Krebs, C., and Bollinger, J. M., Jr., *J Am Chem Soc*, **2003**, *125*, 13008-9.
11. Price, J. C., Barr, E. W., Tirupati, B., Bollinger, J. M., Jr., and Krebs, C., *Biochemistry*, **2003**, *42*, 7497-508.
12. Proshlyakov, D. A., Henshaw, T. F., Monterosso, G. R., Ryle, M. J., and Hausinger, R. P., *J Am Chem Soc*, **2004**, *126*, 1022-3.
13. Duncan, T., Trewick, S. C., Koivisto, P., Bates, P. A., Lindahl, T., and Sedgwick, B., *Proc Natl Acad Sci U S A*, **2002**, *99*, 16660-5.
14. Aas, P. A., Otterlei, M., Falnes, P. O., Vagbo, C. B., Skorpen, F., Akbari, M., Sundheim, O., Bjoras, M., Slupphaug, G., Seeberg, E., and Krokan, H. E., *Nature*, **2003**, *421*, 859-63.
15. Samson, L., *personal communication*.

16. Kurowski, M. A., Bhagwat, A. S., Papaj, G., and Bujnicki, J. M., *BMC Genomics*, **2003**, *4*, 48.



MICHIGAN STATE UNIVERSITY LIBRARIES



3 1293 02504 5216